AD-A062 998 ARCON CORP WALTHAM MA F/G 4/1

IONOSPHERIC MODELING AND PROPAGATION ANALYSIS.(U)

JUL 78 D C MILLER, J GIBBS F19628-77-C-0051

UNCLASSIFIED SCIENTIFIC-1 RADC -TR-78-163 NL

1 OF 1

AD A062998

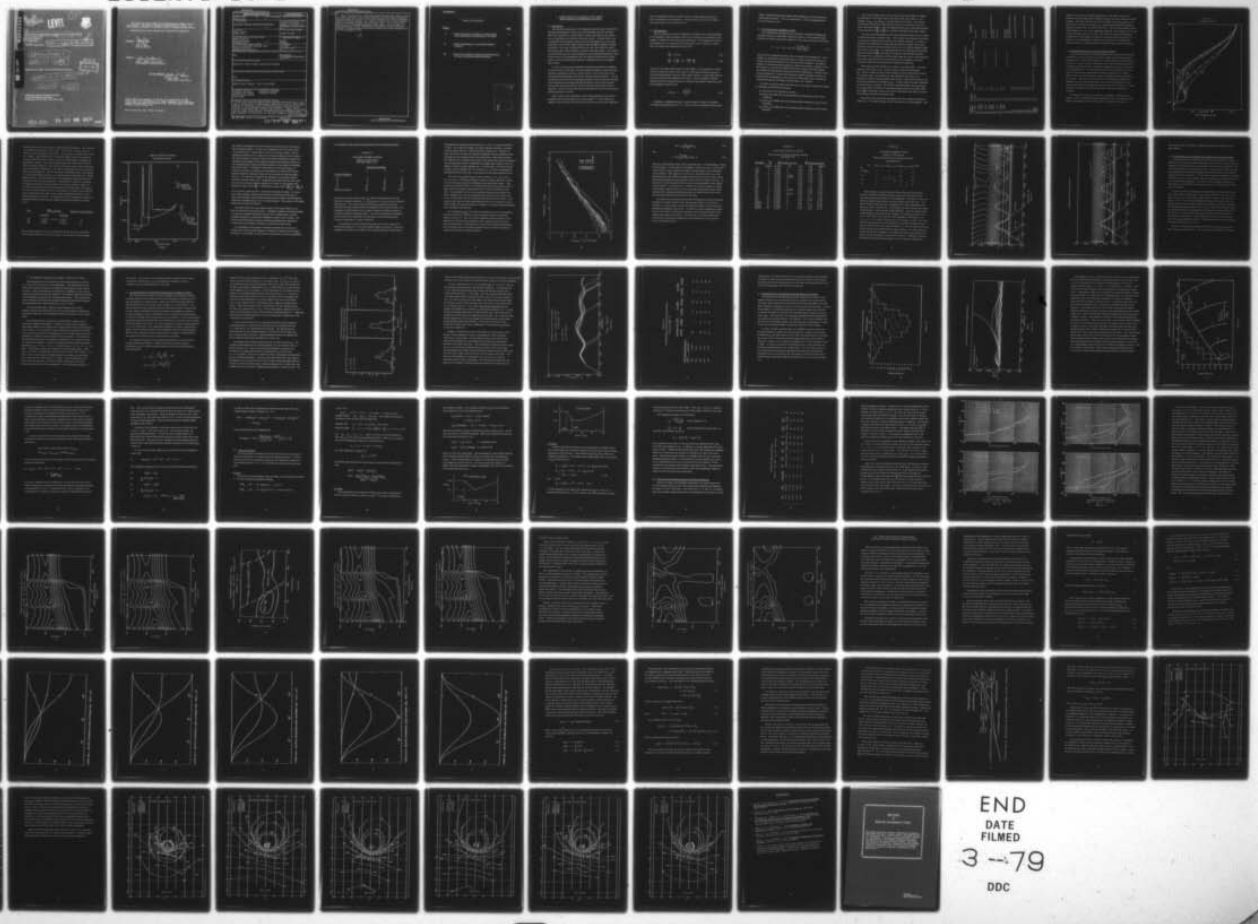

END

DATE FILMED

3 -79

DDC

(18) (19) RADC-TR-78-163
Interim Report
July 1978

LEVEL

(14)

IONOSPHERIC MODELING AND PROPAGATION ANALYSIS

(10) David C. Miller
Joseph Gibbs

ARCON Corporation

(9) Interim rept for Nov 76-Oct 73

(14) SCIENTIFIC-1

(11) Jul 78 (12) 93p.

Approved for public release; distribution unlimited

(15) F19628-77-C-0051

(16) 2305 (17) J2

ROME AIR DEVELOPMENT CENTER
Air Force Systems Command
Griffiss Air Force Base, New York 13441

This report has been reviewed by the RADC Information Office (OI) and is releasable to the National Technical Information Service (NTIS). At NTIS it will be releasable to the general public, including foreign nations.

RADC-TR-78-163 has been reviewed and is approved for publication.

APPROVED: Gary S. Sales

GARY S. SALES
Contract Monitor

APPROVED: Allan C. Schell

ALLAN C. SCHELL, Acting Chief
Electromagnetic Sciences Division

FOR THE COMMANDER: John P. Huss

JOHN P. HUSS
Acting Chief, Plans Office

If your address has changed or if you wish to be removed from the RADC mailing list, or if the addressee is no longer employed by your organization, please notify RADC (EEP) Hanscom AFB MA 01731. This will assist us in maintaining a current mailing list.

Do not return this copy. Retain or destroy.

UNCLASSIFIED

SECURITY CLASSIFICATION OF THIS PAGE (When Data Entered)

REPORT DOCUMENTATION PAGE		READ INSTRUCTIONS BEFORE COMPLETING FORM
1. REPORT NUMBER RADC-TR-78-163	2. GOVT ACCESSION NO.	3. RECIPIENT'S CATALOG NUMBER
4. TITLE (and Subtitle) IONOSPHERIC MODELING AND PROPAGATION ANALYSIS		5. TYPE OF REPORT & PERIOD COVERED Scientific Report No. 1 November 76 - October 77
		6. PERFORMING ORG. REPORT NUMBER N/A
7. AUTHOR(s) David C. Miller Joseph Gibbs		8. CONTRACT OR GRANT NUMBER(s) F19628-77-C-0051
9. PERFORMING ORGANIZATION NAME AND ADDRESS ARCON Corporation 260 Bear Hill Road Waltham MA 02154		10. PROGRAM ELEMENT, PROJECT, TASK AREA & WORK UNIT NUMBERS 61102F 2305J220
11. CONTROLLING OFFICE NAME AND ADDRESS Deputy for Electronic Technology (EEP) Hanscom AFB MA 01731 Monitor/Gary Sales/EEP		12. REPORT DATE July 1978 13. NUMBER OF PAGES 90
14. MONITORING AGENCY NAME & ADDRESS(if different from Controlling Office) Same		15. SECURITY CLASS. (of this report) UNCLASSIFIED 15a. DECLASSIFICATION/DOWNGRADING SCHEDULE N/A

16. DISTRIBUTION STATEMENT (of this Report)

Approved for public release; distribution unlimited.

17. DISTRIBUTION STATEMENT (of the abstract entered in Block 20, if different from Report)

Same

18. SUPPLEMENTARY NOTES

RADC/ET Project Engineer: Gary S. Sales (EEP)

19. KEY WORDS (Continue on reverse side if necessary and identify by block number)

Ionospheric Modeling
Ionospheric Ray Tracing
Electron Density Models
Ducted Modes
Ionospheric Parameters
Ionospheric Heating

20. ABSTRACT (Continue on reverse side if necessary and identify by block number)

This report describes several studies performed toward improving our knowledge of the properties of High-Frequency communication circuits. These studies included the development of three dimensional electron density models and the analysis of various propagation modes in the ionosphere. Several vertical electron density models were constructed that proved to be useful in both global and polar region HF applications. In constructing these models improvements were ~~have been~~ made to existing models for individual ionospheric layer parameters.

(Cont'd on reverse)

DD FORM 1 JAN 73 1473 EDITION OF 1 NOV 65 IS OBSOLETE

1

UNCLASSIFIED

SECURITY CLASSIFICATION OF THIS PAGE (When Data Entered)

(cont'd)

Some of the properties of long range ducted modes have been isolated using ray tracing techniques. The relative probability of establishing and maintaining ducted modes as a function of HF circuit parameters for various ionospheric conditions has been explored. The stability of these modes for small perturbations to the ambient ionosphere has also been studies. Injection into ionospheric ducts by artificially heating localized regions of the ionosphere has been investigated. Spatial distributions and intensity patterns have been obtained for irregularities in the electron density which align themselves with the local geomagnetic field.

TABLE OF CONTENTS

I. COMPUTATIONAL STUDIES OF LONG-RANGE HIGH-FREQUENCY IONOSPHERIC DUCTING

I.1 Introduction

Ray-tracing calculations for HF propagation studies using various three dimensional ionospheric models for rays originating from the earth has shown the existence of a small number of long-range ducted modes which are a strong function of the time of day and season. A ducted mode is one in which HF electromagnetic waves traverse long distances by successive reflections from various height regions of the ionosphere without reaching the ground. For some conditions they do not exist at all while for others they appear with a small efficiency relative to all other modes. The search for these ducted rays in a given ionosphere by searching through many values of the various circuit parameters does not yield the kind of results which would be useful in predicting the general conditions necessary to support these modes.

In order to have greater flexibility in exploring ionospheric conditions we have chosen to work with a two dimensional ionospheric model where the individual ionospheric profiles could be constructed to reflect more arbitrarily specified horizontal and vertical electron density gradients. For the assessment of the effects of ionization gradients on ray injection and ducting at HF frequencies we assume that both the effects of the earths magnetic field and the interaction between the electrons and neutral atoms can be neglected. We also assume that lateral deviations do to transverse electron density gradients are small.

Some results on the dependence of the ducting efficiency upon various gradients have been presented in an earlier paper.[1] In this report we expand on these results and extend the discussion to include some additional

work concerning the stability of these modes to both random and deterministic fluctuations of the ionosphere. We also include a discussion of these long-range modes for an elevated source.

I.2 Ray Equations

The six canonical equations in spherical coordinates for a ray propagating in an ionosphere without magnetic field[2] can be reduced to two equations if the medium is confined to vary only in two dimensions. The propagation geometry corresponds then to a spherical system where the ray is confined to a plane. These two differential equations have the form[3]

$$\frac{dr}{dx} = \frac{r}{a} \tan\alpha \tag{I-1}$$

$$\frac{d\alpha}{dx} = \frac{1}{\mu}\frac{\partial\mu}{\partial h} + \frac{1}{a} - \frac{\tan\alpha}{\mu}\frac{\partial\mu}{\partial x} \tag{I-2}$$

where a is the radius of the earth, h is the height, r is the distance of a point on the ray from the center of the earth, x is the angular distance measured from the starting point of the ray at the earth's surface, α is the angle between the ray direction and the tangent to the earth. For the ionosphere without magnetic field the refractive index μ is related to the plasma frequency f_N and the propagation frequency f by

$$\mu^2(x,h) = 1 - \frac{f_N^2(x,h)}{f^2} \quad . \tag{I-3}$$

Equations, resulting from Eqs. (1) and (2) after a change of variables, are integrated analytically for $\mu = 1$. For $\mu < 1$ they are integrated numerically

using a standard fourth-order Runge-Kutta technique for two simultaneous differential equations.[2] For ray computations, a 10-km stepping interval in ground range is used.

I.3 Two-Dimensional Ionospheric Model

For mathematical and numerical convenience and without implying any unusually superior relationship to physical reality, electron-density height profiles are formed using three segments of sine-square functions of the type

$$N = N_1 + (N_2 - N_1) \sin^2 \left\{ \frac{\pi}{2} \left(\frac{h-h_1}{h_2-h_1} \right) \right\} \qquad \text{(I-4)}$$

specifying the relationship between electron density (N) and height (h). These profiles are changeable through the choice of critical-frequency parameters without causing discontinuities in vertical ionization gradients. Ionospheric profiles are parametrically specified in selected increments of distance along the surface of a curved earth while intermediate values of electron density are obtained by interpolation using second-order polynomials. With the choice of these parameters, vertical and horizontal ionization gradients may be introduced into an ionospheric cross-section to which radio rays, specified by 'operating' frequency and initial elevation angle, are confined.

A profile at any given point along the great circle path is entirely described by specifying the following parameters:

h_o the bottom of the ionospheric E layer,

h_E and f_E the height and corresponding plasma frequency of the E layer maximum,

h_{F1} and f_{F1} the height and corresponding plasma frequency of the F1 layer maximum,

h_{F2} and f_{F2} the height and corresponding plasma frequency of the F2 layer maximum.

Any of the individual layers can be omitted from the profile by setting the parameters of the layer equal to the ones of the layer below it. For example, if $h_{F1} = h_E$ and $f_{F1} = f_E$ there will be no F1 layer. One feature of the model is that the vertical gradient of the electron density is zero at each of the layer heights. The interpolation between any of the given profiles is such that $N(x,h)$, $\frac{\partial N}{\partial h}$ and $\frac{\partial N}{\partial x}$ are continuous throughout the entire region.

For most of the ionospheres used in this study the profiles were specified at 2000 km intervals in ground range. This spacing was adequate to describe a variety of horizontal and vertical electron density gradients. In order to determine the capability of an individual ionosphere to support long-range modes we extend the electron density model over a 10,000 km distance along the surface of the earth. For approximately the first 5000 km the horizontal ionozation gradients $\frac{\partial N}{\partial x}$ were made to be negative and thereafter positive. This allowed for a comparison of the ground range for various ray parameters since those rays which were first injected into an ionospheric duct were eventually reflected to the ground by the symmetric gradients.

Some features of the profiles are common to all the models. The ionospheric E layer starts at h_o = 90 km and has a maximum ionization at h_E = 110 km. While the value of this maximum varies from model to model it is always taken to be constant over the ray path so that there is no horizontal electron density gradient below 110 km. When an F1 layer is used the plasma frequency is specified at h_{F1} = 160 km and the F2-layer maximum is located at h_{F2} = 300 km. The choice of constant heights for h_{F1} and h_{F2} in no way restricts the kinds of ionization gradients that we can study since the net $\frac{\partial N}{\partial x}$ at any point in space can still be controlled by the choice of values of the plasma frequencies along the path.

Parameters for many of the ionospheres that were studied are shown in TABLE I.1. The labels indicate some of the features of the ionosphere. The

TABLE I-1

Parameters for Two Dimensional Ionospheric Models

Ionospheric Models	f_E(110 km)	f_1(160 km)	f_2(300 km)	Comments
1A (1AD)	3.5 MHz	2.0 MHz	8.5, 8.0, 7.5, 7.0, 7.5, 8.0 MHz	
1A'	2.0			No f_1 layer
1B (1BD)	3.5	2.5		
1C (1CD)	3.5	3.0		
1D (1DD)	3.5	3.5		
1D'	3.5			No f_1 layer
2A (2AD)	3.5	2.0	9., 8., 7., 6., 7., 8.	
2A'	2.0			No f_1 layer
2B (2BD)	3.5	2.5		
2C (2CD)	3.5	3.0		
2D (2DD)	3.5	3.5		N_e = constant $110 \leq h \leq 160$ km.
2D'	3.5			No f_1 layer
3A (3AD)	3.5	2.0	9. 7.5, 6.0, 6.0, 7.5, 9.	
3A'	2.0			No f_1 layer
3B (3BD)	3.5	2.5		
3C (3CD)	3.5	3.0		
3D (3DD)	3.5	3.5		
3D'	3.5			No f_1 layer
2B'	2.5		9., 8., 7., 6., 7., 8.	No f_1 layer
2C'	3.0			No f_1 layer
2AA	2.0	2.0		N_e = constant $110 \leq h \leq 160$ km.
2AB	2.5	2.0		
2AC	3.0	2.0		
2BB	2.5	2.5		N_e = constant $110 \leq h \leq 160$ km.
2BC	3.0	2.5		
2BA	2.0	2.5		
2CA	2.0	3.0		
2CB	2.5	3.0		
2CC	3.0	3.0		N_e = constant $110 \leq h \leq 160$ km.
2DA	2.0	3.5		
2DB	2.5	3.5		
2DC	3.0	3.5		
3DCBA	3.5	3.5, 3.0, 2.5, 2.0, 2.5, 3.0	9., 7.5, 6.0, 6.0, 7.5, 9.0	Gradient in f_1 and f_2 layer
2DCBA	3.5		9., 8., 7., 6., 7., 8.	
1DCBA	3.5		8.5, 8.0, 7.5, 7.0, 7.5, 8.0	

number refers to the horizontal gradient due to the change in foF2 as a function of ground range with 1 being the smallest and 3 the largest horizontal gradient. The letters specify one of four possible values of f_E and f_1, the first refers to f_1 and the second to f_E. Some typical profiles are shown in Figure I-1 where foF2 = 8.0 MHz in all cases. The electron density in three of the profiles, A', D', D are monotonic functions of the height and A, B, and C have ionization valleys at 160 km. The values the horizontal ionization gradients at several heights for the three models is shown in TABLE I-2. A large variety of ionospheric conditions can be studied by combining the separate models for the horizontal and vertical electron density gradients.

I.4 Ducting Efficiency for Various Ionospheric Models

In order to determine the relative efficiency for ducting for each of the ionospheres we trace an array of rays in 0.5 MHz steps in the frequency domain between 6 and 25 MHz and in 0.5° steps in ground elevation between 0° and 11°. In some cases we reduced the size of the frequency interval in an attempt to determine the sensitivity of finding ducted rays as a function of the sampling size. For all of the profiles shown in Figure I-1 no long range ducted rays were found when horizontal gradients were omitted. This was the case even when the frequency sampling interval was reduced to 0.1 MHz. Each ray is traced until one of the following conditions is fulfilled: the ray touches the ground, the local elevation angle is 0° in a non-ionized portion of the path, the ray penetrates at h = 400 km., or when a ducted ray reaches the limit in range over which the ionosphere is specified.

For model 3D' 22 rays were found to be trapped, reaching ground ranges in excess of 8000 km before touching the earth. The behavior with distance and height of some of these rays is illustrated in Figure I-2,

Figure I-1

Ionospheric Profiles

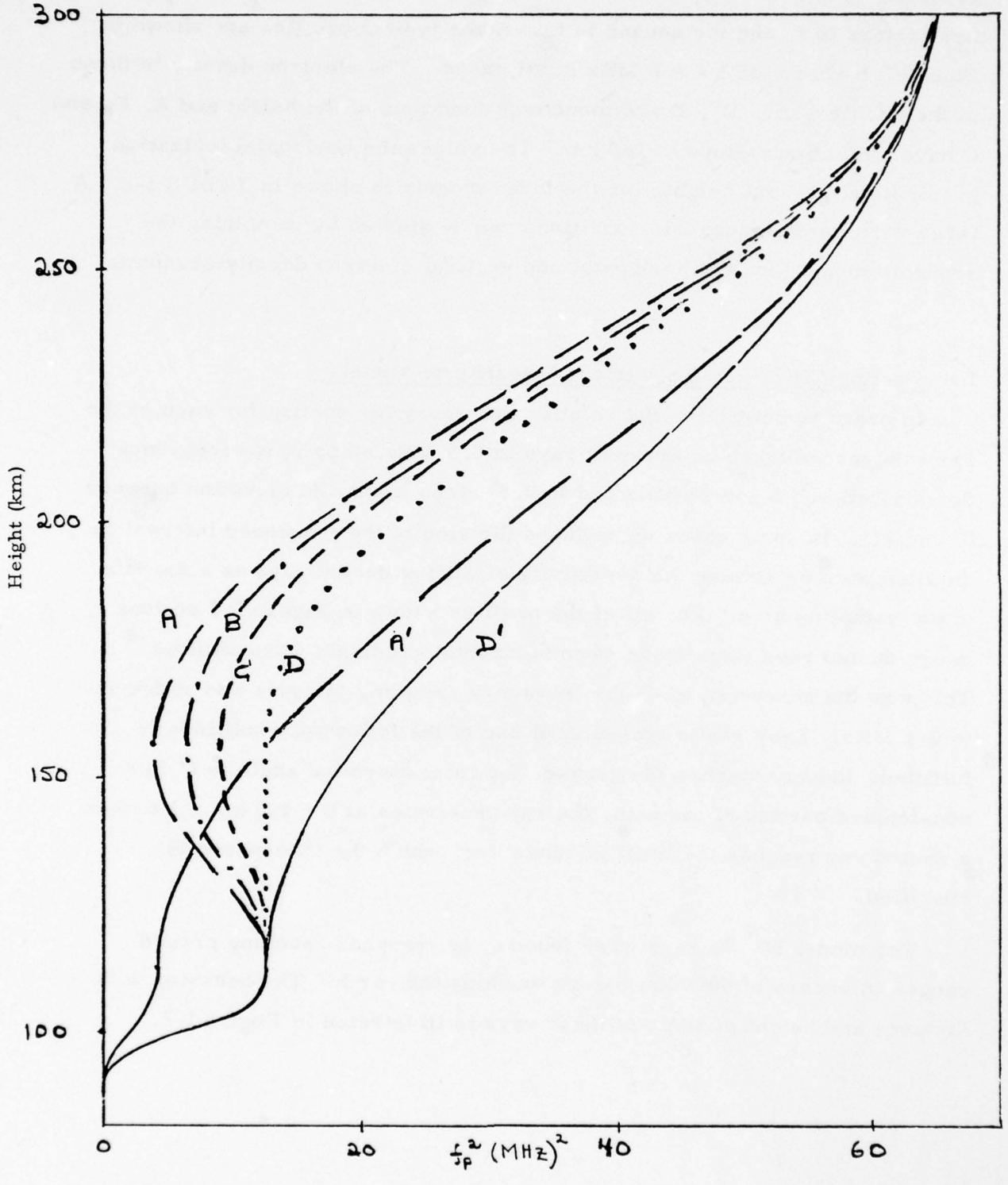

TABLE I-2

Horizontal Electron Density Gradients

Ionospheric Models	$\frac{\partial N_e}{\partial x}$ at x = 2000 km. (el./cc./m.)		
	Height		
	300 km	200 km	185 km
1 (A, B, C, and D)	-0.05	-0.0093	-0.0038
2 (A, B, C, and D)	-0.099	-0.019	-0.0076
3 (A, B, C, and D)	-0.140	-0.026	-0.011

TABLE I-3

Long Range Ionospheric Ducting

Number of Rays Ducted: Fixed Horizontal Electron Density Gradient (Ionosphere #2)

Electron Density Models without Ionization Valleys

f_E		$N_{f\alpha}$		$N_{f\alpha}$
2.0 MHz	A'	0	AA	2
2.5	B'	0	BB	3
3.0	C'	4	CC	11
3.5	D'	9	DD	16

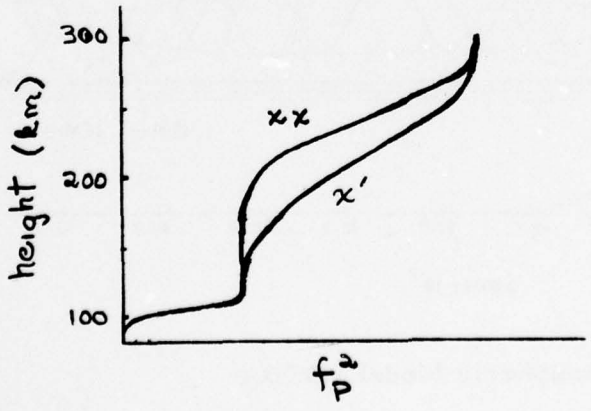

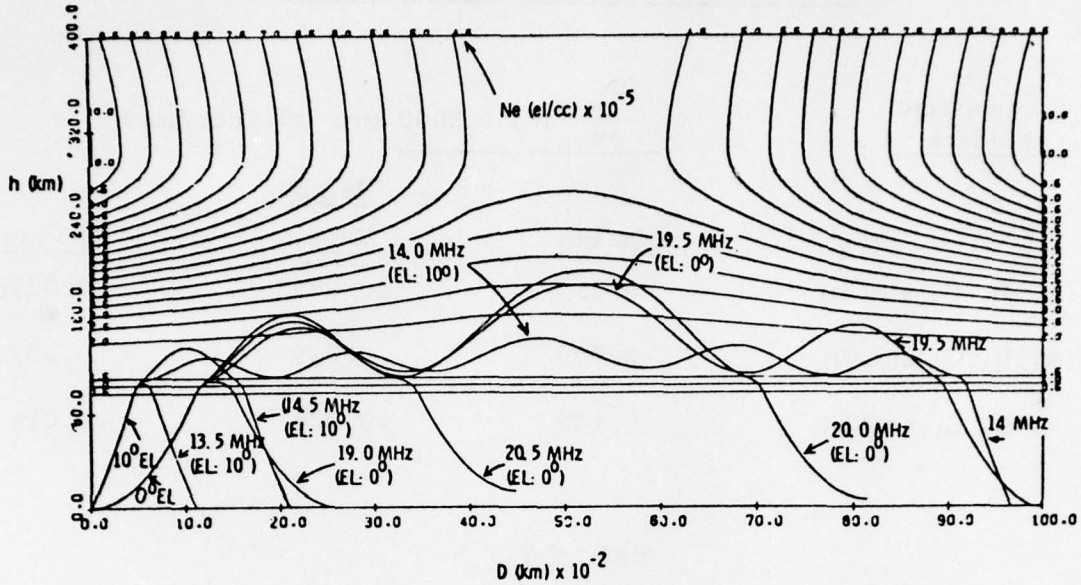

Ionospheric Model 3D'

Figure I-2

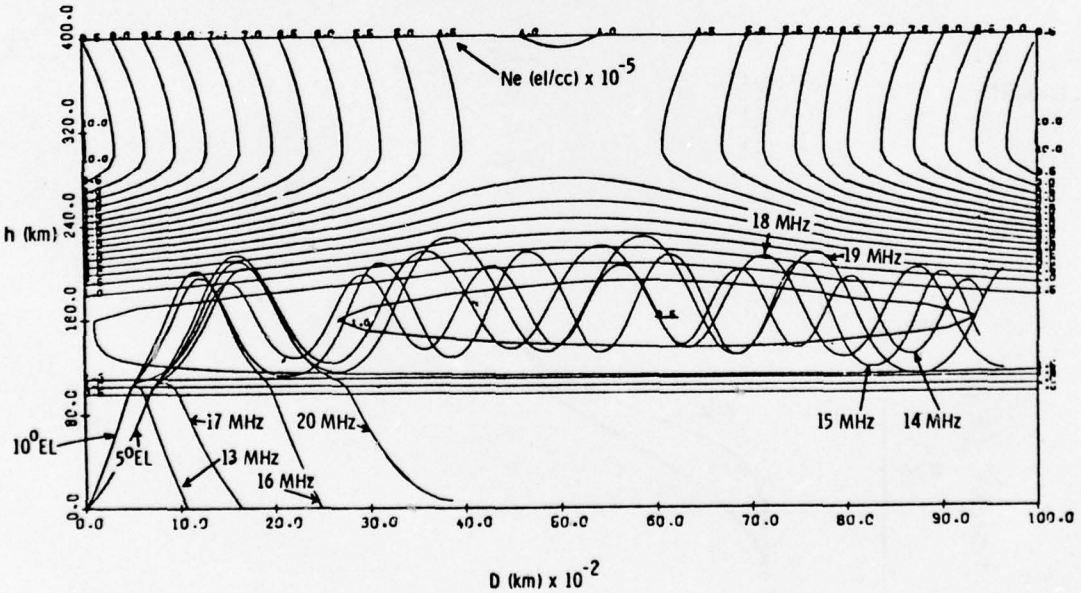

Ionospheric Model 2DCBA

Figure I-3

together with the iso-ionic contours of the modeled ionosphere. The contours are identified by number of el/cc x 10^{-5}. Four of the 22 ducted rays are shown for elevation angles of 0° and 10°. For an initial elevation angle of 10°, for example, rays computed for 13.5 and 14.5 MHz return to the ground at relatively short distances, while a ray for 14.0 MHz appears trapped in an ionospheric channel. For zero-elevation angle, two rays at 19.5 and 20.0 MHz reach large distances, while rays of 19 and 20.5 MHz reach a short and moderate distance respectively. The nature of the paths for the two elevation angles is quite different. The 10° ray has five oscillations and is constrained to a 40 km height interval while the 0° ray has three oscillations over a 90 km height interval. The ducted rays occur for frequencies just above those for penetration of the E layer maximum. A detailed plot of range as a function of frequency for initial elevation angles of 3° and 6° is shown in Figure I-4. For these curves the frequency was sampled in 0.25MHz steps. The gaps in the curves around 20 MHz are due to rays which are reflected once in the F2 layer but penetrate down range on the second oscillation when the F2 layer plasma frequency is reduced. A comparison of three ionospheres without an ionization valley but with the three different horizontal gradients is shown below.

Case	$\frac{\partial N}{\partial x}$ (x=2000 km)			Number of Trapped Rays
	h=230 km		h=185 km	
1D'	-0.0348	el/cc/m	-0.0167	4
2D'	-0.0695		-0.0335	9
3D'	-0.0978		-0.0471	22

The horizontal gradient is given at only one point but its value is indicative of the relative behavior over a large region. For the same vertical profile

Range as a function of frequency

Ionospheric Model 3D'

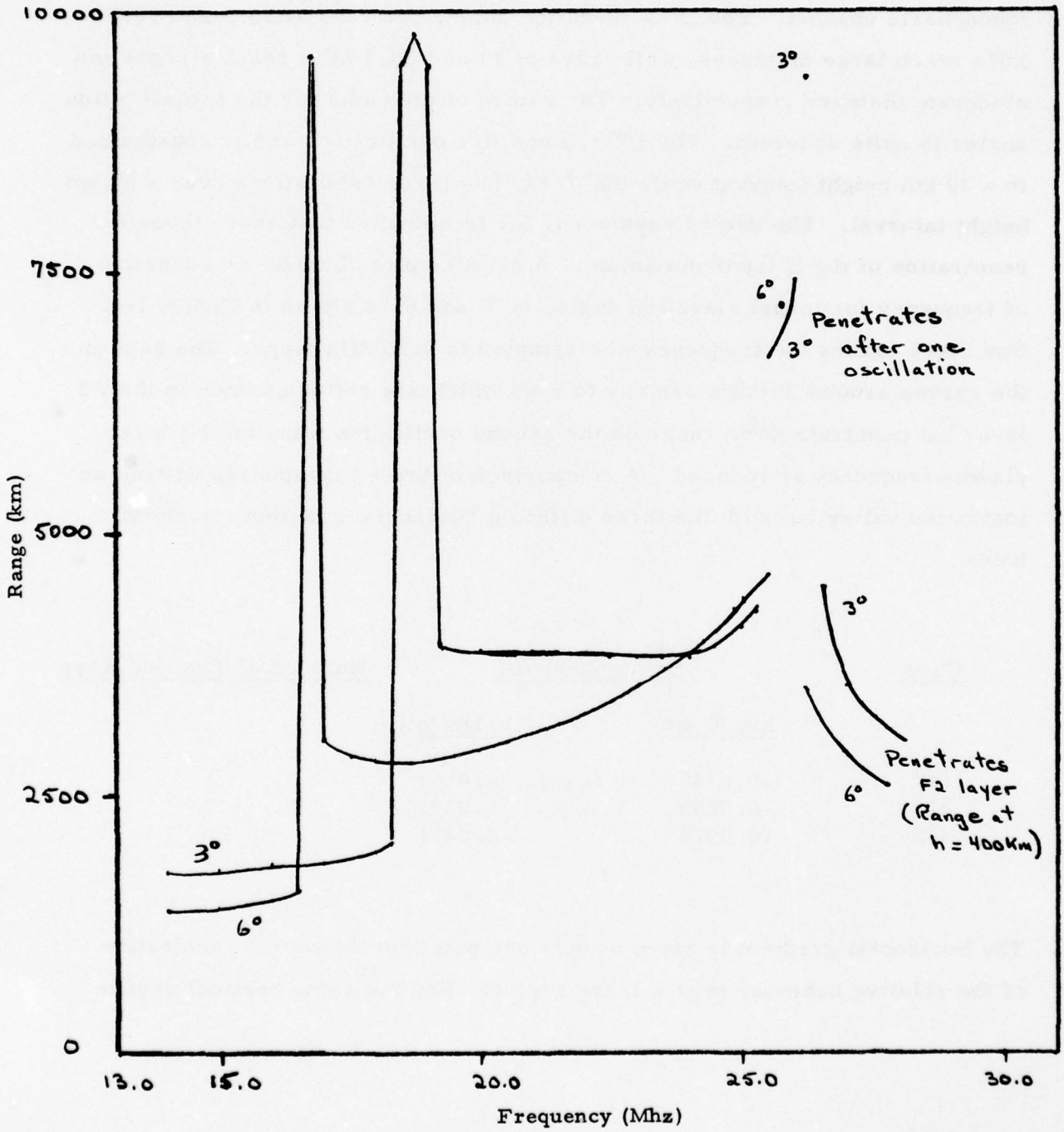

Figure I-4

the number of trapped rays increases faster than linearly as a function of the horizontal gradient. No rays were trapped for any of the three cases of the profile type A' which differs from D' by having a weaker vertical ionization gradient in the E region but a stronger gradient in the F2 region. The effectiveness of ducting of rays in a two-layer ionospheres without an ionization valley appears to be influenced both by the ionization density of the underlying layer and the horizontal gradients in the region immediately above the E layer. In TABLE I-3 the number of rays ducted ($N_{f\alpha}$ as a function of frequency and initial elevation angle) is presented for several profiles without an ionization valley and for the same horizontal gradient (Case 2). For both sets of profiles the efficiency of long range ducting increases with the value of foE. Comparing the models that have the same value of foE we observe that the efficiency is larger for the profiles that have both a region where $\frac{\partial N}{\partial h} = 0$ followed by a region where $\frac{\partial N}{\partial h}_{xx}(h) > \frac{\partial N}{\partial h}_{x'}(h)$ for $h > 160$ km, where xx and x' denote the two kinds of models. To determine which condition produces the increase in the ducting efficiency we traced rays through a model which incorporates the steeper vertical gradient without the extended region of zero vertical gradient. This model is 2D' where hmF2=250 km instead of 300 km.

Only three rays were long-range ducted for this model which is less than for both the two previous models. Although a negative horizontal gradient is required to facilitate ducting the nature of its coupling with a vertical ionization gradient in a particular ionospheric model is very critical. For certain ionization profiles negative horizontal gradients may represent a necessary but not sufficient condition for efficient ducting of rays.

For ionospheres with negative ionization gradients the occurance of valleys in the vertical profile appears to enhance the efficiency for ducting. In TABLE I-4 the number of rays ducted is presented for several ionospheres

as a function of both vertical and horizontal electron density gradients.

TABLE I-4

Long Range Ionospheric Ducting

Number of Rays Ducted
(Elevation Angle ≤ 15°)

	Horizontal Gradients		
	1	2	3
Vertical Gradients			
A'	0	0	0
D'	4	9	22
D	8	16	33
C	9	20	44
B	11	24	50
A	14	28	58
DCBA Combination	>62	>74	>110

For a given vertical profile model $N_{f\alpha}$ shows the same behavior for the different horizontal gradients; i.e. $N_{f\alpha}$ increases at least as fast as linearly with gradient. For a given horizontal ionization gradient the ducting efficiency increases slowly with the deepening of the ionization valley. The ionospheric model DCBA is one in which a negative horizontal gradient is introduced along the ionization valley. The vertical ionization distribution has no valley at the transmitter but one begins to develop downstream reaching a minimum at a range of 6000 km.

A ray pattern for model 2DCBA along with the iso-ionic contours is illustrated in Figure I-3. For two elevation angles of 5° and 10°, rays were computed for frequencies on either side of and including the ducting bands.

Examining the conditions encountered for EL = 10°, it is seen that both the 13 MHz- and 16 Mhz ray satisfy a one-hop reflection condition, returning to the ground at about D = 1050 and 2400 km respectively. Both the 14 MHz-ray and the 15 MHz-ray encounter favorable injection conditions when entering into the ionization valley and remain there, apparently tracking the expansion and subsequent contraction of the ionization valley with distance with an undulation-height to undulation-wavelength ratio of about 0.0275 for both the 14 MHz-ray (for example, Δh = 32.88 km and λ = 1191 km) and the 15 MHz-ray (for example, Δh = 42.66 km and λ = 1555 km), indicating the possibility that this ratio may be invariant over the ducted frequency band.

The ratio of $N_{f\alpha}(DCBA)/N_{f\alpha}(A)$ varies between 2. for case 3 and 4. for case 1 but is a significantly larger change in ducting efficiency relative to any of the profiles with fixed although deeper ionization valleys. This increase in efficiency holds even though the gradient in the valley causes a small positive horizontal ionization gradient in the first 2000 km of the path. An examination of the ray trajectories indicates this gradient may aid in trapping some rays that might otherwise penetrate the E layer and return to the ground after one downward reflection from the F layer. This suggests that from the study of an initially ducted ray no inferences can be drawn whether the ray will or will not continue to be ducted without knowledge of the ionosphere downstream.

The distribution $N_{f\alpha}$ for the discrete sampling of the set of ionospheric models of TABLE I-3 with the largest horizontal ionization gradient is shown on Figure I-5. Each successive ionosphere shown includes all the ducted rays of the previous ionosphere with a smaller ionization valley. Since the ionosphere is stratified below 110 km the boundary specifying the lower frequency limit of the ducting region can be calculated analytically using the secant law for oblique incidence

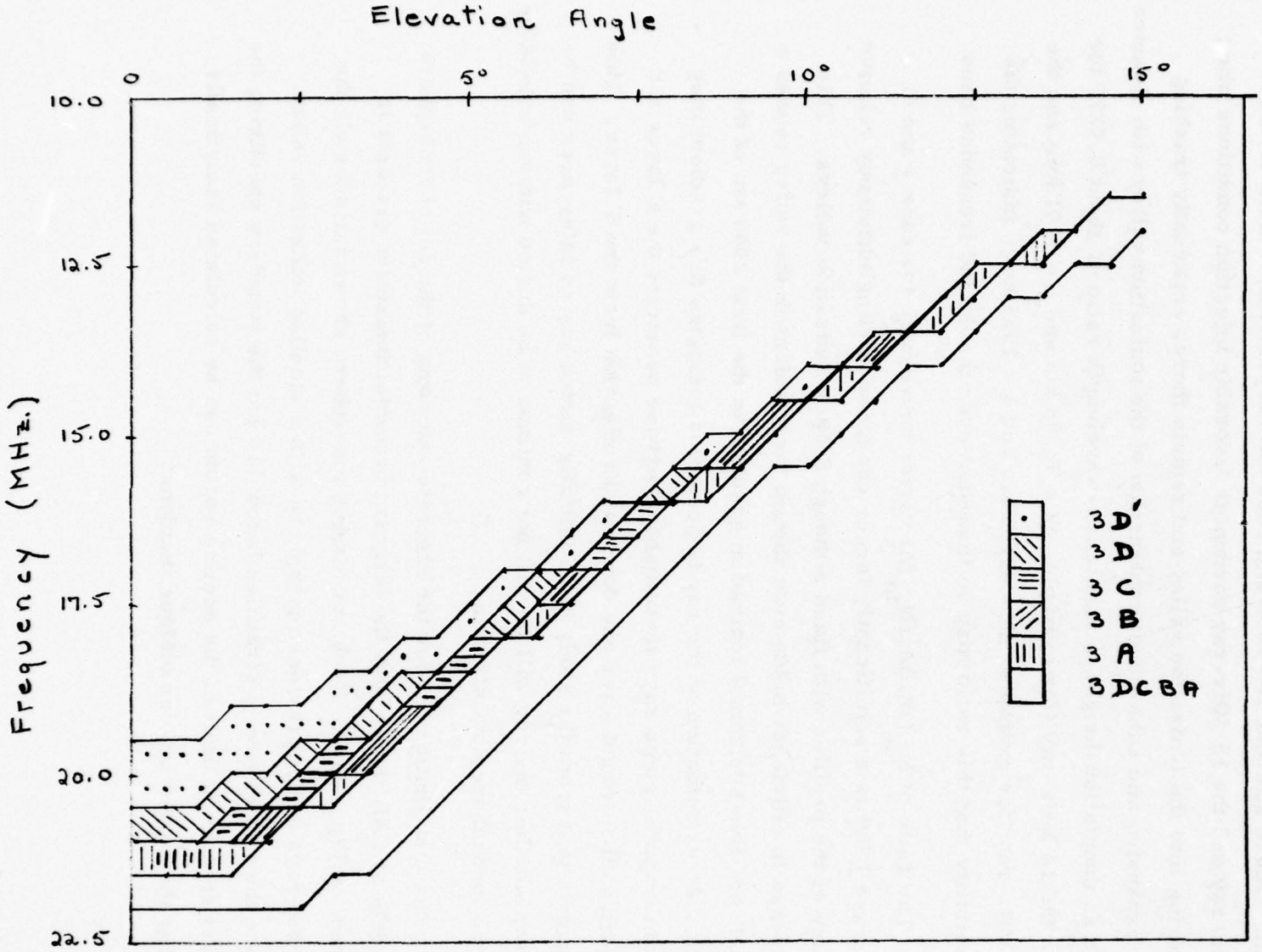

Horizontal Gradient Case 3

Figure I-5

$$\sin \alpha = \left(\frac{a}{a + h_E}\right) \sin \alpha_o \tag{I-5}$$

and

$$f = foE \left(\frac{a + h_E}{a}\right) \sec (90^\circ - \alpha) \tag{I-6}$$

where α_o is the elevation angle at the ground and foE = 3.5 MHz and h_E = 110 km for this model. For the first five ionospheric models we observe an increase in the number of rays trapped at any given elevation angle as the ionization valley deepens. This appears to be due to the reflection of the ray on the downward part of the path in the height region between 110 and 160 km where the ionization gradient is increasing in the direction of motion of the ray. We note that for these ionospheres there is no horizontal gradient in this region (below 160 km). For the last case, 3DCBA, the vertical gradient is weaker in this height region but there is now a horizontal ionization gradient which enlarges the net positive gradient along the rays which tends to reduce the local elevation angle and return them to the duct.

The number of rays ducted and various horizontal and vertical ionization gradients for models with the same foF2 gradients (Case 2) is shown in TABLE I-5. Some of these results are shown in TABLE I-6 for each of the possible permatations of f_E and f_1. We observe several examples (enclosed values in the Table) of three layer monotonic electron density profiles that support long range ducted modes. For the same f_1 and foF2 parameters increasing the underlying ionization by increasing the value of f_E results in more rays being ducted.

TABLE I-5

Long-Range Ionospheric Ducting

Fixed Horizontal Electron Density Gradient
(Ionosphere #2)

Ionosphere	$N_{f\alpha}$	$\frac{\partial N}{\partial x}$ (x=2000) el/cc/m.		$\frac{\partial N}{\partial h}$ (x=2000) el/cc/m.		
	$\alpha \leq 11^0$	h = 185	135	185	135	100km.
2BA	0	-0.0076	0	4.27	0.88	3.9
2CA	0	-0.0076	0	4.07	1.95	3.9
2DA	0	-0.0076	0	3.83	3.21	3.9
2A'	0	-0.0335	-0.0042	5.82	2.47	3.90
2B'	0	-0.0335	-0.0042	5.60	2.39	6.09
2DB	2	-0.0076	0	3.83	2.34	6.08
2CB	2	-0.0076	0	4.07	1.07	6.08
2AA	2	-0.0076	0	4.44	0	3.90
2BB	3	-0.0076	0	4.27	0	6.08
2DC	4	-0.0076	0	3.83	1.27	3.51
2C'	4	-0.0335	-0.0042	5.33	2.26	8.76
2AB	9	-0.0076	0	4.44	-0.88	6.09
2D'	9	-0.0335	-0.0042	5.02	2.13	11.93
2CC	11	-0.0076	0	4.07	0	3.51
2BC	14	-0.0076	0	4.27	-1.07	6.08
2AC	15	-0.0076	0	4.44	-1.95	8.78
2D(DD)	16	-0.0076	0	3.83	0	11.93
2C(CD)	20	-0.0076	0	4.07	-1.27	11.93
2B(BD)	24	-0.0076	0	4.27	-2.34	11.93
2A(AD)	28	-0.0076	0	4.44	-3.21	11.93

TABLE I-6

Long-Range Ionospheric Ducting
Number of Rays Ducted
Fixed Horizontal Electron Density Gradient
(Ionosphere #2)

f_1 \ f_E:	2.0	2.5	3.0	3.5 MHz.
2.0 MHz.	2	9	15	28
2.5	0	3	14	24
3.0	0	2	11	20
3.5	0	2	4	16

The ionospheres described thus far have been characterized by a negative horizontal ionization gradient produced by the value of foF2 decreasing along the direction of ray propagation. In Figure I-6 four ray paths are plotted along with the iso-ionic contours for model 2A'. For the 2° elevation angle two rays, separated by 0.5 MHz with similar ray paths are ducted. In Figure I-7 we show the iso-ionic contours of a model in which foF2 = 8 MHz over the entire 10000 km. Here the negative horizontal gradient is generated by the change of f_1 along the surface of the earth. The values of f_1 at 160 km and at spacings of 2000 km are 3.0, 2.5, 2.0, 2.0, 2.5 and 3.0 MHz and f_E is a constant 3.5 MHz. Four rays with the same parameters as in Figure I-6 are traced through this ionospheric model and are also shown in Figure I-7. The ray paths for the two ducted frequencies in both models are quite similar. The total number of ducted rays for this ionosphere is 40 which falls between the numbers for models 2A and 3A which are respectively 28 and 55. Although a negative horizontal ionization gradient appears to be a necessary condition for

Ionospheric Model 2A'

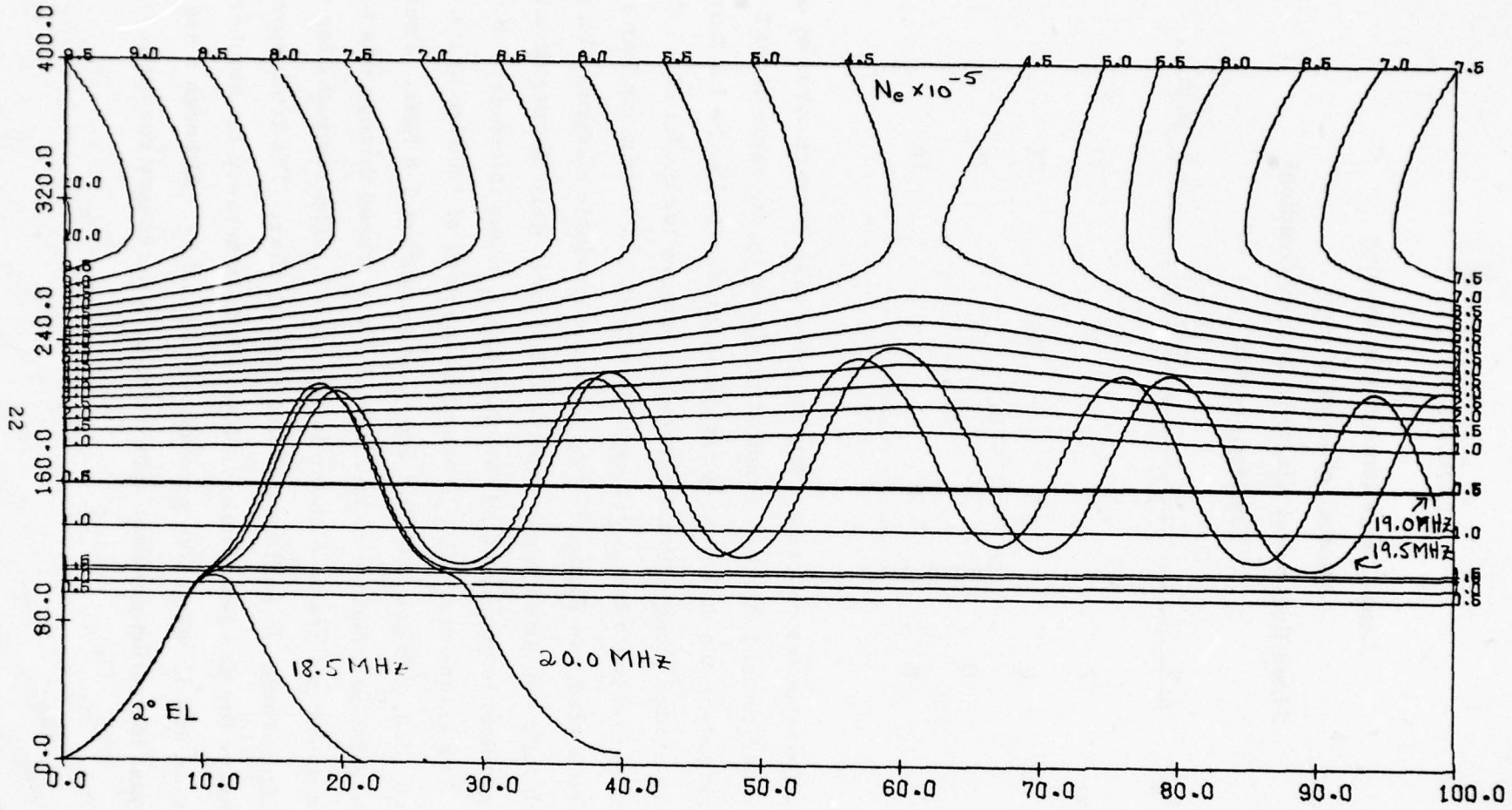

Range (km x 100)

Figure I-6

Ionospheric Model with foF2=constant

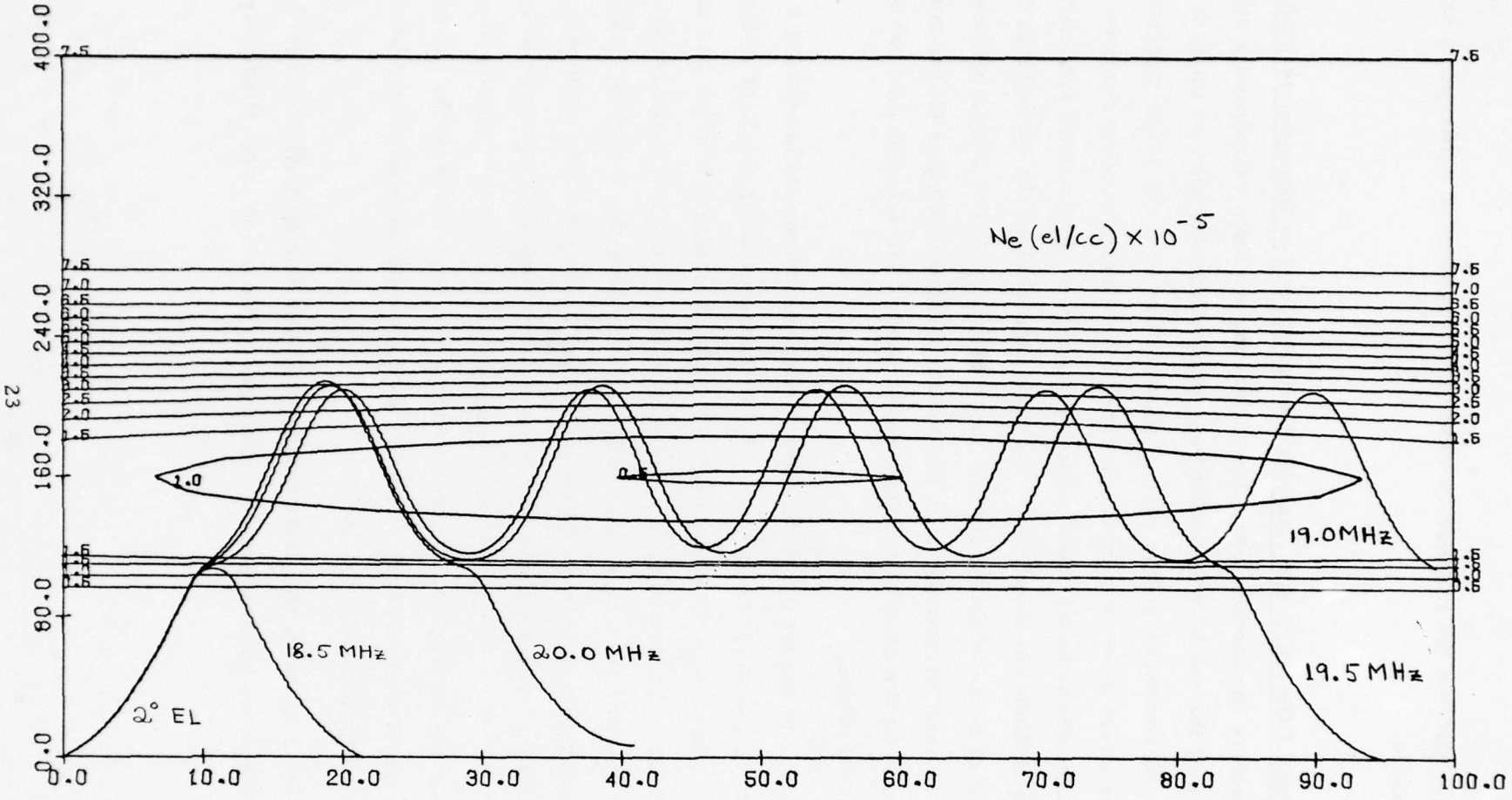

Range (km x 100)

Figure I-7

long-range ducting the manner in which this gradient is achieved is still quite flexible.

I.5 Ducting Efficiency and Analytic Perturbations to Ionospheric Models

In each of the models considered thus far we have calculated a relative efficiency of the model to support long range ducted modes by using a discrete sampling of communications circuit parameters in a ray trace program. All of these models have been characterized by a slowly varying electron density distribution whose horizontal gradients have been determined from profiles specified at 2000 km intervals. We have also studied the changes in the ducting efficiency of some of these models for various localized perturbations to the electron density distributions. The nature of these changes yields some information on the stability of long range modes for a particular set of ionospheric conditions.

In order to insert perturbations to the ionosphere we have used a three layer model and vary the values of f_1 for some profiles for part of the ray path. We generate a three layer profile which is similar to the two layer model of 3D'. Values of f_1 are determined from the two layer model at a height of 160 km at each of the profiles given along the ray path. Although the resulting ionosphere matches 3D' at each of the critical altitudes there are deviations between the two models at intermediate heights between 110 and 300 km. We now use two sine-squared profiles in this region where previously we only had one. This results in a zero value of the vertical electron density gradient at 160 km. Both models have non-zero horizontal ionization gradients above 110 km.

Figure I-8 shows the distribution of the 48 ducted rays for this three layer ionosphere (dotted area). For a given elevation angle these rays are

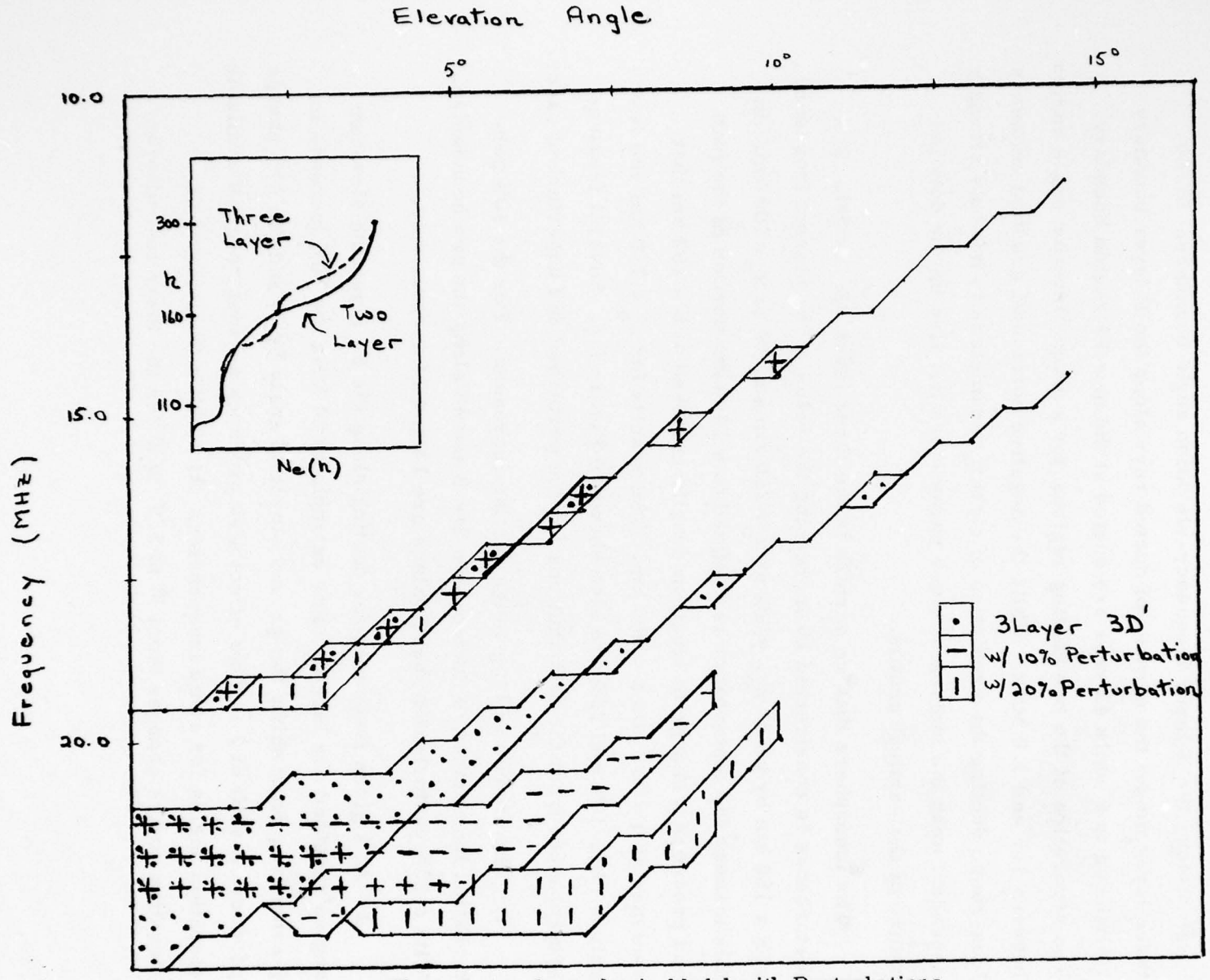

Three Layer Ionospheric Model with Perturbations

Figure I-8

located at frequencies just above those for penetration of the layers at 110 and 160 km. The 22 rays ducted for the two layer 3D' model were all located along the E layer frequency-elevation angle boundary. In the three layer model the number of ducted rays along the E layer boundary is reduced to 5 while 43 rays are ducted at the new F1 region boundary. The separation of the two ducting regions for a given elevation angle varies between 1.5 and 3.0 MHz. While the negative horizontal gradient enhances long-range ducting the prediction of circuit parameters is not only strongly dependent upon the individual layer parameters but also on the detailed nature of the vertical profile.

The ionosphere that we perturb is the three layer 3D' model. The disturbance is constructed by increasing the value of the plasma frequency at h = 160 km by y% at x_o, y/2% at $x_o \pm 250$ km and 0% at $x_o \pm 500$ km. In this manner the disturbance is confined to a 1000 km portion of the path and produces a change in electron density centered at h = 160 km that vanishes at h = 110 and h = 300 km. The results for x_o = 750 km and two values of y, 10% and 20% are also shown in Figure I-8. Several features are apparent from the distributions for the perturbed and unperturbed cases.

1. The amount of long range ducting increases. For the 10% perturbation the number of ducted rays are 9 and 48 along the two boundaries. With a 20% perturbation these values are 14 and 44 respectively.

2. At a given frequency for ducting along the F1 layer the elevation angles required are larger. For example at 20 MHz the 10% increase in plasma frequency shifts the ground elevation angle by 3° and the 20% change produces a shift of 5°. This effect also produces a wider range of available elevation angles for some frequencies. At 22 MHz the interval of elevation angles changes from 3° to 5.5° to 8° for the three ionospheres.

3. The maximum frequency for ducting is reduced by 0.5 MHz.

This analysis was also carried out for the same values of y but with x_o = 500 km (250 km closer to the transmitter). The parameters for the ducted rays along the E layer were shifted but the number of them did not increase. This is probably due to the discrete sampling of a very narrow region of parameters along this boundary. The number of ducted rays along the F1 boundary increased to 46 for both perturbations. These showed the same tendency of narrowing the available frequency interval and widening the angular interval as the previous case of x_o = 750 km.

We conclude that while relatively small changes from a given plasma frequency distribution do not destroy the possibility of supporting long-range modes they can substantially change the required circuit parameters.

Our sampling interval revealed no ducted modes in either a two or three layer stratified ionosphere. Ducting was observed when negative horizontal gradients were applied over a large portion of the total ionospheric cross section. It is of interest to know whether these gradients need exist over such a large portion of the potential path or are only required near the transmitter in order to obtain injection into a ducted mode. We have used the method described above to introduce gradients over a restricted region of a stratified ionosphere. We have considered two basic models with fixed parameters, f_E = 3.5, f_1 = 5.0, f_2 = 8.0 MHz and f_E = 2.5, f_1 = 5.0, f_2 = 8.0 MHz. Both of these models were subjected to perturbations with y = 20% and x_o = 500 km. No ducted rays were observed for the model with f_E = 2.5 MHz. Three rays along the E region frequency-elevation angle boundary were ducted for the model with f_E = 3.5 MHz. The elevation angles for these rays were between 4.5° and 7.0° which corresponds to the rays intersecting the bottom of the ionosphere (h = 90 km) at ground ranges of

640-540 km. The presence of a negative horizontal gradient in this region is sufficient to inject into a duct even though the ionosphere remains stratified for the remaining 9000 km of the path.

I.6 Ducting Efficiency and Random Perturbations to Ionospheric Models

The results of the previous section are helpful in accessing the changes in ducting efficient due to differences in actual ionospheric parameters from those predicted by a median model. These may represent measureable but unknown differences over a large region of space, e.g. 200-2000 km. It is also of interest to make estimates about the stability of various ducted modes to more random and highly localized fluctuations of ionospheric conditions. We have developed a scheme which allows one to combine the modeled effects of random scatterings with a deterministic ray trajectory. Our two-dimensional ray tracing program calculates the ray coordinates at a discrete series of points along the surface of the earth. We solve for $h_i(x_i)$ and $\alpha_i(x_i)$ for equal spacing in x_i. In our scheme the ray is repeatedly subjected to a series of perturbation using a scale size that is related to the probability of the ray being disturbed. When the ray, advancing in 10 km steps reaches a distance corresponding to the average local scale size the ray direction is perturbed.

The magnitude and sign of the angular perturbation are derived from a random Gaussian distribution. Both the scale size S_i and the angular perturbation $\Delta\alpha_i$ are weakly dependent upon the electron density through the following models:

$$S_i = S_o \left\{ 1 - a \frac{(N - N_o)}{N_o} \right\} \quad \text{and}$$

$$\Delta\alpha_i = g\,\alpha_o \left\{ 1 - b \frac{(N - N_o)}{N_o} \right\}$$

where N is the electron density per cubic centimeter, $N_o = 10^5$ el/cc and both a and b have been chosen to be 0.1 in this study. S_o and α_o are chosen to describe the nature of the fluctuations present in a particular ionosphere. We have used various combinations of S_o, α_o with 100 km $\leq S_o \leq$ 400 km and 0.005 radians $\leq \alpha_o \leq$ 0.02 radians. In the expression for the angular perturbation g is a Gaussian random number with average zero, $\sigma = 1.0$ and g is limited to values in the interval to $\pm 6\sigma$. Since the value of S_i changes with each step in the integration we use an averaged value of the scale length over several steps in order to determine when to apply the angular perturbation. When this average value is exceeded the ray trace continues with the value of α_i replaced by $\alpha_i + \Delta\alpha_i$. The average angular change in a 10 km step in the deterministic ray trace calculation is approximately 0.2°. Depending upon the perturbation parameters chosen the instantenous changes due to the scattering are less than 4°.

We have used the model 3D[1] to determine the effect of this repeated scattering process. This was first carried out for an unducted ray with f = 21 MHz and $\alpha = 10°$ launched from the ground. The unperturbed ray penetrates the E layer maximum height, is reflected in the F2 layer and has a ground range of 2600 km. The perturbation scheme was applied 100 times using the same initial conditions for a given ray.

The analysis was performed for three sets of values of S_o and α_o. The frequency distribution for the calculated ranges for each of these cases is shown in Figure I-9. The second and third distributions each have one parameter in common with the first case which has S_o = 200 km and α_o = 0.01 radians so that we can isolate the effect of changing each parameter on the resultant distribution. For the second distribution the scale length is unchanged but we one-half the value of the average scattering angle while for the third case the scattering angle remains unchanged but we double the scale length (decrease the number of applied perturbations by a factor of two). We

Random Perturbation of Ray Direction

Number of rays as a function of Range.

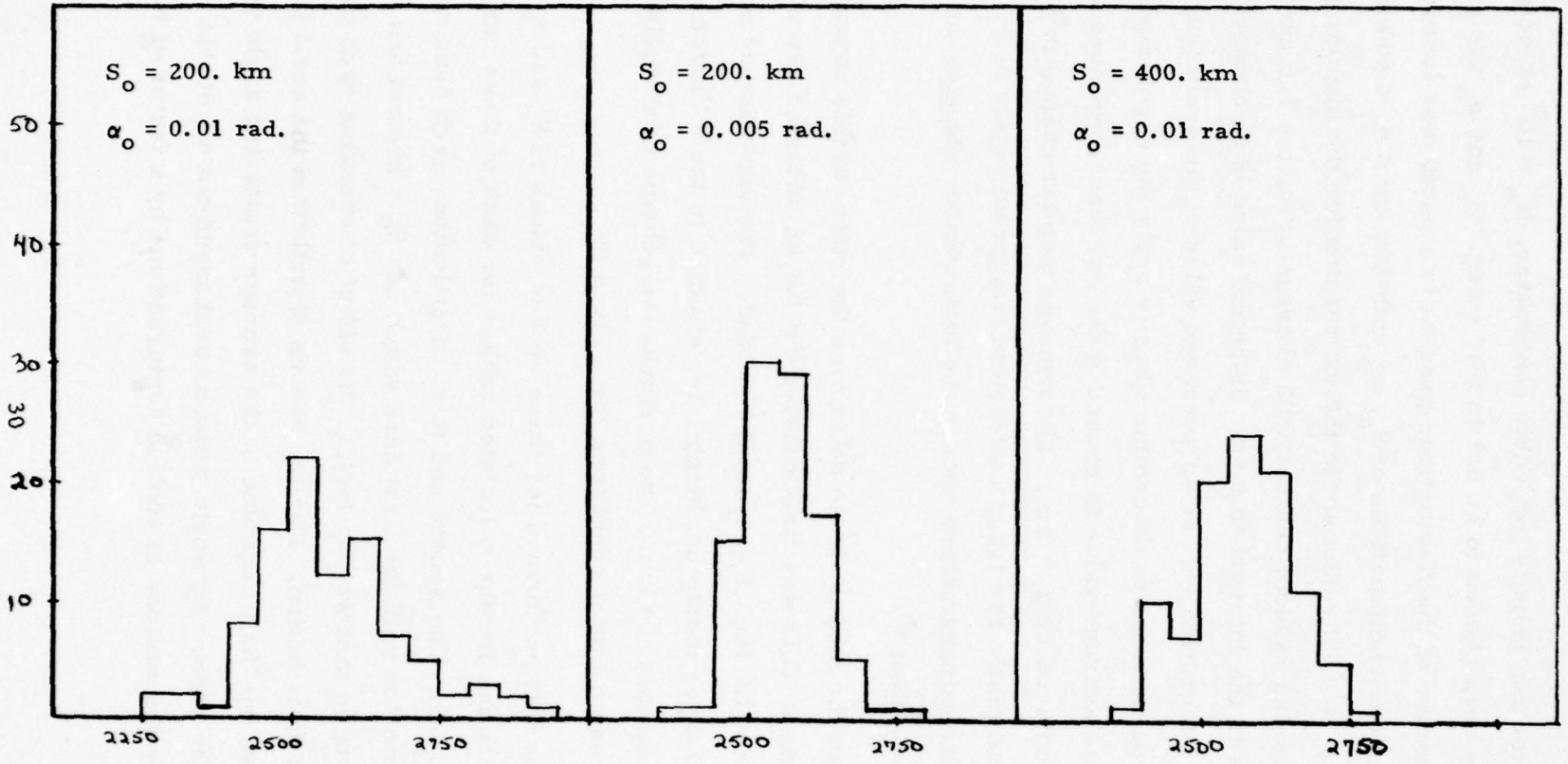

frequency = 21.0 MHz Elevation angle = 10.0°

Figure I-9

observe that for this algorithm the magnitude of each scattering has a considerably stronger effect on the range distribution than the number of such perturbations.

We have sampled the 3D' for an elevation angle of 3° every 0.1 MHz in the vicinity of the penetration of the E layer maximum. We found that for f = 18.3 MHz the ground range was 2000 km and the long-range ducted region extends from 18.4 - 19.0 MHz. We have chosen to study the effect of repeated small angle scatterings on three rays; 18.3 MHz (an unducted ray), 18.5 MHz (a ducted ray very close to the edge of the frequency band for ducting), and 18.7 MHz (a ducted ray in the center of the ducted band). Ten perturbed rays for f = 18.5 MHz, experiencing approximately ten angular perturbations per 2000 km, are illustrated in Figure I-10. For the chosen perturbation parameters we observe that some rays remain in the elevated duct while others are deflected to the ground. As a measure of the ducting stability we use the percentage of the total number of rays whose range remains greater than 5000 km. The results for the three ray frequencies chosen and various combinations of perturbation parameters are given in TABLE I-7.

Keeping in mind that the values in the table are effected by the total number of rays sampled for each set of parameters some consistent observations can be made. For the frequency that is not ducted in the unperturbed ionosphere the introduction of the scattering mechanism produces some long-range rays. The probability of entering the long-range duct is seen to increase with the frequency and size of the scatterings. Correspondingly the initial conditions which normally yield long-range rays are observed to suffer some losses due to the repeated scatterings. For both rays the probability of leaving the duct also increases with the frequency and size of the scatterings. The stability for ducting does not appear to be strongly correlated with the position of the frequency in the

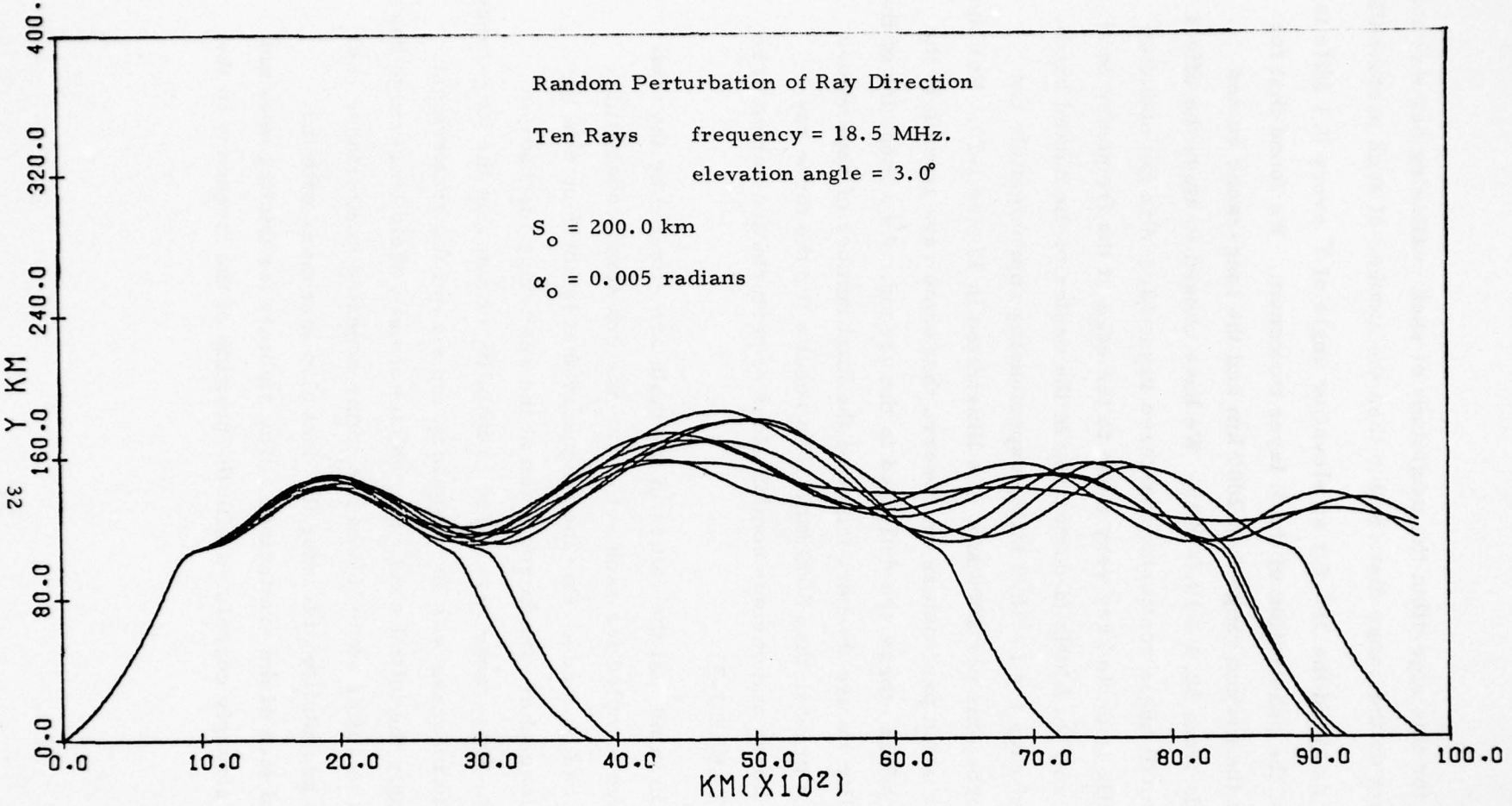

Range KM(x 10^2)

Figure I-10

TABLE I-7

PERCENTAGE OF RAYS THAT ARE DUCTED

Elevation Angle = 3°

Perturbation Parameters		Frequency 18.3MHz		18.5MHz		18.7MHz	
		R<5000	R>5000	R<5000	R>5000	R<5000	R>5000
S_o(km)	α_o(radians)						
200.	0.005	98	2	14	86	24	76
400.	0.01			19	81	33	67
200.	0.01	90	10	43	57	31	69
200.	0.02	92	8	68	32	52	48
100.	0.01	85	15	71	29	70	30

ducting band. For the last three sets of scattering parameters the stability of ducting is larger for the frequency which is in the middle of the ducting band than that for the frequency that is at the edge of the band while for first two sets of parameters the results are reversed.

I.7 Elevated Sources and Injection and Maintenance of Ray Ducts

We have had several indications that the conditions necessary for the support of long-range ducted modes from the ground may be separated into two parts; those required for injection into an elevated ionospheric duct and those required to maintain the ray in a duct once it has been injected. A small perturbation to a stratified ionosphere in a localized region was sufficient to provide the means for injection when the underlying ionization was above some value. Once injected, this stratified monotonically increasing profile was sufficient to maintain the duct for 9000 km. For a series of models all with the same horizontal gradient, the introduction and deepening of a valley in the electron density profile increased the efficiency of the ducting.

In order to further examine these two conditions we have traced rays through ionospheric models with elevated sources. Figure I-11 shows the distribution $N_{f\alpha}$ for long-range rays for model 3A with the source at 160 km. The search is at 4° intervals in local elevation angle and every 2 MHz in frequency. Figure I-12 is a plot of ray paths for $\alpha = 0°$ and f between 12 and 34 MHz. We observe many more ducted modes for a source placed at the ionization minimum than for one at the ground. For one of these modes to be reached from the ground the underlying ionization and the horizontal gradients have to be such that if the ray reaches 160 km it will have local elevation angle which falls within the boundary of the curve shown in Figure I-11.

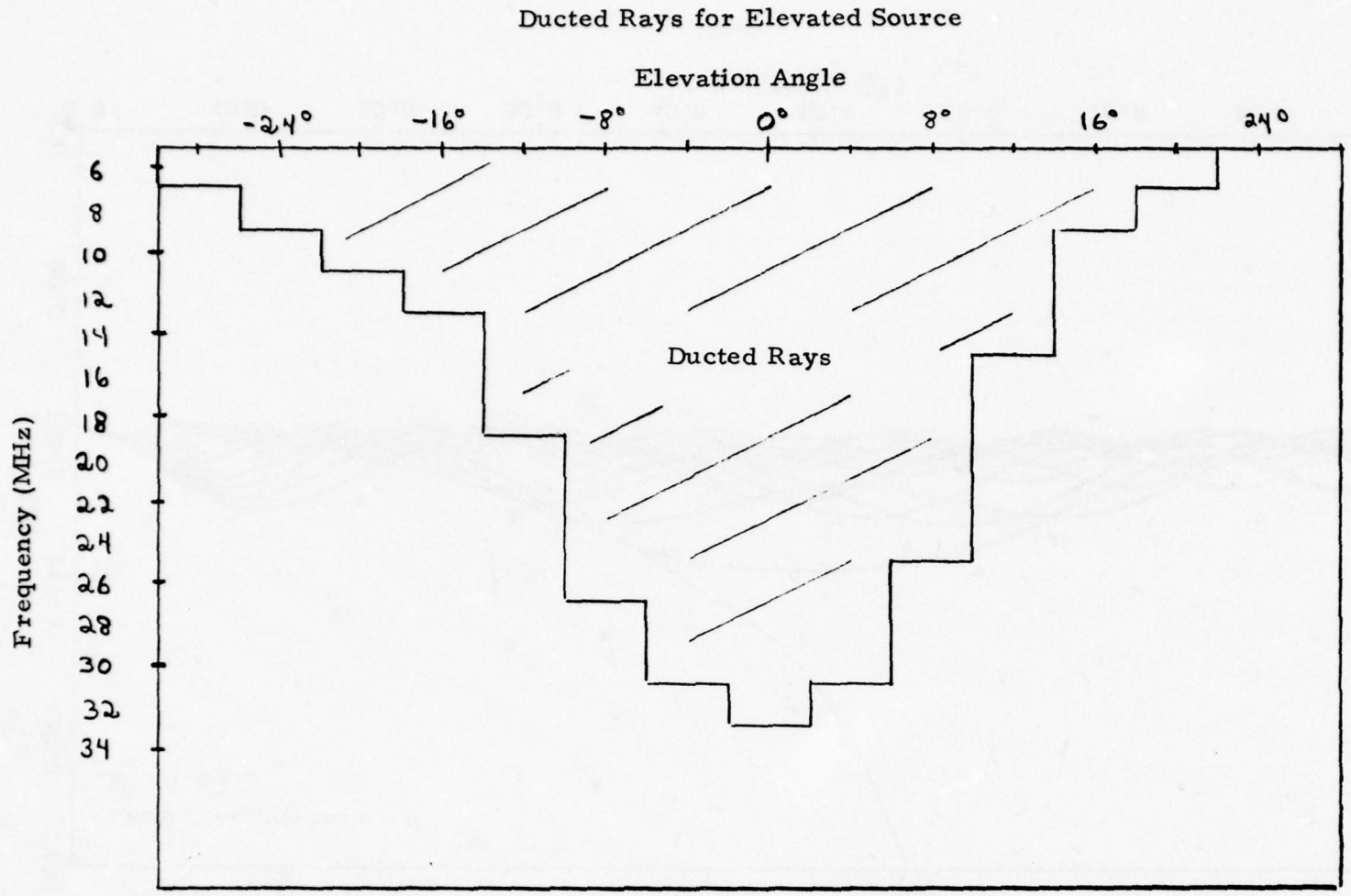
Ducted Rays for Elevated Source
Elevation Angle
-24°
-16°
-8°
0°
8°
16°
24°
Frequency (MHz)
6
8
10
12
14
16
18
20
22
24
26
28
30
32
34
Ducted Rays

Figure I-11

Rays for Elevated Source: Ionospheric Model 3A'

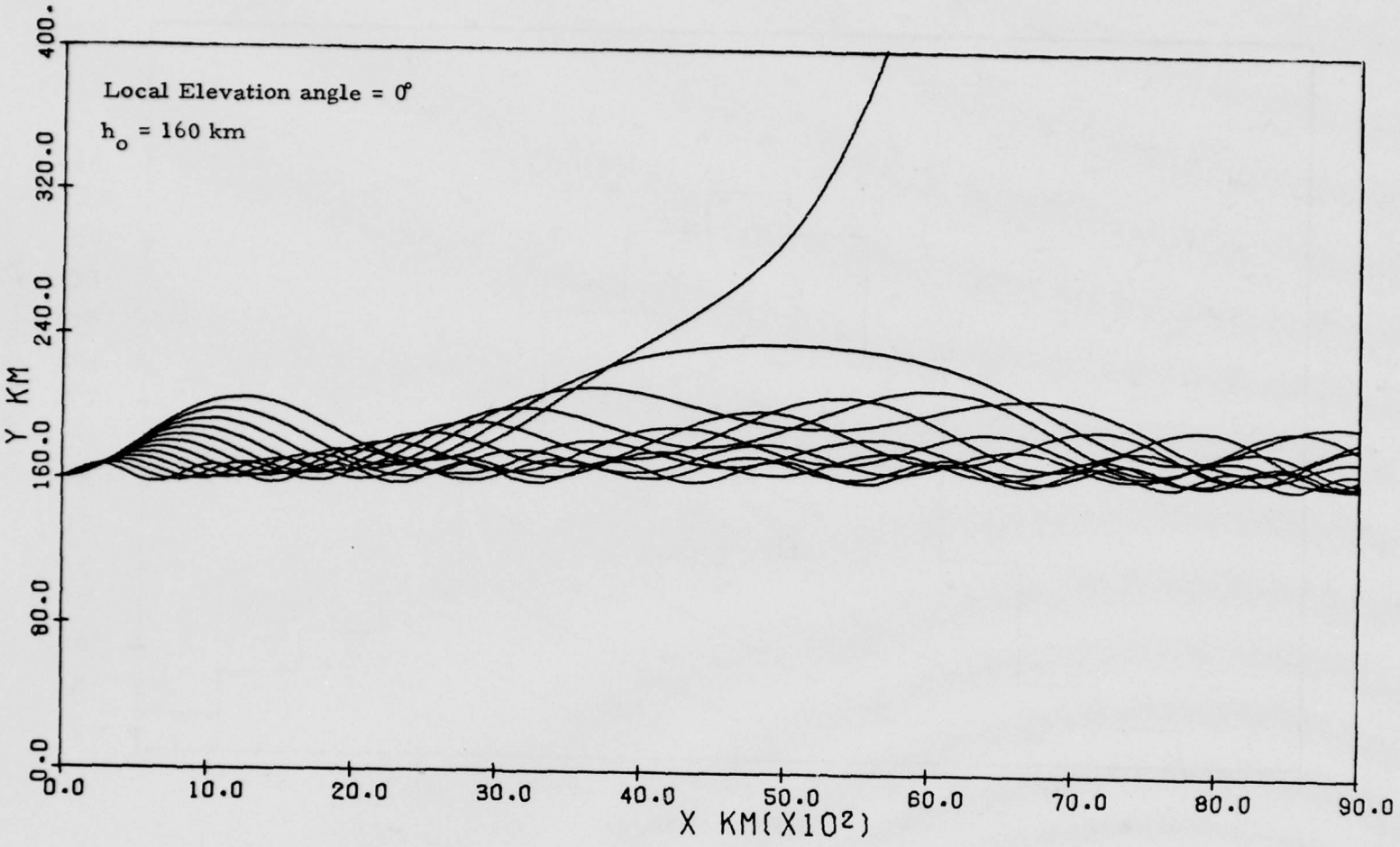

Range

Figure I-12

The changes in the $N_{f\alpha}$ distribution for an elevated source brought about by a horizontal ionization gradient is shown in Figure I-13 where the solid curve is the boundary for the model 3A and the dashed curve is for a stratified model with f_E = 3.5 MHz, f_1 = 2.0 MHz and f_2 = 8.0 MHz. This latter model does not support any ducted modes for a ground based transmitter. Only positive angles are traced and the region of interest is shown finer detail with a 0.5 MHz and 0.5° sampling interval. At small elevation angles the effect of the horizontal gradient is to reduce the maximum frequency that will support a ducted modes. At elevation angles above 10° the horizontal gradient tends to increase the maximum possible ducted frequency. Also shown in Figure I-13 are the curves representing the transformation between ground elevation angles and frequencies to elevation angles at h = 160 km and the same frequency obtained by tracing rays up to a height of 160 km. This height is reached at various points downstream from the transmitter. They can not be made to correspond with the boundary curves for the elevated source since they all originate at the origin of the coordinate system. If an exact matching of elevation angle and the corresponding ground range could be made the overlap of the two curves would denote all the long-range ducted modes that are possible. The cross hatched region shows which rays are in fact ducted for the 3A ionospheric model. The horizontal gradient enhances the overlap area between the two regions. While this method shows the nature of the required gradients for injection it is computionally impractical to use for different ionospheric models. The case considered here used a model with no horizontal gradients below h = 160 km to calculate the required transformation of elevation angles.

Ducted Rays for Elevated Source

Local Elevation Angle at the origin at h = 160 km

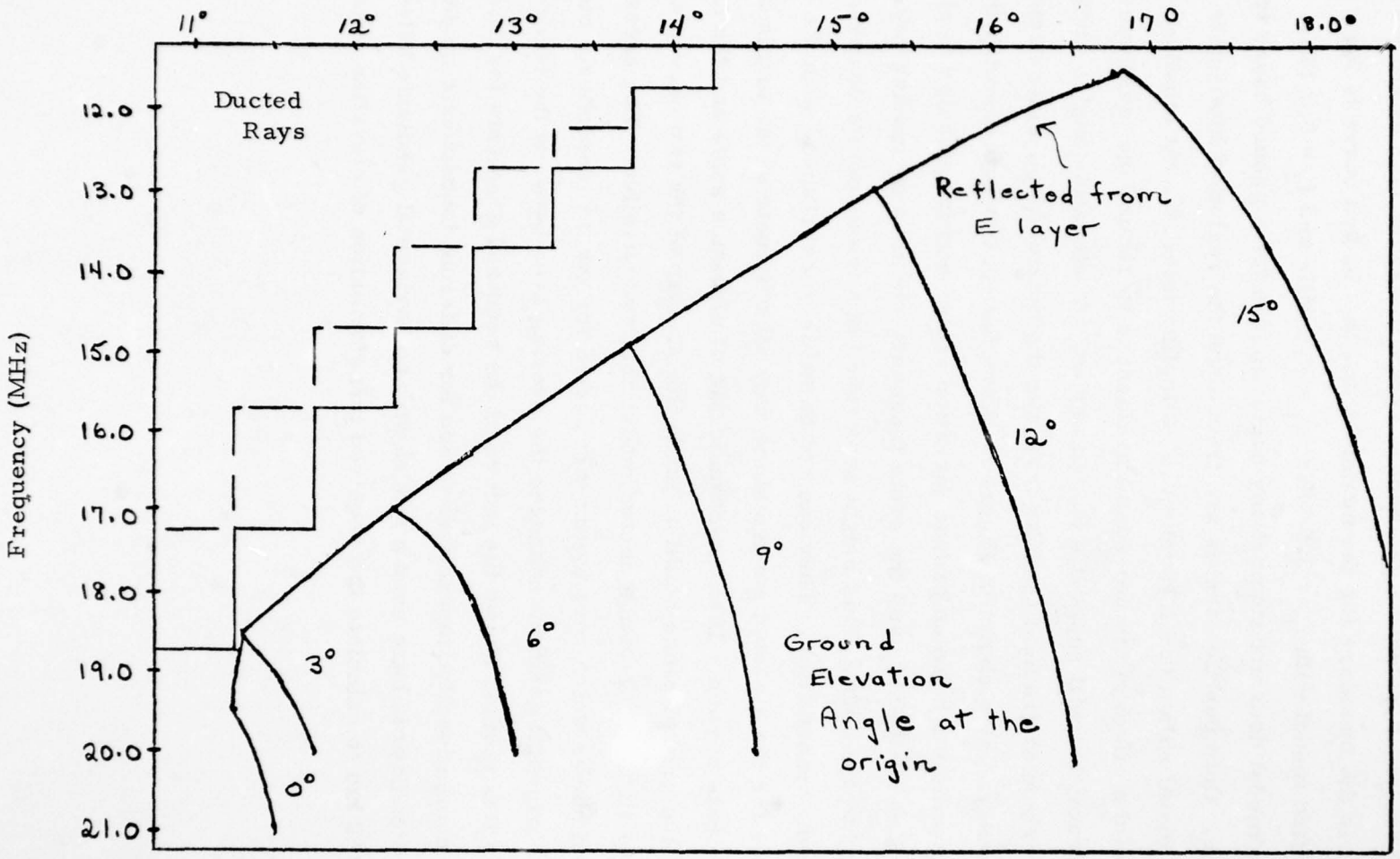

Figure I-13

II. THREE DIMENSIONAL ELECTRON DENSITY MODELS

II.1 Introduction in the Polar Region

In the previous section we have used simple electron density models in the study of a particular HF communication problem. In order to study this problem further and for other ionospheric applications we have continued our work in the development of three dimensional electron density models in the polar region. In reports [4] [5] [6] we have described the two elements of such models. They consist of empirical models for individual ionospheric layer parameters and a method for generating a continuous vertical electron density distribution from these parameters. These vertical profiles have involved the use of simple analytic functions which maintain continuity of both the electron density and its height derivative. Attempts have been made to use these one dimensional distributions to construct physically accurate three dimensional ionospheric models. The extension in space is made using numerical interpolation techniques between the predicted vertical profiles at specified points on a

Examination of the resulting isoionic contours in two dimensions of this model (POLAR 76) revealed several problems and deficiencies with the methods used in constructing the model. We have constructed a new vertical electron density model (POLAR 77) in an attempt to improve the model. No changes were made to the interpolation procedures used to extend the profiles in space. A second order interpolation method is used and appears to be adequate to describe all possible horizontal electron density gradients.

In the development of POLAR 77 we have also found it necessary to modify some of the models for the individual ionospheric parameters so

that the electron density distributions presented here using the POLAR 76 model are not the same as would be constructed from the model of earlier report. We have also modified the daytime profile of this model such that it always is made up of cubic equations between the E and F1 layers and the F1 and F2 layers independent of the relative values of the individual layer parameters. This removes some unphysical gradients that were predicted when the zenith angle is in the region $75^\circ \leq \chi \leq 90^\circ$. Both models use the same parameters based upon median ionospheric conditions when the following are specified: latitude, longitude, universal time, sunspot number and K_p index.

II. 2 Development of Electron Density Model

The two electron density models are identical in the height region above $h_m F2$ and in the daytime for altitudes below $h_m E$. The models differ in the region between $h_m E$ and $h_m F2$. The problems that arose with POLAR 76 in this region include the following:

a) The disappearance of individual layers as a function of space and time and the resulting discontinuity due to the use of different analytic functions depending upon the number of layers present. (e.g., the solar E and F1 layers).

b) The difficulty in predicting the extrema position and magnitude of the electron density in the region between 100 and 200 km when only the auroral E and F2 layers are present at widely separated heights.

c) Changes in the shape of the vertical profile when only the auroral E and F2 layers are present and the sign of the difference between the magnitude of foF2 and foE changes at locations which are close to each other in space and time.

In order to eliminate some of these problems we have replaced the various analytic functions used in the vertical profile model with a single set of functions containing all the possible ionospheric parameters. The coefficients of terms representing individual layers were constructed in a manner which attempts to maintain continuity in the other spatial variables. This required the extension of the individual models of various parameters into regions where they did not exist. An example of this is the prediction of an electron density at a height corresponding to hmF1 for χ (zenith angle) $> 90^{\circ}$.

In order to describe the electron density in the region between hmE and hmF2 we make use of median predictions for the following ionospheric parameters:

$$\text{foF2, hmF2, ymF2, foF1, hmF1, } \text{foE}_{\text{solar}},$$

$$\text{hmE}_{\text{solar}}, \ \text{foE}_{\text{auroral}}, \text{ and } \text{hmE}_{\text{auroral}} \quad .$$

We first assumed that the electron density could be described by the following fifth order polynomial:

$$(1) \quad N_m(x) = ax^5 + bx^4 + cx^3 + dx^2 + ex + f \quad \text{where}$$

$$x = \frac{h - \text{hmE}}{\text{hmF2} - \text{hmE}} \quad .$$

In order to determine the six coefficients, we used the above set of ionospheric parameters to specify the electron density and its height derivative at three points for $0 \leq x \leq 1$. Using this model, all the coefficients were constrained to be continuous functions of latitude, longitude and universal

time. This ensured that no gradients existed in the three-dimensional model that were not consistent with those that existed for the median models of the ionospheric parameters. Since the diurnal variation in some of the parameters (e.g. foE) varied by a factor of 10^3, we also used the expression $\log N_m(x)$ in the polynomial. This form produced more realistic height gradients in the profiles.

In general, the polynomial (1) has four extrema and at least one real root (i.e. $N_m(x) = 0$ for some value of x). Three of the extrema are specified by the parameters. In order for the resultant profile to be physically valid, the fourth extrema and any real roots cannot occur in the interval $0 \leq x \leq 1$. This proved to be a problem as the polynomial obtained from the three data often predicted a spurous maximum in the height region of interest.

In order to remove this difficulty, we used a fourth order polynomial of the form:

$$\log N_m(x) = ax^4 + bx^3 + cx^2 + dx + e \tag{2}$$

The ionospheric parameters were used to form the following constraints:

$$N_m(0) = N_mE \tag{3}$$

$$\frac{d}{dx} \log N_m(0) = 0 \tag{4}$$

$$N_m(1) = N_mF2 \tag{5}$$

$$\frac{d}{dx} \log N_m(1) = 0 \tag{6}$$

$$N_m(x_1) = N_1 \quad \text{where } x_1 = \frac{h_1 - hmE}{hmF2 - hmE} \tag{7}$$

In order to reduce the computational complexity we introduce the cubic equation which satisfies conditions (3) - (6)

$$P(x) = -2 (\log N_m F2 - \log N_m E)\, x^3 + 3 (\log N_m F2 - \log N_m E)\, x^2 + \log N_m E$$

The resulting fourth order polynomial is

$$\log N_m(x) = P(x) + \left\{ \frac{\left[\log N_m(x_1) - P(x_1)\right]}{x_1^2 (x_1 - 1)^2} \right\} \left(x^2 (x - 1)^2 \right)$$

II.3 Layer Parameters

For solar daytime conditions all the parameters that are necessary to define the polynomial are available from the individual models. We have constructed models for nighttime conditions and modified the definition of the parameters given in (3) - (7) so that they are continuous in space and time.

E Layer

The solar E layer parameters foE_s and hmE_s are described in reference 4. We have modified the definition of hmE_s

$$hmE_s = 100. + 20. \log_e(\sec \chi) \qquad \chi < 87.1^\circ$$

$$hmE_s = 100. + 10. \log_e(\sec 87.1^\circ) = 160. \text{ km} \qquad \chi \geq 87.1^\circ$$

For $\chi > 90°$

$N_m E_s = 2 \times 10^3 + 30.0\,S$ el/cc where S is the average sunspot number and $h_m E_s = 110.$ km. The southern and northern boundaries of the auroral oval are defined by

Magnetic Day $\Phi_s = 78.0 - 2.5\,K_p$ deg. $6.0 \leq t < \leq 18.0$

Magnetic Night $\Phi_s = 71.0 - 2.5\,K_p \cos\left(\frac{\pi}{12}(t_c - 1)\right)$, $t_c < 6.0$ or $t_c > 18.0$

and $\Phi_N = \Phi_s + K_p + 4.0$ where t_c is the corrected geomagnetic time and λ_m is the corrected geomagnetic latitude. When $\Phi_s \leq \lambda_m \leq \Phi_N$ the auroral oval blanketing frequency is calculated using

$$f_A = 1.3 + 0.3\,(4.0 + 0.05\,K_p) \quad .$$

For solar night this is replaced by

$$(f_A{}^2 + 1.1^2)^{1/2}$$

The final E layer parameters foE and hmE are generated according to the rules

$$(foE)^4 = (foE_s)^4 + \frac{3}{2}(foE_A)^4$$

$$hmE = \frac{(foE_s)^2\, hmE_s + (foE_A)^2\, hmE_A}{(foE_s)^2 + (foE_A)^2} \quad .$$

F2 Layer

The calculation of the maximum density $N_m F2$ and the semithickness of the F2 layer are given in reference 4 and 5. The model for hmF2 has

been slightly modified. The seasonal variation of $h_m F2$ is incorporated in the behavior of noon and midnight values.

$$h_m F2(\text{noon}) = 197.0 + 0.79S - 0.0011S^2 + 0.55(\lambda_m - 45.0^\circ)$$

$$h_m F2\ (\text{midnight}) = 297.0 + 0.603S + 0.55(\lambda_m - 45.0^\circ) \quad .$$

The diurnal variation of $h_m F2$ is divided into three separate cases. In the first case there is no diurnal variation. This occurs when the sun does not set or when the sun does not rise.

$$h_m F2 = h_m F2\ (\text{noon}) \qquad \text{if} \quad \chi(\text{midnight}) < 102^\circ$$

$$h_m F2 = h_m F2\ (\text{midnight}) \quad \text{if} \quad \chi(\text{noon}) > 102^\circ$$

where χ is the local zenith angle. The remaining two cases depend upon the value of χ(noon) and the behavior of $h_m F2$ is shown in the two following curves. Linear interpolations for $h_m F2$ are performed from one of the two graphs for a given value of χ. In order to determine which case applies, the four parameters; χ(noon), χ(midnight), $T(\chi = 87^\circ)$ are calculated for the given day of the year.

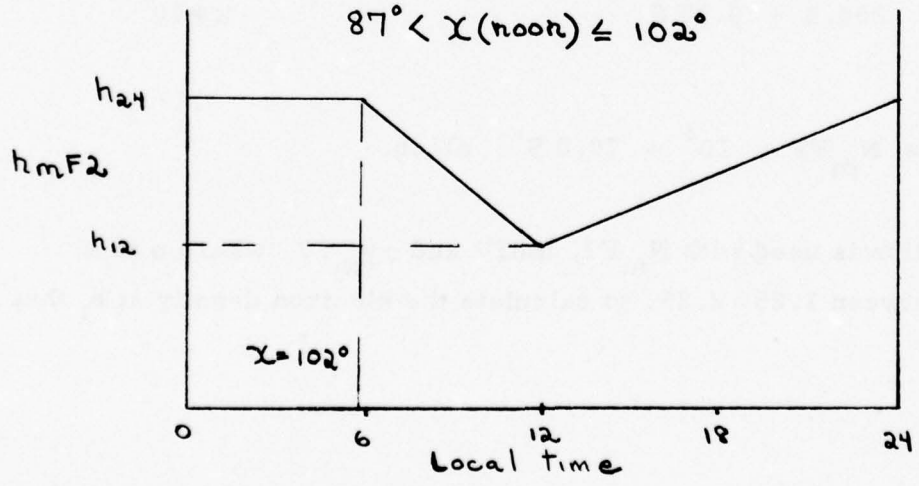

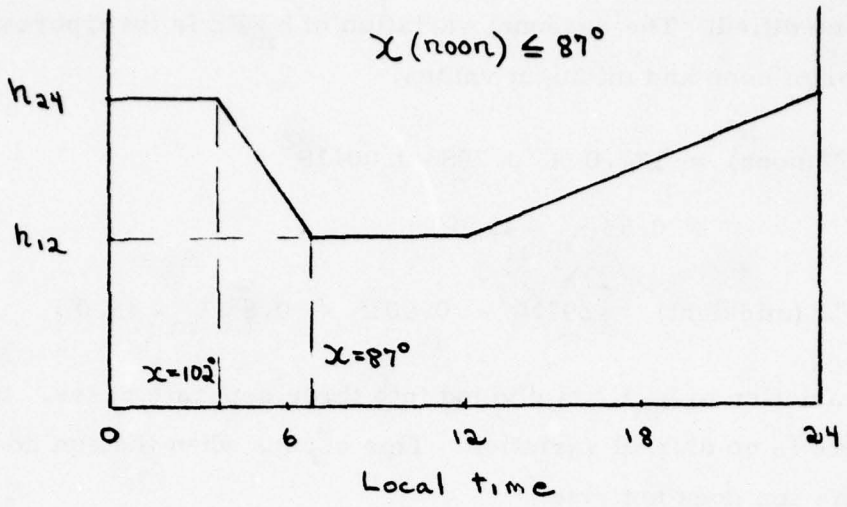

F1 Layer

A twenty-four hour model for an electron density at a height between the E and F2 layers is constructed using the solar F1 layer and the various parameters of the F2 layer. The model for $N_mF1(h_1)$ for $\chi < 90°$ is described in reference 1. The height of this intermediate layer corresponds to h_mF1 and is given by

$$h_1 = h_mF1 = 156. + 0.15\,S + 45.\log_e(\sec\chi), \chi \leq 70°$$

$$h_1 = 156 + 0.15\,S + 45.\log_e(\sec 70°)$$

$$= 204.3 + 0.15\,S \qquad \chi > 70°$$

For $\chi > 90°$

$$N_1 = N_mF1 = 10^3 + 70.0\,S \quad \text{el/cc.}$$

A cubic equation is used with N_mF2, hmF2 and αy_mF2, where α is a parameter between 1.25 - 2.25, to calculate the electron density at h_i that

would be predicted by an F2 layer alone. This value, $N_m F21$ is combined with $N_m F1$ to produce an anchor point on the profile at all times of the day.

The weighting procedure is the following:

$$\Delta_1 \equiv \frac{h_m F2 - h_1}{\alpha\, y_m F2} \qquad \text{with } \Delta_1 \text{ always} \leq 1.0,$$

$$\Delta_2^2 \equiv 1.0 - \Delta_1^2 \qquad \text{and the density at } h_1 \text{ used in the construction of the profile is given by}$$

$$N_1 = N_m F1\, \Delta_1^2 + N_m F21\, \Delta_2^2.$$

As h_1 becomes more removed from $h_m F2$ the less influence the F2 layer has on the determination of N_1. At night $\Delta_1 \to 1$ and N_1 approaches the value $N_m F1$ ($\chi > 90°$). During the day for periods close to the equinox the weighting factors are of the same size and the two densities are close to the same value. The procedure then produces a smoothed value for N_1 for two independent parameter models. For periods close to the solstice $h_m F2$ and h_1 can be approximately the same (as predicted from the models). In this case the F2 layer becomes the important contributor to N_1. This procedure reflects our assessment of the relative merits of the individual empirical models for the F1 and F2 layer parameters.

II.4 One and Two Dimensional Electron Density Distributions

Table II-1 contains the ionospheric parameters for various layers for several locations along a great circle path between California and England for April 15 at UT = 2100 hours. Two of the sets, $\theta = 0°$ and $75°$, are during solar day and night respectively while the remaining three locations are close

Individual Ionospheric Parameters

April 15 UT = 2100 K_p = 2.0 SSN = 50.0

	Lat.	Long.	Local Time	f_oE	f_oF1	f_oF2	h_mE	h_l	h_mF2	y_mF2	χ
1	45.0N	114.0W	13.4	3.5MHz	4.4MHz	6.8MHz	105.km	175.km	249.km	60.km	39
2	63.2N	37.8W	18.5	2.1	3.3	6.5	146.	212.	297.	69.	84
3	61.5N	27.5W	19.2	1.3	2.7	5.8	160.	212.	301.	70.	89
4	59.6N	18.4W	19.8	0.0	0.0	5.4	110.	212.	303.	70.	94
5	46.0N	6.6E	21.4	0.0	0.0	5.5	110.	212.	324.	69.	114

TABLE II-1

to the terminator at sunset. In figure II-1 we show the dependence of the POLAR 77 model using these parameters for various values of α. Three profiles are shown with α = 1.25, 1.75, and 2.25 along with the profile constructed using the POLAR 76 model. It is not our intent to compare one model with another but to determine under what conditions either can be used to describe realistic median ionospheric conditions. For daytime conditions both POLAR 76 and POLAR 77 with α = 1.25 and 1.75 contain the general features of the three layers. The height derivative $\frac{\partial N}{\partial h}$ for POLAR 76 is more slowly varying in a larger region around the layer heights. POLAR 77 with α = 2.25 produces an unphysical peak in the electron density larger than $N_m F2$ at a height between h_1 and $h_m F2$.

If we restrict our examination of the nighttime profile to $N_e > 7000$ el/cc (0.75 MHz.) we observe that the gradient decreases with increasing values of α. For α = 2.25 the profile predicts relatively large densities in the height region between 160 and 200 km. The POLAR 76 model is a single parabolic layer with a semithickness of 1.414 $y_m F2$. For a fixed value of α (1.75) we wish to examine the relative spatial and temporal dependence of the two models.

Figure II-2 shows the profiles using POLAR 77 for the three locations bracketing the terminator and one for low zenith angle. Figure II-3 also contains the same profiles using POLAR 76. In the height region between h_1 and $h_m F2$ the two models are almost identical near midday and remain similar until past sunset when $\frac{\partial N}{\partial h}$ becomes larger with the POLAR 77 model. In the height region below h_1 the POLAR 77 model predicts a smaller value of the total electron content (TEC) for low zenith angle and a larger TEC during solar night. The shape of the profiles for the POLAR 77 model changes more slowly than those of the POLAR 76 model as the terminator is crossed.

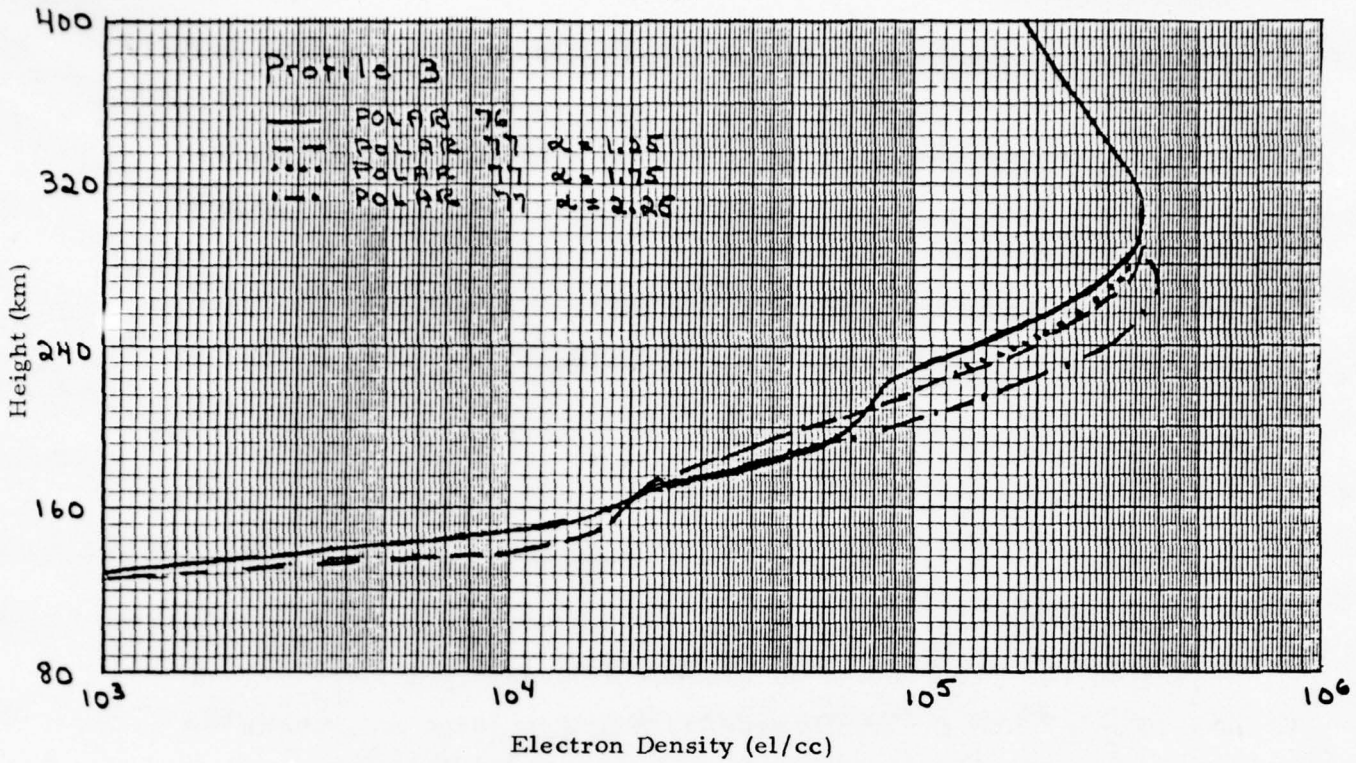

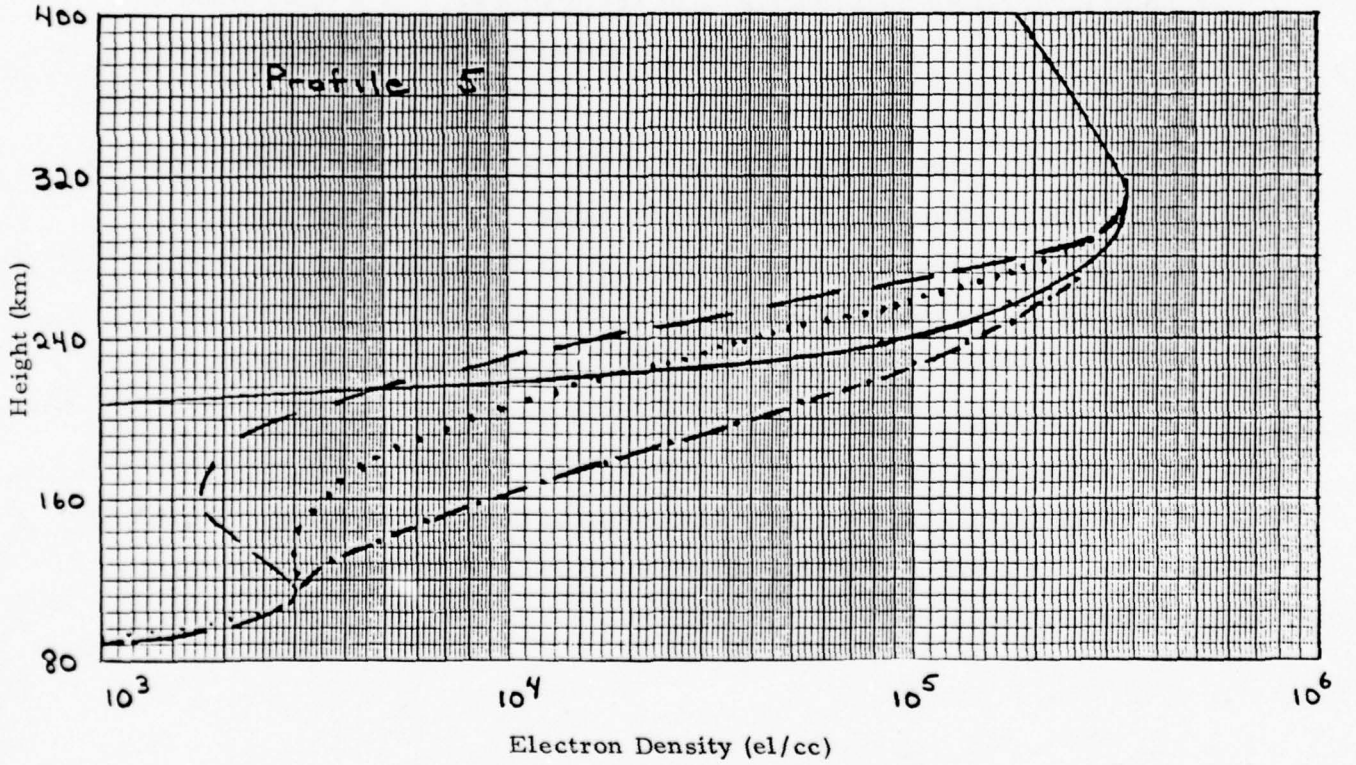

ELECTRON DENSITY PROFILES
April 15 K_p = 2.0 SSN = 50.0
Figure II-1

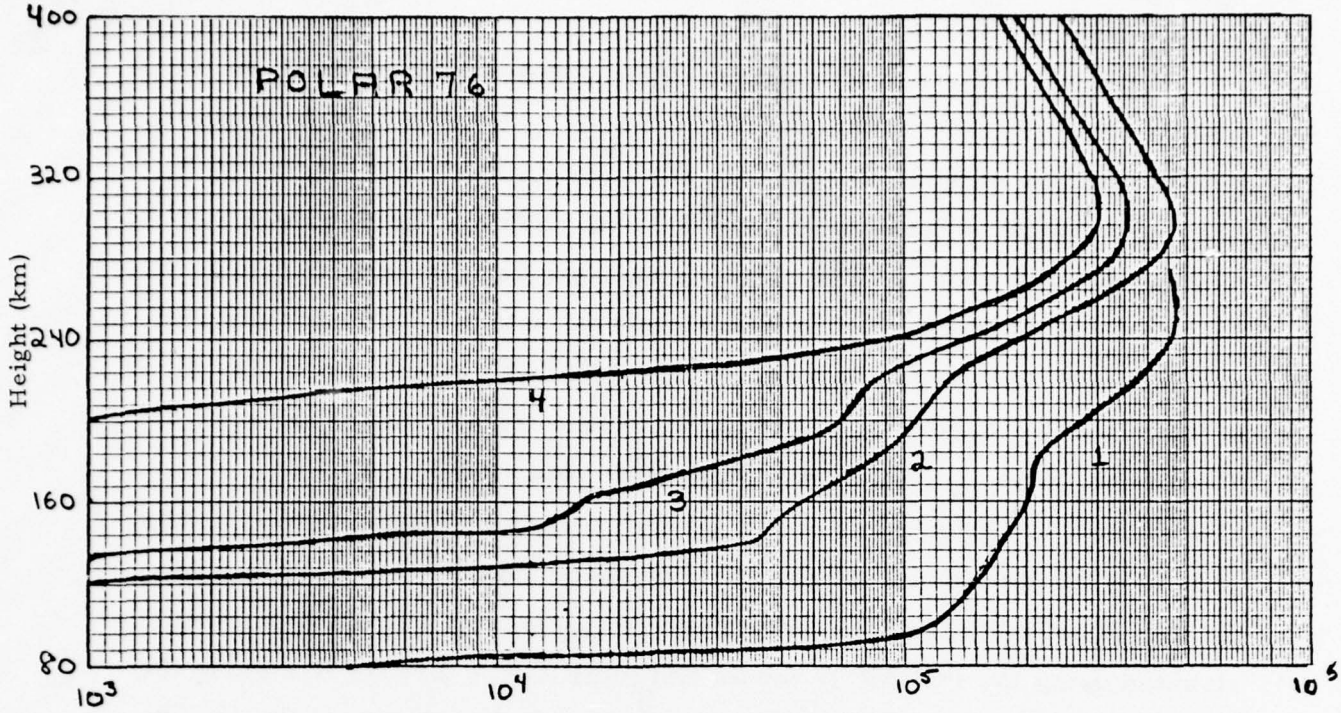

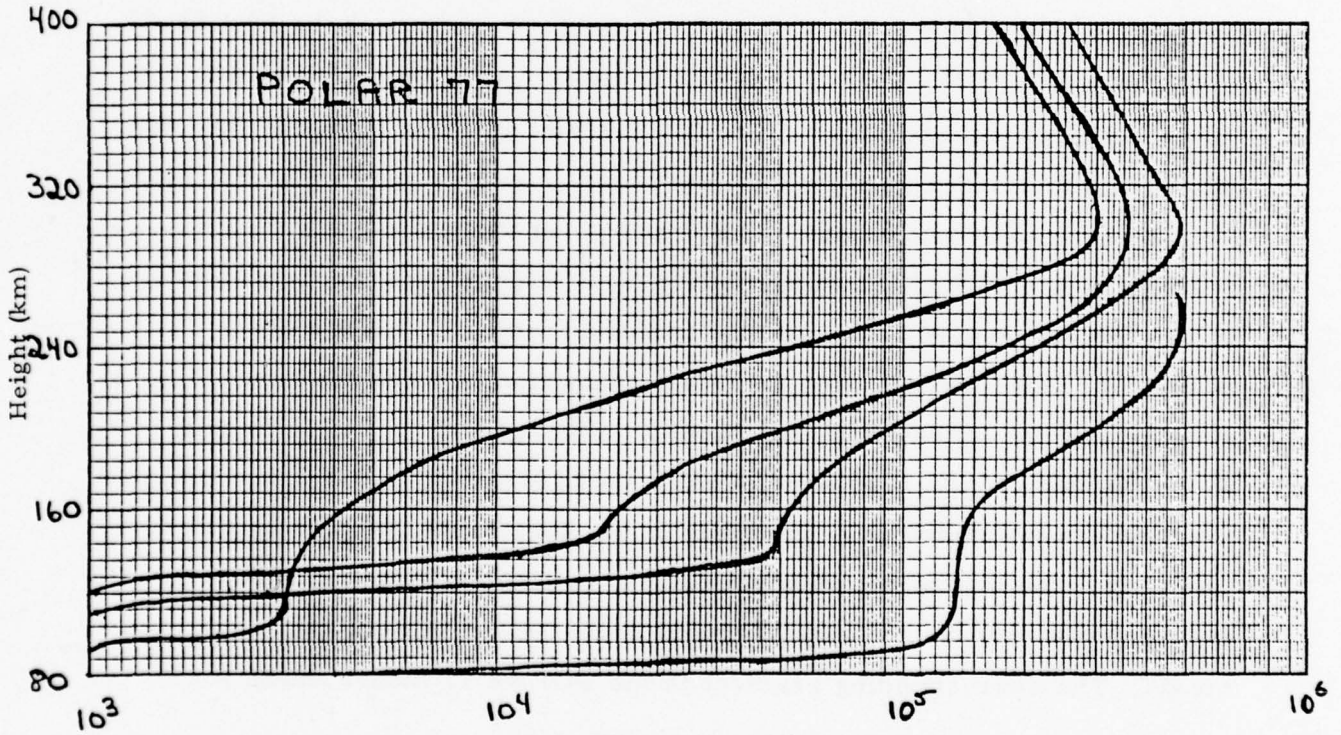

ELECTRON DENSITY PROFILES
April 15 K_p = 2.0 SSN = 50.0

Figure II-2

Figures II-3 through II-6 are iso-ionic contour maps of electron density for a 75° great circle path with the origin at 45°N, 114°W and an azimuthal angle of 38.2° East for the time and date given in TABLE II-1. The height range is between 80. and 400. km and the contour labels are electron density x 10^{-5}. The origin is during solar day and the path is such that we cross the auroral oval at approximately 25° and exit the oval and cross the terminator between 45° and 50°. The contours are constructed using a quadratic smoothing technique from profiles that are given every 3° in arc length and every 10.0 km in height. Figure II-7 is plot showing the boundaries of the auroral oval and the terminator for this path as a function of universal time. These boundaries are contained in the individual models of the ionospheric parameters. Figure II-3 is constructed using the POLAR 76 model and figures II-4 through II-6 using the POLAR 77 model with α = 1.25, 1.75, and 2.25. For heights above $h_m F2$ all the models are identical. Several features of the nighttime part of the ionosphere are clearly apparent. The POLAR 76 model and the POLAR 77 model with α = 1.75 are very similar. The POLAR 77 model with α = 2.25 produces significantly larger electron densities at lower altitudes than the others and the model with α = 1.25 produces an exceptionally thin F2 layer. This leads to very large horizontal gradients at the terminator. Both POLAR 76 and POLAR 77 with α = 2.25 have a large horizontal gradient in 150-200 km region at the auroral oval boundary. The other two POLAR 77 models generate a smoother transition between the auroral E layer and the corresponding F layers. Figures II-8, POLAR 76 and II-9, POLAR 77, α = 1.75 are the same as figures II-3 and II-5 but the profiles are generated at 1° intervals in arc length. In the region of the terminator the horizontal electron density gradient does not change significantly with the POLAR 76 model in the height region just below hmF2. The corresponding gradient in the POLAR 77 model shows a

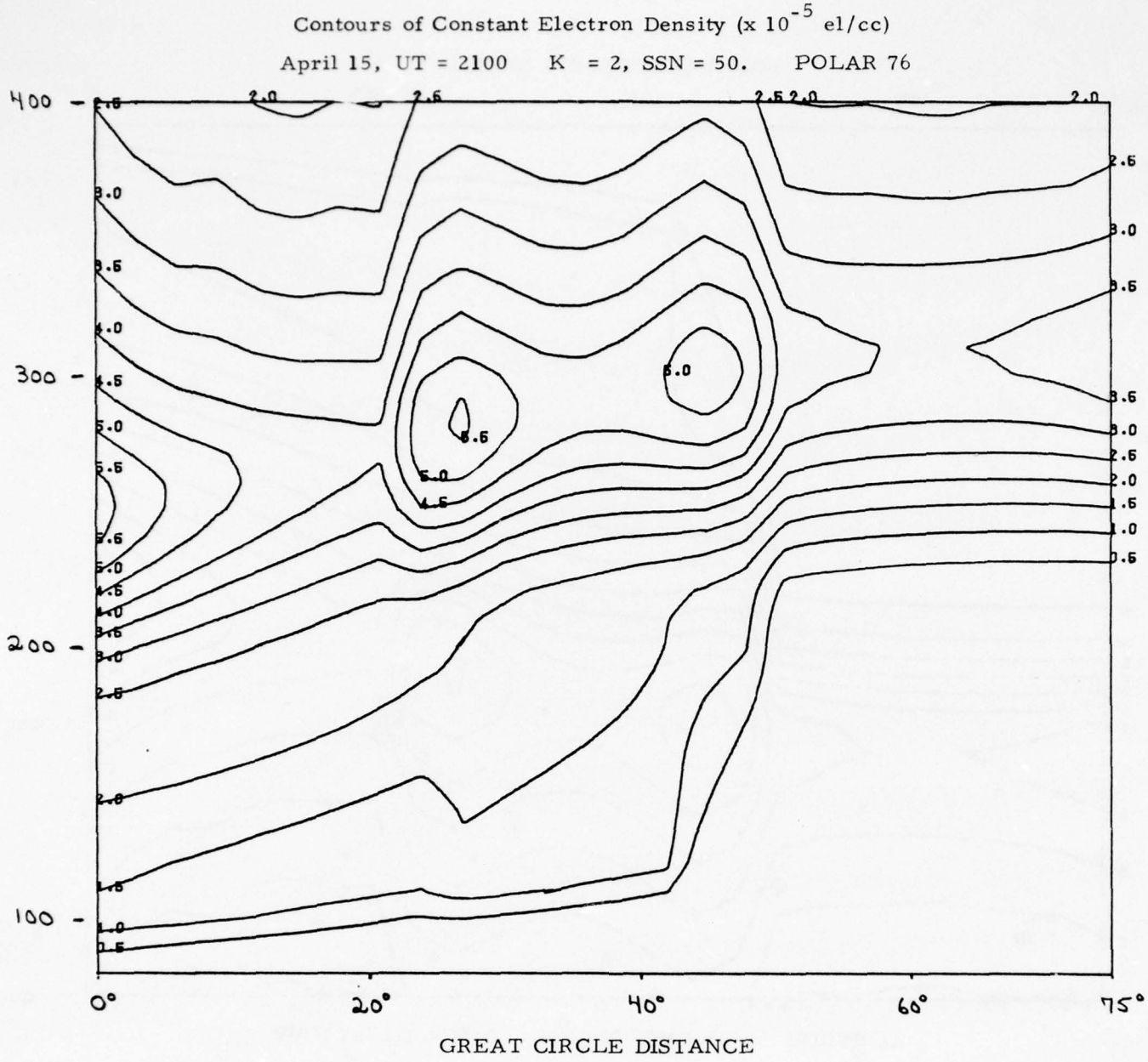
Contours of Constant Electron Density (x 10^{-5} el/cc)
April 15, UT = 2100 K = 2, SSN = 50. POLAR 76
400
300
200
100
Height (km)
0°
20°
40°
60°
75°
GREAT CIRCLE DISTANCE

Figure II-3

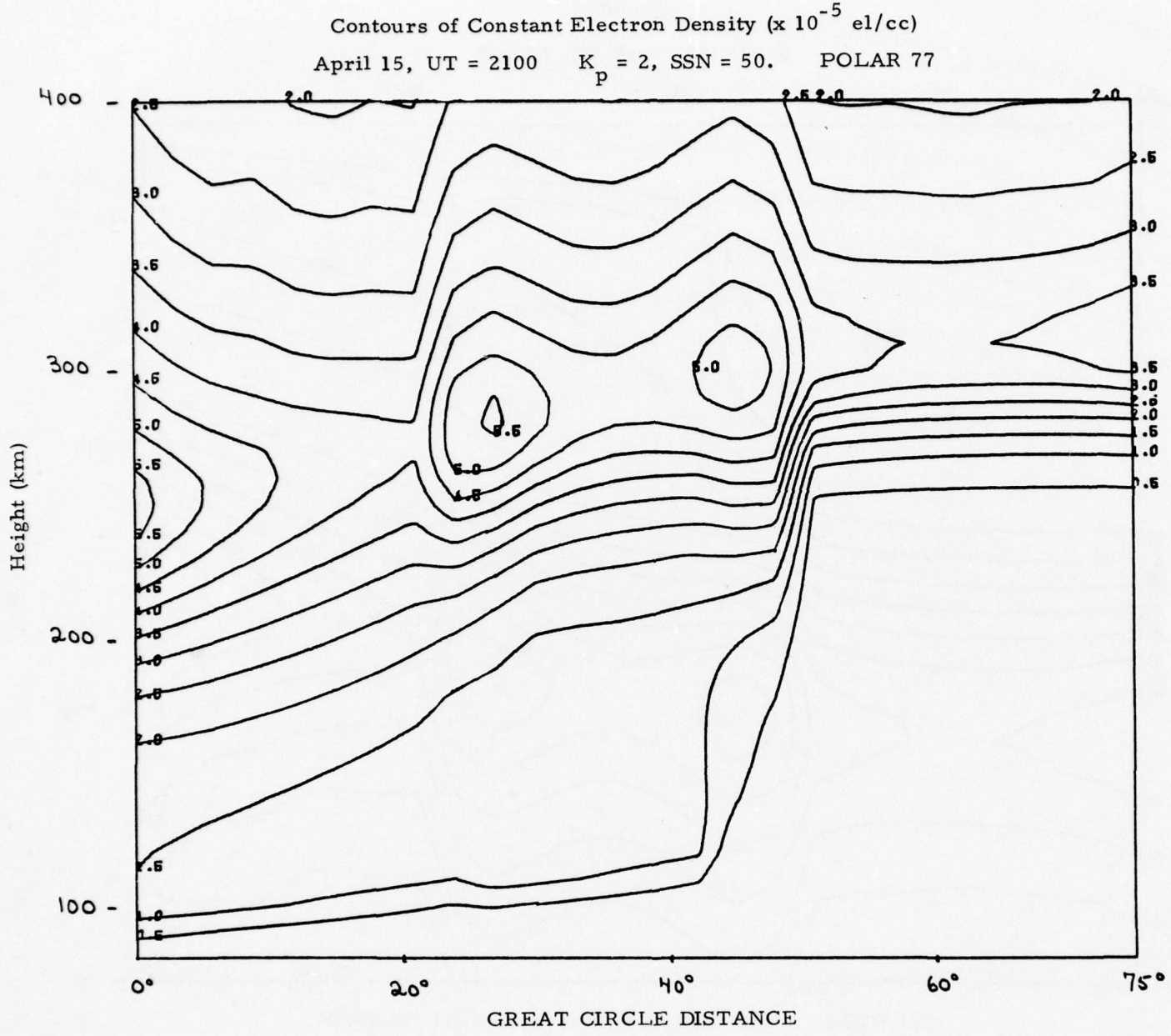
Contours of Constant Electron Density (x 10^{-5} el/cc)
April 15, UT = 2100 K_p = 2, SSN = 50. POLAR 77
400
300
200
100
Height (km)
0°
20°
40°
60°
75°
GREAT CIRCLE DISTANCE

Figure II-4

Contours of Constant Electron Density (x 10^{-5} el/cc)

April 15, UT = 2100 K_p = 2, SSN = 50. POLAR 77

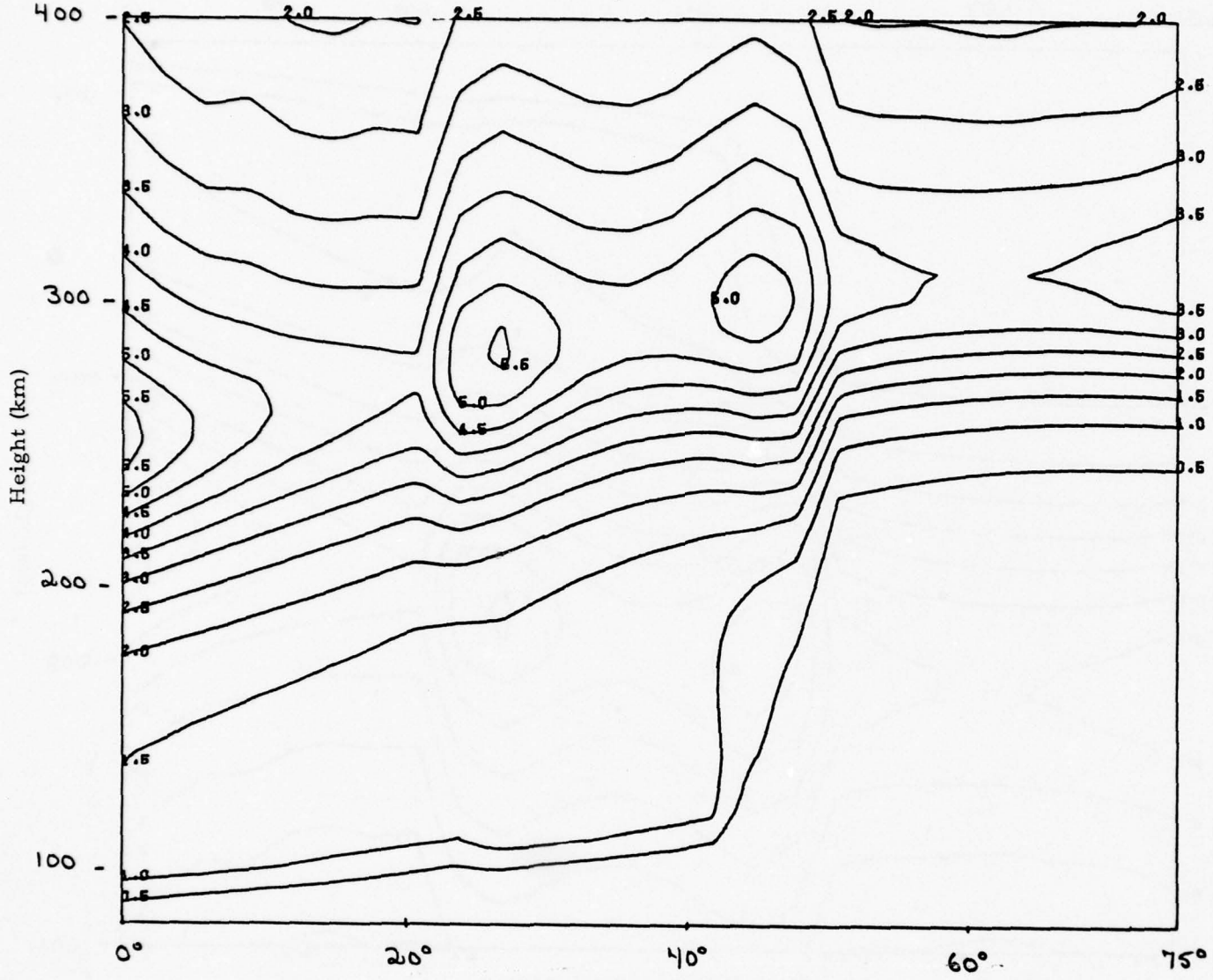

Figure II-5

Contours of Constant Electron Density (x 10^{-5} el/cc)

April 15, UT = 2100 K_p = 2, SSN = 50. POLAR 77

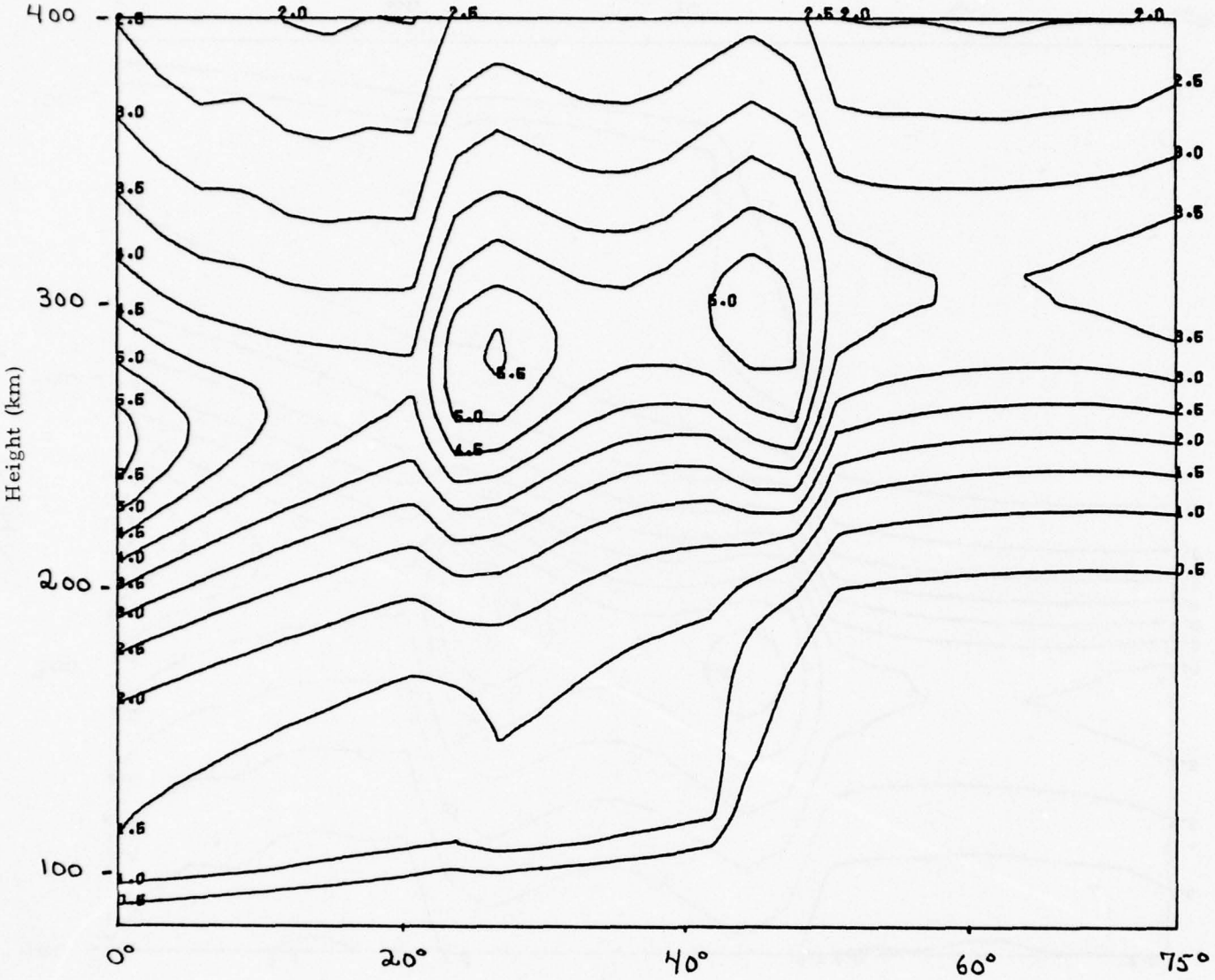

Figure II-6

Geophysical Boundaries vs. Time

Transmitter Location 45°N, 114°W Azimuth = 38.2°

April 15 K_p = 2.0

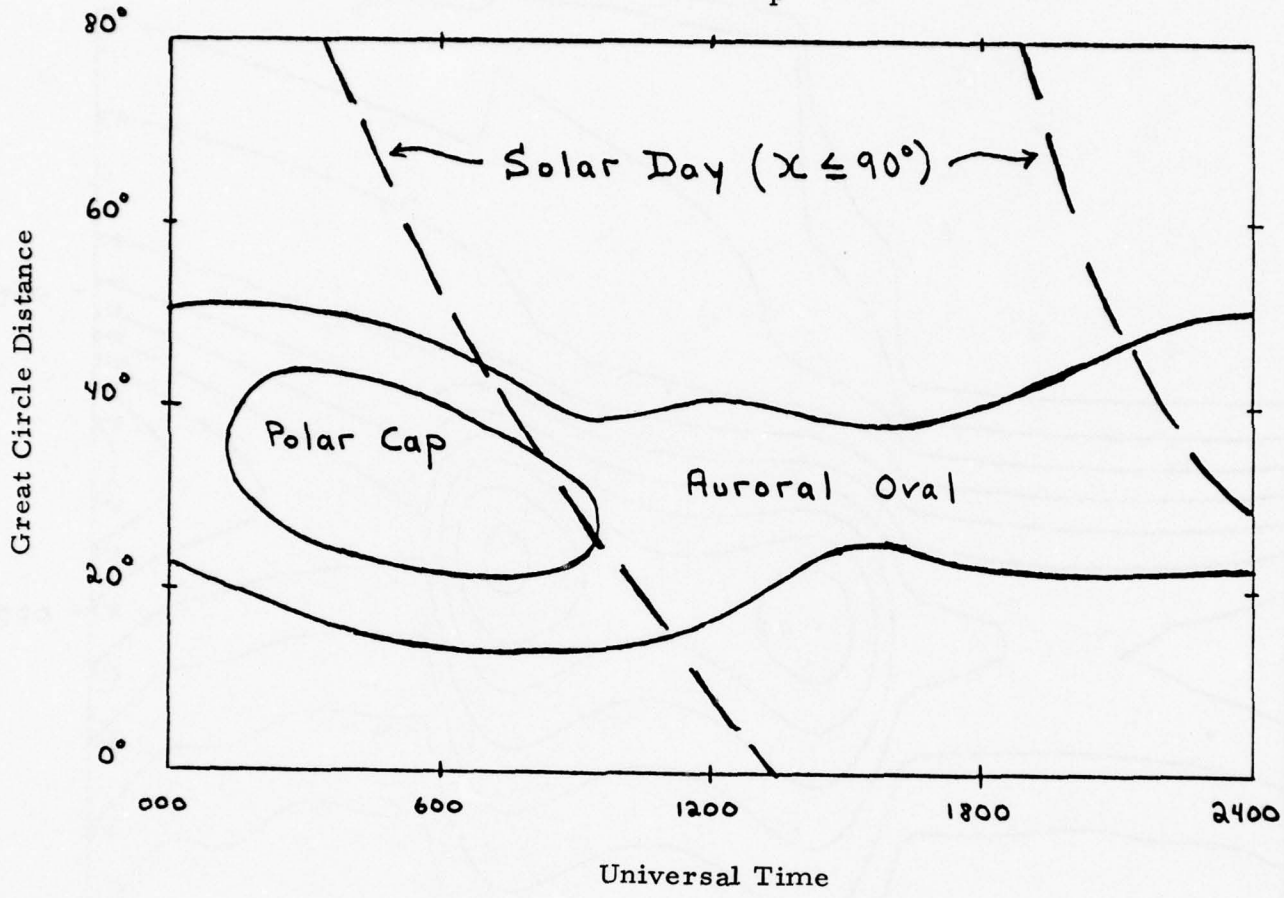

Figure II-7

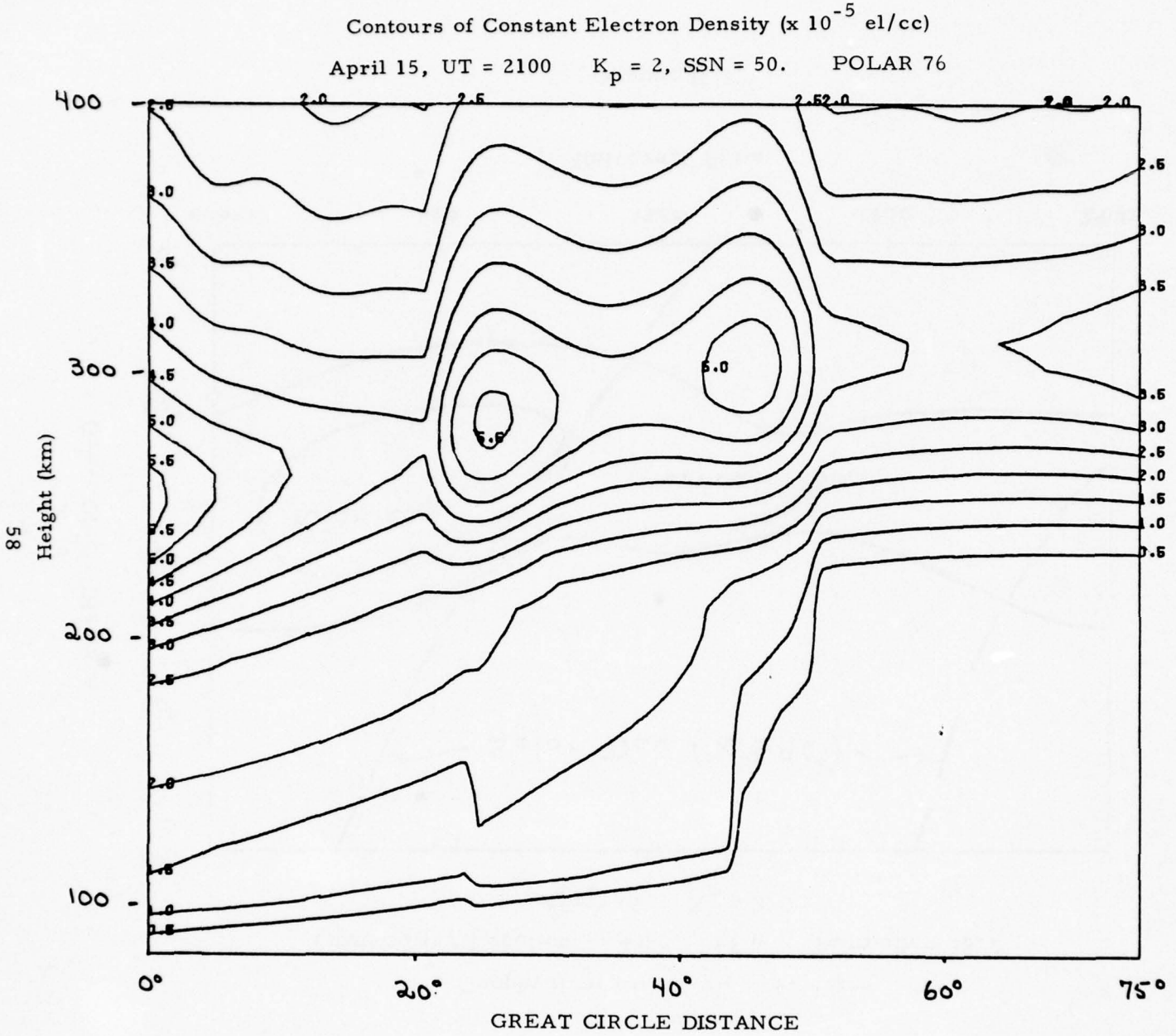
Contours of Constant Electron Density (x 10^{-5} el/cc)
April 15, UT = 2100 K_p = 2, SSN = 50. POLAR 76
400
300
200
100
Height (km)
0°
20°
40°
60°
75°
GREAT CIRCLE DISTANCE

Figure II-8

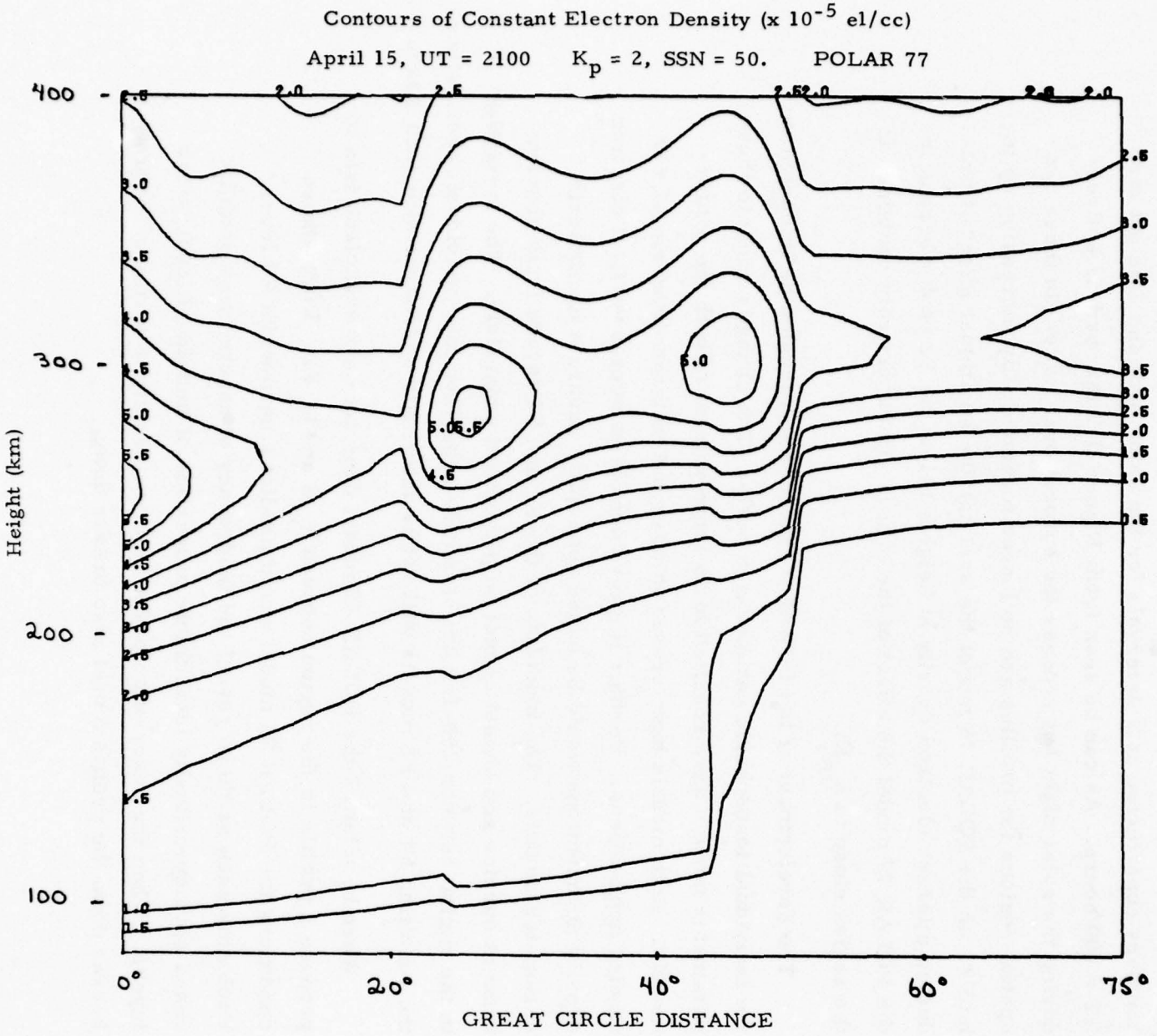
Contours of Constant Electron Density (x 10^{-5} el/cc)
April 15, UT = 2100 K_p = 2, SSN = 50. POLAR 77
400
300
200
100
Height (km)
0°
20°
40°
60°
75°
GREAT CIRCLE DISTANCE

Figure II-9

sharper increase in this region.

Figures II-10, POLAR 76 and II-11, POLAR 77, $\alpha = 1.75$ are iso-ionic contours constructed at 3° intervals for the same path and date but for UT = 400 hours. As can be seen from Figure II-7 this path is entirely during the solar night but crosses the auroral oval twice. In these two spatial regions the profiles are no longer monotonically increasing up to hmF2. In the POLAR 76 model the oval has the additional effect of producing a larger electron density at heights below the F2 peak whereas in the POLAR 77 model the effect of the oval is almost entirely contained in the region close to $h_m E$.

The development of the POLAR 77 model has revealed deficiencies in the individual ionospheric parameter models. The changes made to these parameter models have resulted in an improvement of both the profile models. Both models have proved to be useful in three dimensional ray tracing applications. Further improvement in predicted vertical electron density distributions would be based upon more accurate ionospheric parameter models. The modeling of the F2 and F1 layers from observations at sunrise and sunset cannot be performed separately. The ionization in the region between 200-250 km cannot be separated into individual layers since the resulting F1 and F2 models will not be internally consistent with each other.

When h_1 = hmF2 the POLAR 77 model does not have sufficient data to produce a profile in the region between $h_m E$ and $h_m F2$. Under these conditions the POLAR 76 model would predict a zero-width F2 layer. Problems such as these reveal the inadequacy of constructing profiles based upon specifically identifiable properties of individual ionospheric layers. When the description of the electron density in terms of layers breaks down the profile model also breaks down.

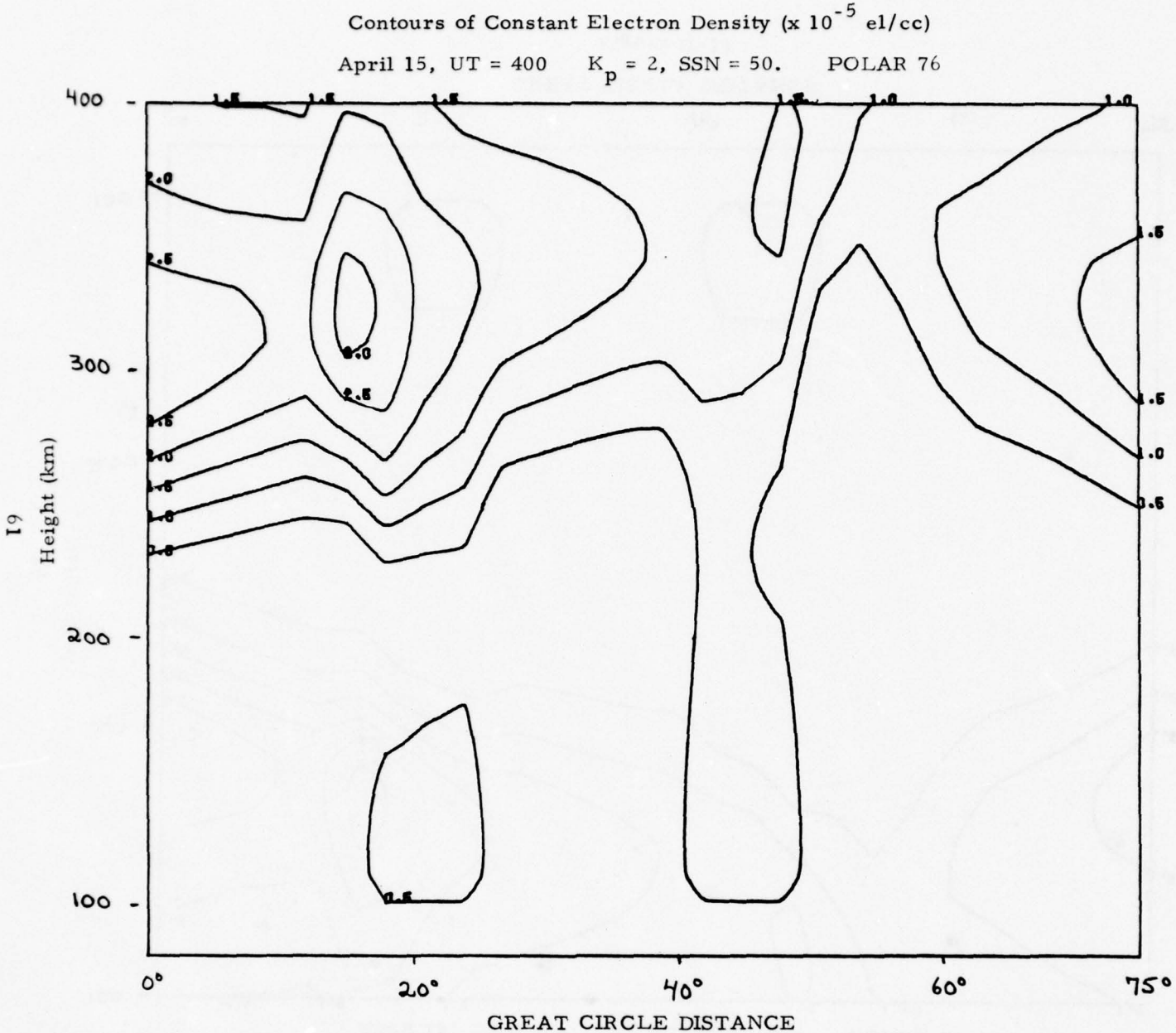
Contours of Constant Electron Density (x 10^{-5} el/cc)
April 15, UT = 400 K_p = 2, SSN = 50. POLAR 76
400
300
200
100
Height (km)
0°
20°
40°
60°
75°
GREAT CIRCLE DISTANCE

Figure II-10

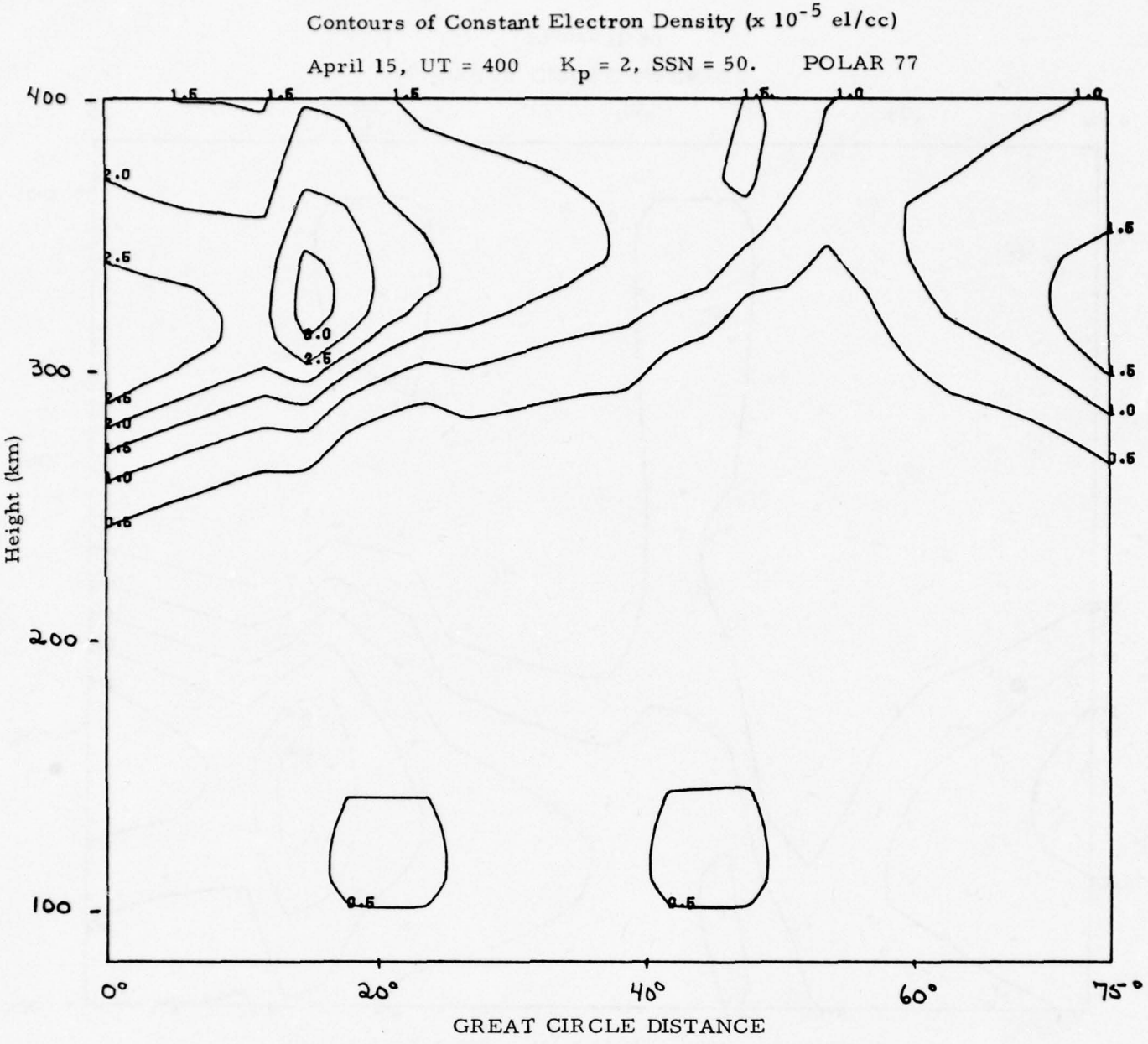
Contours of Constant Electron Density (x 10^{-5} el/cc)
April 15, UT = 400 K_p = 2, SSN = 50. POLAR 77
400
300
200
100
Height (km)
0°
20°
40°
60°
75°
GREAT CIRCLE DISTANCE

Figure II-11

III. EARTH DETACHED RF PROPAGATION INDUCED BY FIELD ALIGNED IRREGULARITIES

There are modes of radio propagation controlled by the regular ionospheric regions by which HF and even VHF radio waves can travel to great distances with low attenuation without intermediate ground reflections. An important class of these modes is the Earth Detached, or Chordal Hop, mode whereby a ray is refracted in the ionosphere so as to travel above the earth's surface, reentering the ionosphere. Such modes of propagation could be extremely useful for long range HF communication or over the horizon backscatter radar applications.

However, it is clear that in a spherically symmetric ionosphere such modes cannot be excited by a ground based transmitter. On the other hand, the naturally occurring horizontal gradients in the ionosphere could create sufficient ionospheric "tilt" to inject a ray into earth detached propagation. Generally, even at grazing angles, a ray leaving the ground arrives at ionospheric altitudes with too large an angle with the layer for injection into earth detached propagation. Furthermore, the occurrence of favorable conditions for such injection is so fortuitous and for such short duration as to preclude reliance on the mode for routine use.

Other natural mechanisms capable of coupling HF radio waves into or out of earth detached propagation consist of (a) sporadic E ionization, (b) auroral columns and curtains, (c) meteor trails, (d) equatorial F-region ionization troughs, and (f) travelling ionospheric disturbances. Clearly, these all lack the reliability criterior for routine utilization of the mode.

Artificial scattering centers such as rocket-launched ionization trails, rocket-launched ionospheric seeding, or an RF induced ionization cloud, are also conceivable and have been shown to be effective to create a local

modification of the ionosphere to create coupling into and out of earth detached modes. These methods suffer from the defect that the coupling efficiencies are small compared to what one might obtain from injection by naturally occurring ionospheric tilts. In the first place, the fraction of the incident energy scattered from these ionospheric irregularities is generally small; secondly, much of the scattered energy is spread out into undesired directions.

High power, high frequency radio transmitters have been used[7] to intentionally modify the electron temperature and density in the F region of the ionosphere. Under the influence of a passing electromagnetic wave, an oscillatory motion is imparted to the electrons in the plasma constituting the ionosphere absorbing energy from the wave, and consequently heating the electrons in a local region creating irregularities in the ionization and electron temperature. As electron temperature increases, the plasma pressure increases, and the plasma tends to expand. However, the electrons are constrained to spiral about the magnetic field lines; thus, the plasma expands along these lines.

Consequently, the irregularities in the electron density and temperature become aligned with the local geomagnetic field, and serve as scattering centers for incident HF radiation.

These scattering centers may be modeled by long thin cylinders, and the incident radiation will be coherently scattered into a cone centered about the local magnetic field line with apex angle θ equal to the angle between the directions of the incident radiation and the local magnetic field. The lengths of the scattering centers are presumed to be of the order of tens of kilometers, while the wavelengths of interest are from 0.1 km (3 MHz) to 0.01 km (30 MHz); under these conditions, the scattered radiation is effectively confined to the surface of the scattering cone, and the far field pattern R of the time averaged

radiated power is given by[7]

$$R = \sin^2 \chi \quad , \tag{3.1}$$

where χ is the angle between the electric field vector of the incident radiation and the direction of the scattered radiation. This pattern is relative to the forward scattered radiation.

The geometry of the situation is shown in Figure III.1, which displays the geometry referenced to a spherical polar coordinate system constructed with the direction of the incident radiation as the pole; therefore, the $\vec{E}$ field of the incident radiation will lie in the equatorial plane. The "longitude" is measured from the plane containing the incident radiation direction and the local geomagnetic field. The angle χ, then, is given by

$$\cos \chi = \sin \Theta \cos (\Phi - \Phi_E) \quad , \tag{3.2}$$

and the far field radiation pattern is given by

$$R(\Theta, \Phi, \Phi_E) = 1 - \sin^2 \Theta \cos^2 (\Phi - \Phi_E) \tag{3.3}$$

Three special cases will be considered: (a) plane polarization with the electric field of the incident radiation in the plane containing the geometric field line and the direction of incident radiation ($\Phi_E = 0$); (b) plane polarization with the electric field perpendicular to this plane ($\Phi_E = \pi/2$); (c) circular polarization. The far field radiation patterns are respectively given by

$$R_a(\Theta, \Phi) = \cos^2 \Theta + \sin^2 \Theta \sin^2 \Phi \tag{3.4}$$

$$R_b(\Theta, \Phi) = 1 - \sin^2 \Theta \sin^2 \Phi \tag{3.5}$$

$$R_c(\Theta, \Phi) = 1 - \frac{1}{2} \sin^2 \Theta = \frac{1}{2} (1 + \cos^2 \Theta) \tag{3.6}$$

It is desirable that these results be expressed in a local spherical coordinate system rather than the ray coordinate system. Choosing the magnetic field line as the pole of the coordinate system, the incident radiation direction is described by ($\theta_h = \theta$, $\varphi_h = 0$) and the locus of the scattering cone is given by ($\theta_s = \theta$, $\varphi_s = \varphi$; $\varphi = 0, 2\pi$). Referring to the spherical triangle KMK' in Figure III. 1, we have,

$$\cos\Theta = \cos^2\theta + \sin^2\theta\cos\varphi = 1 - \sin^2\theta(1 - \cos\varphi) \qquad 3.7$$

$$\sin\Theta \sin\Phi = \sin\theta \sin\varphi \qquad 3.8$$

and,

$$R_a(\theta, \varphi) = 1 - \frac{1}{2}\sin^2\theta\cos^2\theta[3 - 4\cos\varphi + \cos2\varphi] \qquad 3.9$$

$$R_b(\theta, \varphi) = 1 - \frac{1}{2}\sin^2\theta[1 - \cos2\varphi] \qquad 3.10$$

$$R_c(\theta, \varphi) = 1 - \frac{1}{4}\sin^2\theta[(1 + 3\cos^2\theta) - 4\cos^2\theta\cos\varphi - \sin^2\theta\cos2\varphi] \qquad 3.11$$

These, then, are the expressions for the far field intensity patterns for the three special polarizations: Polarization in the plane defined by the incident radiation and geomagnetic field line R_a; polarization perpendicular to this plane R_b; and circular polarization R_c. Note that the elements on the scattering cone are specified by the angle φ measured from the direction of the incident radiation, and that the radiation patterns are relative to this direction.

These three intensity patterns are plotted in Figures 2 through 7 for incident angles $\theta = 15°$, $30°$, $45°$, $60°$, $75°$, and $90°$ respectively. Pattern R_a reaches a minimum at $\varphi = 180°$, where pattern R_b reaches a maximum. The minimum of R_b occurs at $\varphi = 90°$; and that of R_c varies from $\varphi = 180°$ when $\theta = 45°$ to $\varphi = 90°$ when $\theta = 90°$.

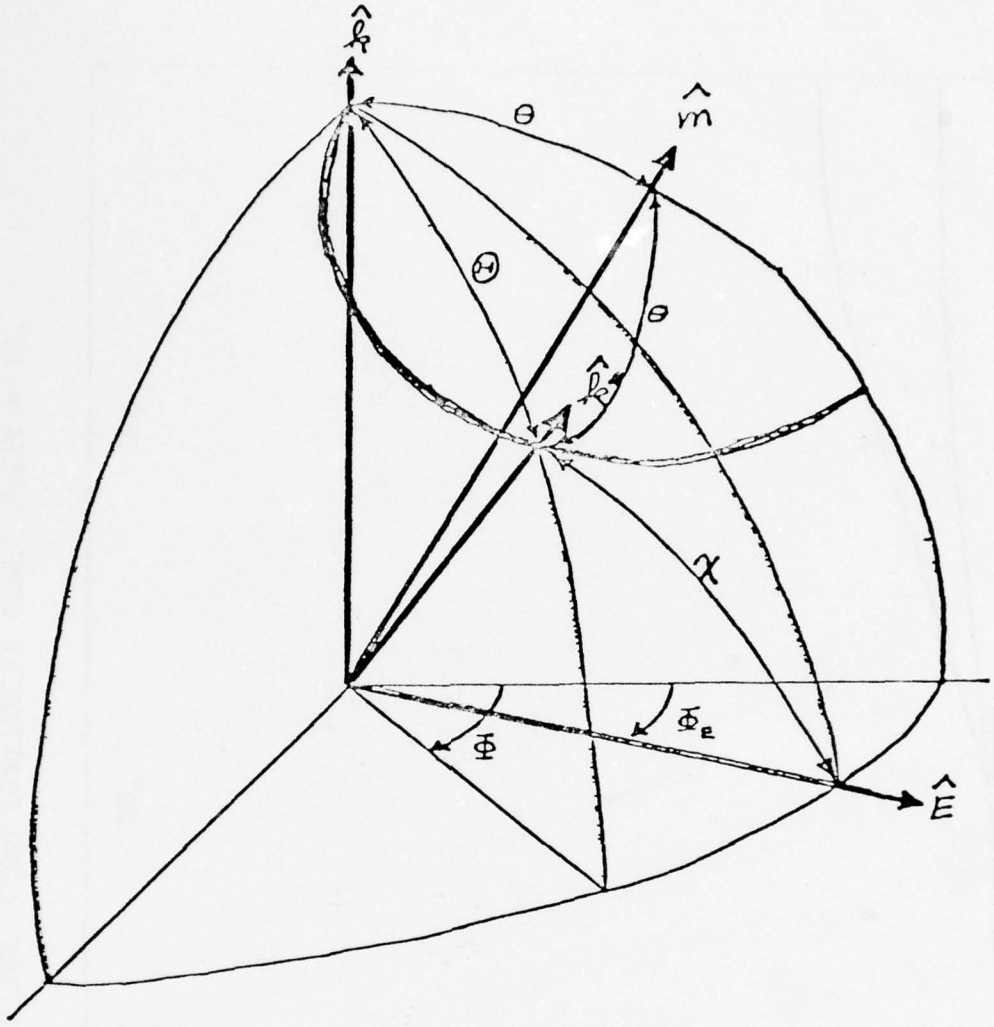

$\hat{k}$ – direction of incident radiation

$\hat{k}'$ – direction of scattered radiation

$\hat{E}$ – direction of electric field vector

$\hat{m}$ – direction of magnetic field

Figure III-1: Geometry of Scattering Cone

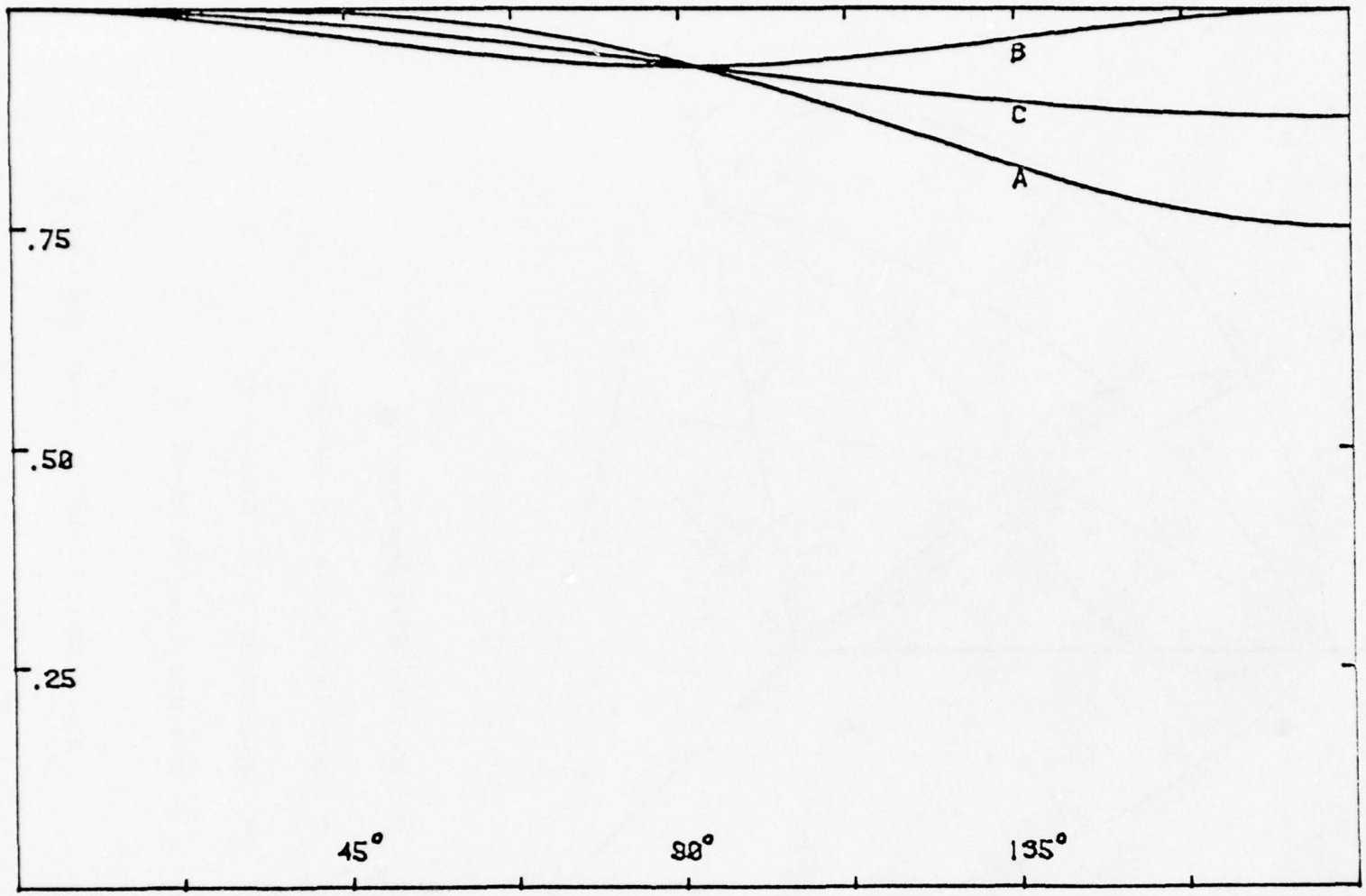

FIGURE III.2. RELATIVE INTENSITIES ALONG SCATTERING CONE. THETA = 15°

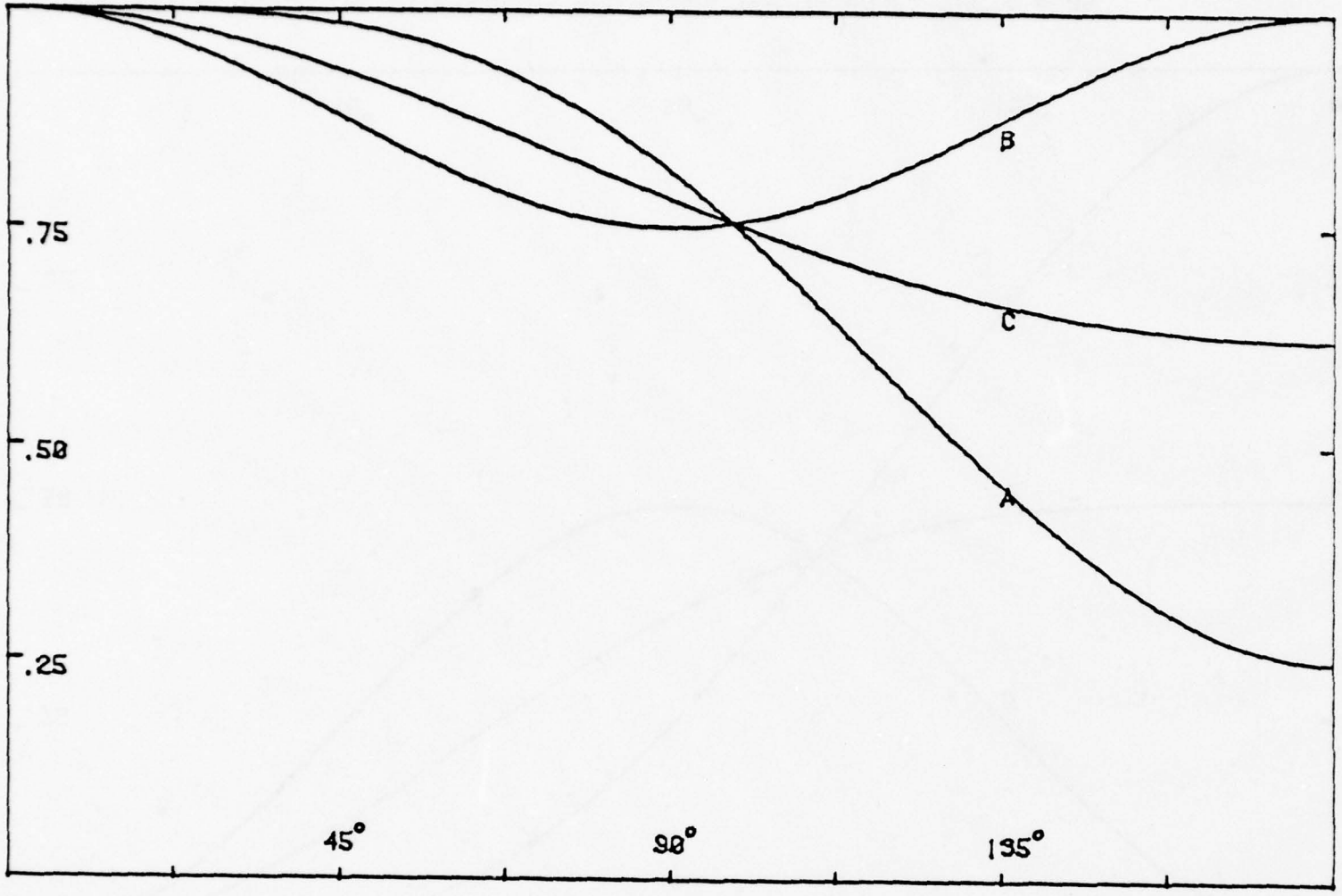

FIGURE III.3. RELATIVE INTENSITIES ALONG SCATTERING CONE. THETA = 30°

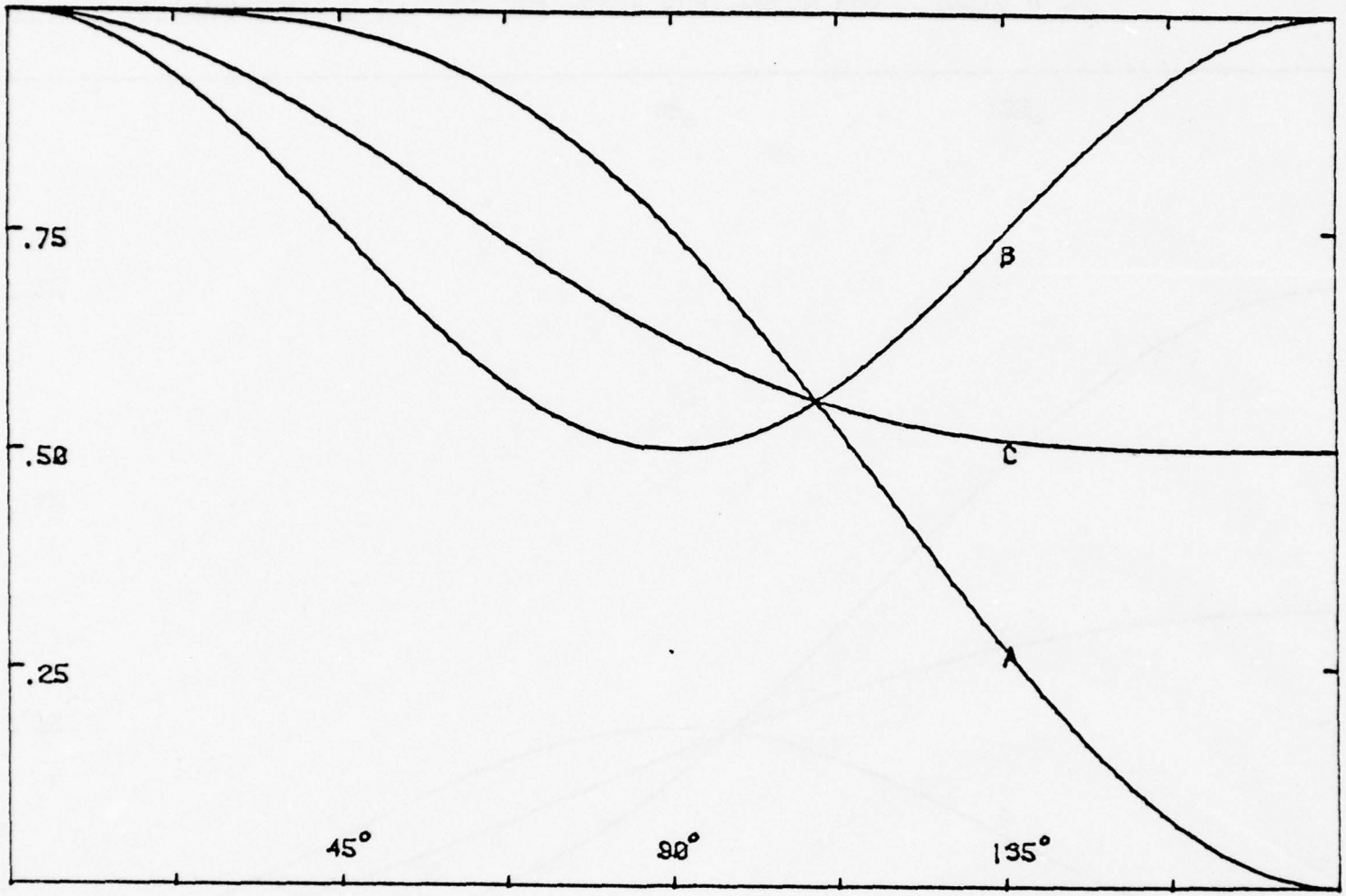

FIGURE III.4. RELATIVE INTENSITIES ALONG SCATTERING CONE, THETA = 45°

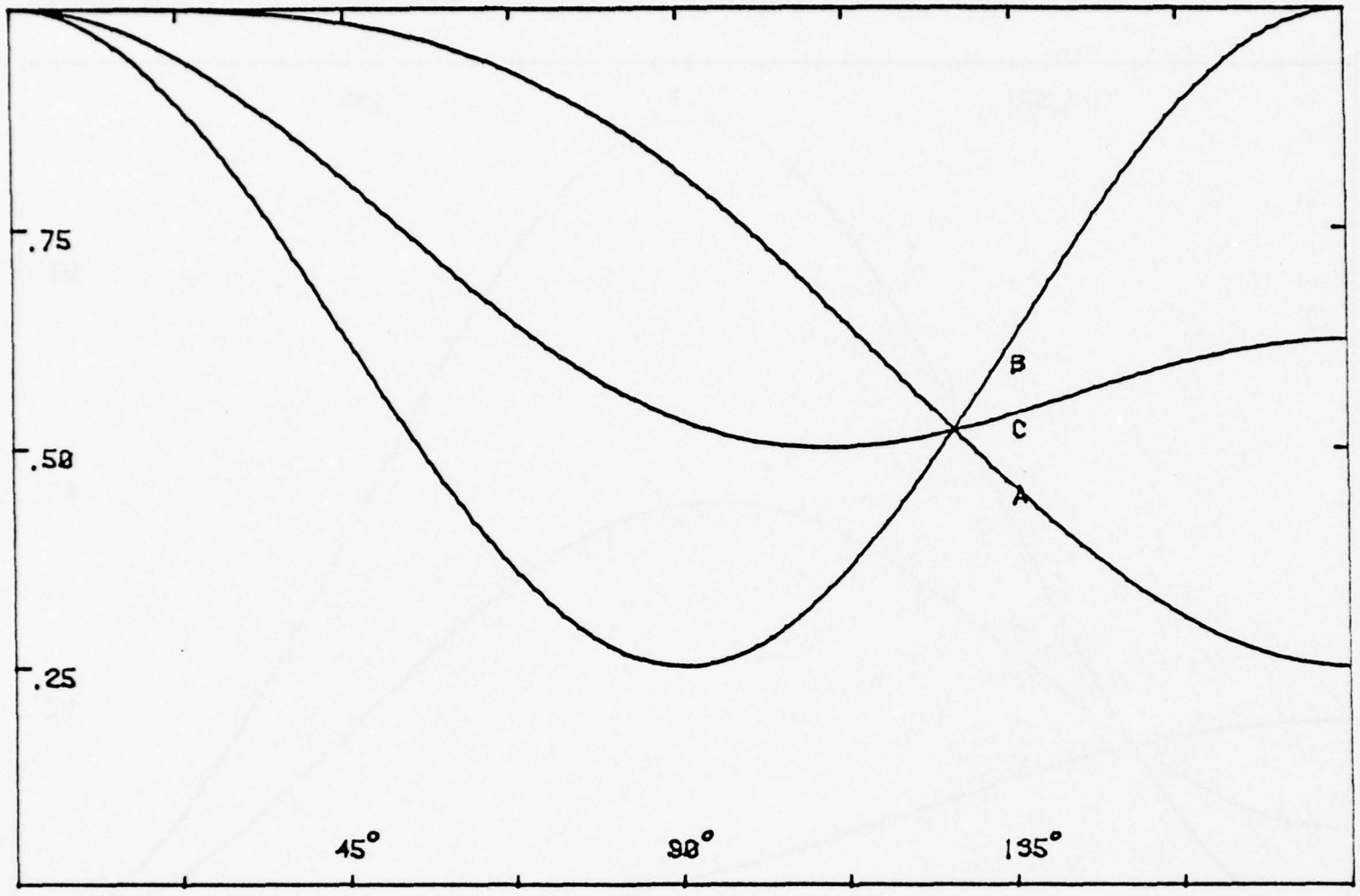

FIGURE III.5. RELATIVE INTENSITIES ALONG SCATTERING CONE. THETA = 60°

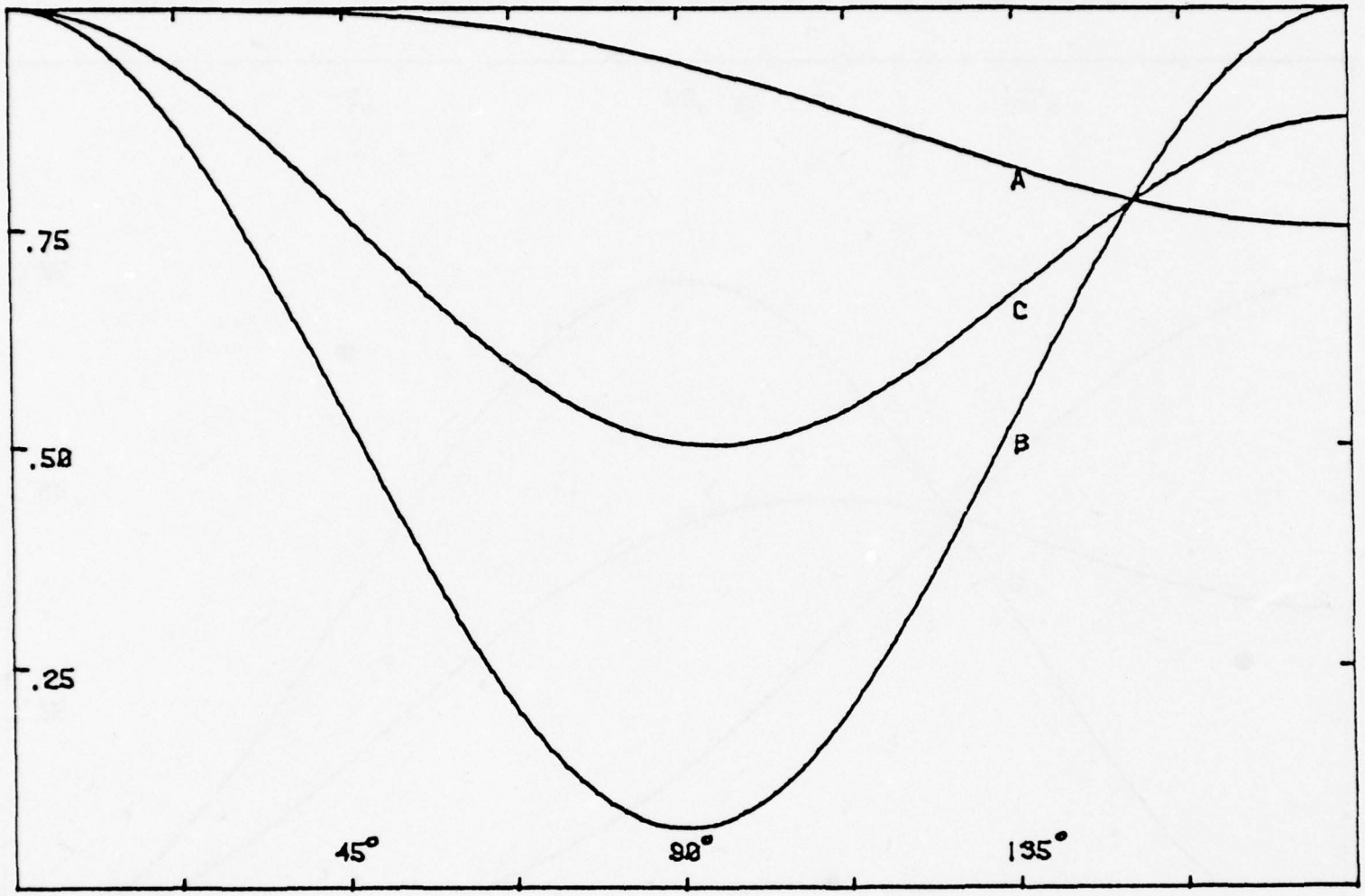

FIGURE III.6. RELATIVE INTENSITIES ALONG SCATTERING CONE. THETA = 75°

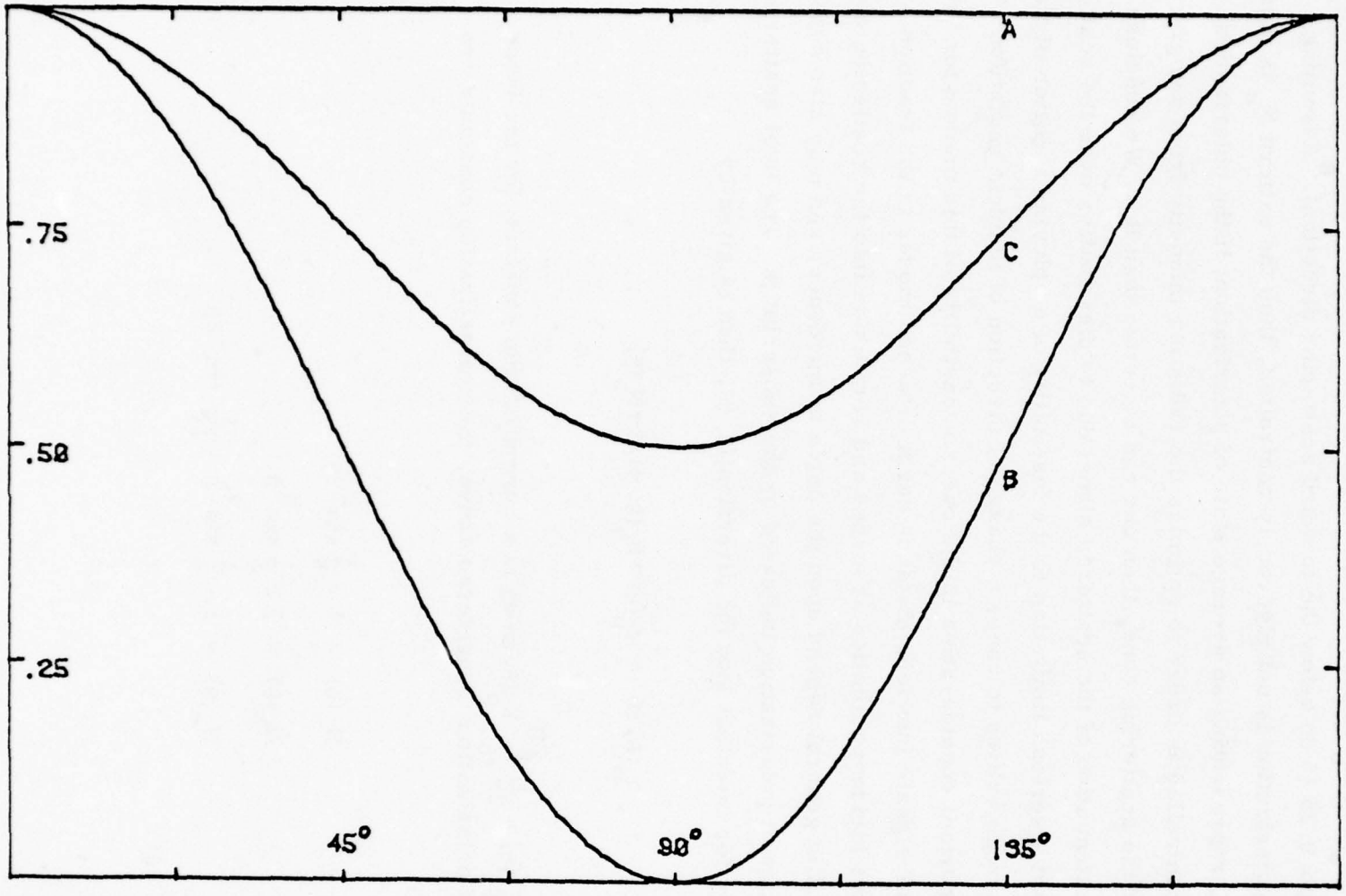

FIGURE III.7. RELATIVE INTENSITIES ALONG SCATTERING CONE, THETA = 90°

The worst case for R_a occurs at $\theta = 45°$, and for R_b and R_c when $\theta = 90°$. Although R_a and R_b vanish in their respective worst case minima, R_c never falls below 0.25 (6 db below the forward scattering direction). Assuming that the polarization is not rigorously controlled, then the pattern R_c is most relevant, representing an average state of polarization; if the polarization may be controlled in order to optimize the radiation intensity from any given region of the scattering cone, then one can do better than R_c. We conclude that the attenuation of the scattered signal due to distribution over the scattering cone is not a serious limitation to the feasibility of employing a region of field aligned irregularities to cause a change of direction of incident radiation. The most important consideration in the overall feasibility of this method for injecting RF signals into long distance earth detached modes is the fraction $\epsilon_p(\theta)$ of the incident radiation absorbed and reradiated into the scattering cone, which will in general depend upon the angle of incidence, and may also depend on the state of polarization indicated by the subscript p. The total scattering efficiency for injection into the direction (θ, φ), then is given by

$$\eta_p(\theta, \varphi) = \epsilon_p(\theta) * R_p(\theta, \varphi)/2\pi N_p(\theta) \quad , \tag{3.12}$$

where $N_p(\theta) = \frac{1}{2\pi} \int_o^{2\pi} R_p(\theta, \varphi)\, d\varphi$ is a normalization constant; for the three states of polarization considered above, the normalization constants are given by,

$$N_a(\theta) = 1 - \frac{3}{8} \sin^2 2\theta \quad , \tag{3.13}$$

$$N_b(\theta) = 1 - \frac{1}{2} \sin^2 \theta \quad , \tag{3.14}$$

$$N_c(\theta) = 1 - \frac{1}{4} \sin^2 \theta - \frac{3}{16} \sin^2 2\theta \quad . \tag{3.15}$$

The derivation of the expressions R_p and N_p for arbitrary polarization is straightforward, although cumbersome. The polarization is specified by the angle Φ_E measured in the plane perpendicular to the direction of the incident radiation from the plane containing the incident direction and the focal magnetic field line. The expression for the radiation pattern becomes:

$$R(\Theta, \Phi, \Phi_E) = 1 - \sin^2\Theta \left\{ \begin{array}{l} \cos^2\Phi \cos^2\Phi_E \\ + \sin^2\Phi \sin^2\Phi_E \\ + \sin\Phi \cos\Phi \sin 2\Phi_E \end{array} \right\} \qquad 3.16$$

A little trigonometric manipulation yields:

$$\sin^2\Theta \cos^2\Phi = \frac{1}{2} \sin^2\theta \cos^2\theta f^2(\varphi) \qquad 3.17$$

where

$$f^2(\varphi) = 3 - 4\cos\varphi + \cos 2\varphi \quad . \qquad 3.18$$

The radiation pattern then becomes:

$$R_p(\theta, \varphi) = 1 - \frac{1}{2} \sin^2\theta \left[\cos^2\theta f^2(\varphi) \cdot \cos^2\Phi_E + (1 - \cos 2\varphi) \cdot \sin^2\Phi_E + \sqrt{2} \cos\theta \cdot \sin\varphi \cdot f(\varphi) \cdot \sin 2\Phi_E\right] \qquad 3.19$$

And the normalization factor becomes:

$$N_p(\theta) = 1 - \frac{1}{2} \sin^2\theta \left[3 \cos^2\theta \cos^2\Phi_E + \sin^2\Phi_E\right] \qquad 3.20$$

The locus of the scattering cone may be transformed from the local geomagnetic coordinate system into the local horizon coordinate system,

specified by elevation and azimuth, in which the criterior for earth detached modes (EDM) of propagation are defined, presumably by upper and lower elevation limits at each local azimuth. The intersections of the scattering cone with this band will in general select two windows into which EDM is injected from the incident radiation. The intensity patterns may be integrated across these windows to determine the fraction of the incident radiation, relative to the forward scattered radiation, injected into EDM.

A problem not considered in the present analysis is the question of the coupling efficiency of the field aligned irregularities. This would be expressed as the fraction of the incident energy scattered into the forward direction of the scattering cone.

The problem of the criterior of injection and sustaining radiation in EDM propagation is considered in detail elsewhere in this report. This is a difficult, and to some extent undefined, problem depending on the global electron density distribution, the operating frequency, the (arbitrary) minimum range qualifying for EDM, the (arbitrary) minimum altitude of ray perigee qualifying for EDM.

Clearly, the weakest criterion is to determine the elevation angle for the straight line (high frequency limit) tangent to the earth from the elevated source, and specify the elevation limits as between plus and minus this angle. These limits may be further restricted by raising the minimum ray perigee height. Ultimately, the limits are determined by detailed ray tracing through a model ionosphere. In the study described below, the criterior selected is that radiation incident upon an elevated scattering with a local elevation angle up to plus or minus 5° is presumed to arrive via long distance earth detached propagation. Clearly, this presumption is subject to qualification based upon analysis of the results of the ray tracing program.

Given the existence of a heated region of the ionosphere, it is of interest to determine the locus of transmitter sites suitable to inject RF signals into earth detached modes of propagation via scattering from the field aligned irregularities. This problem may be attacked by considering incident radiation on the heated regions from various azimuths at small local elevation angles, selecting a set of scattered rays along the scattering cone, and tracing these rays to the ground or penetration of the ionosphere. Those rays that strike the ground trace out the locus of suitable transmitter sites, from the principle of reciprocity.

This ray tracing simulation program was carried out for frequencies of 6, 12, 18, 24 and 30 MHz incident on field aligned irregularities located above Plattville, Colorado at altitudes of 150, 200, and 250 km. The radiation was presumed to have come from earth detached propagation modes, incident from magnetic azimuths 0°, 45°, 90°, 135° and 180°, at local elevation of 0°. Elevations of ± 5° were also included at the 200 km level.

The results of this simulation are presented in Figures III. 8 through III. 17. These charts trace the locus of those rays on the scattering cone which strike the ground within the limits of the charted region; sixteen rays were traced on each scattering cone. The numbers annotated to each curve represent the magnetic azimuth <u>from</u> which the incident horizontal (or nearly horizontal) ray comes; and therefore, from reciprocity, the magnetic azimuth into which radiation will be horizontally scattered from a transmitter located on the charted curve.

Figure III. 8 shows the geometry of the scattering cones, without refraction, in the vertical plane containing the local geomagnetic field line appropriate to Plattville, Colorado where the local geomagnetic dip is approximately 67°. The rays labeled 000M and 180M are incident horizontally <u>from</u> the indicated magnetic azimuth on a scattering center at a height h above

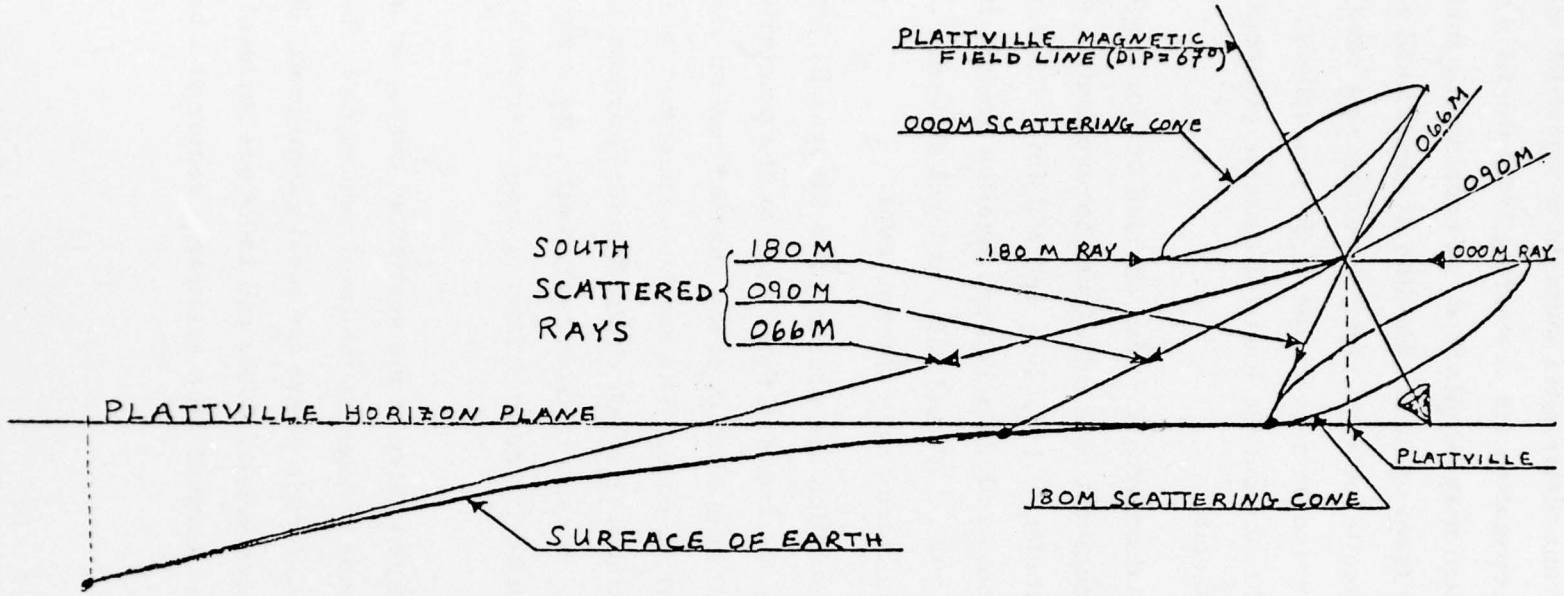

FIGURE III. 8. GEOMETRY OF SCATTERING CONES WITHOUT REFRACTION

the surface of the earth; the scattering cones generated by these rays are as indicated. The ray from this elevated source, just grazing the earth magnetically south of Plattville must leave the source at a local elevation $-\beta_m$ and grazes the earth at a ground range $R_o\beta_m$ from Plattville, where

$$\cos\beta_m = R_o/(R_o + h)$$

This ray lies on the scattering cone generated from a horizontally incident ray from magnetic azimuth z_m given by

$$\cos z_m = \cos(\Delta + \beta_m)/\cos\Delta \quad .$$

For $h \approx 200$ km, $\beta_m \approx 14°$, and $z_m \approx 066M$.

Figures III. 9, III. 10, and III. 11 show the locus of the intersection on the earth's surface of the rays on the scattering cone after refraction within the midnight ionosphere in the neighborhood of Plattville. In Figures III. 9 and III. 10, for scattering centers at 150 km and 200 km respectively, the scattering centers lie below the bottom of the nighttime ionosphere (which, of course, is not technically possible for the presumed method of creation) and the downward scattered rays are unrefracted; a single locus is generated for all frequencies. These loci are the 090M, 135M and 180M curves. At 6 MHz, portions of the 000M, 045M, and 090M scattering cones undergo refraction in the F layer and a subsequent return to the ground.

As the scattering center is raised to 250 km the effects of refraction in the ionosphere become evident as shown in Figure III. 11, most clearly in the 090M traces. Note also that the 6 MHz curves at azimuths 090M, 135M and 180M become closed, and that the 000M and 045M traces appear. Noting that the undeviated incident ray is a member of the scattering cone, a closed

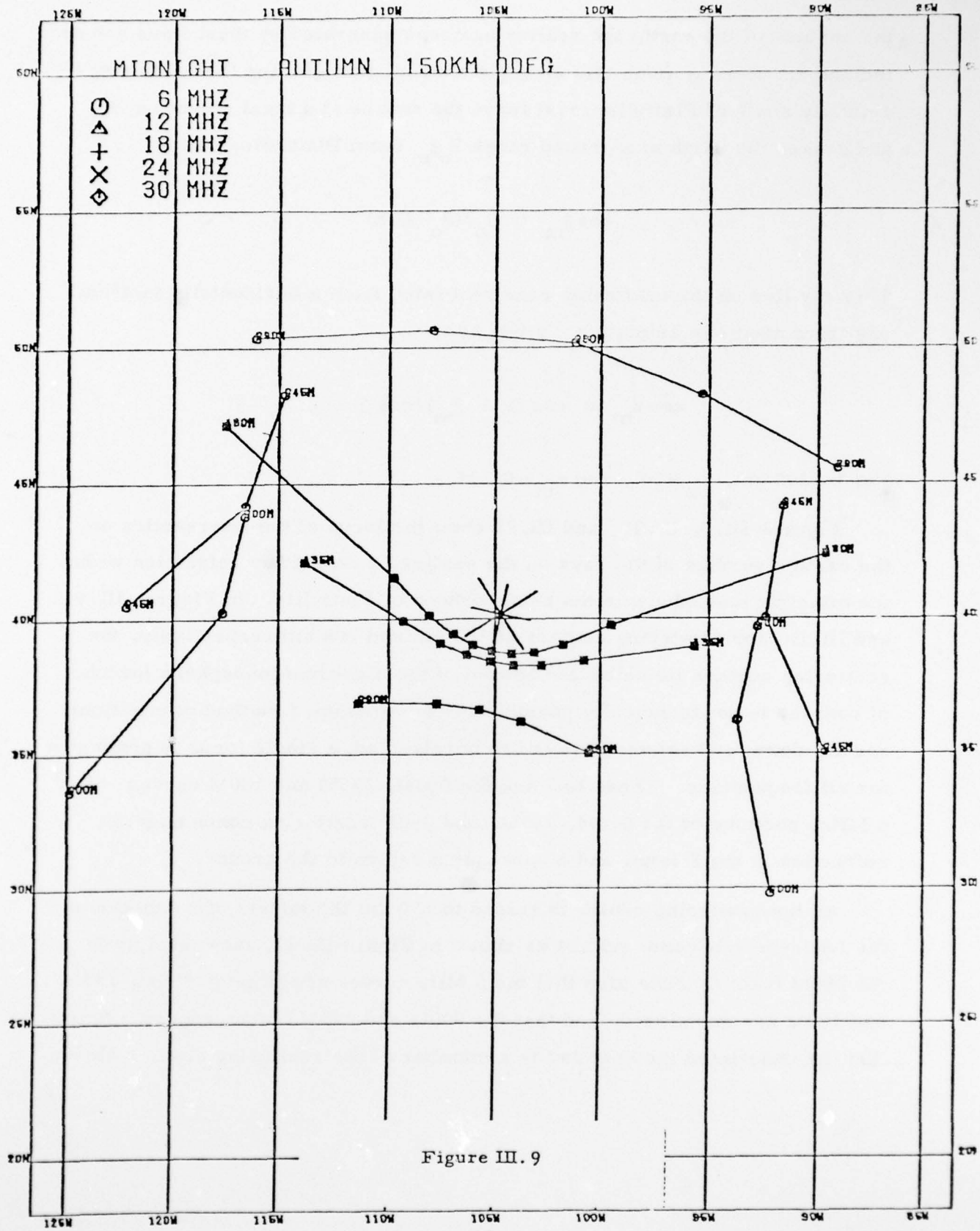
MIDNIGHT AUTUMN 150KM 0DEG
6 MHZ
12 MHZ
18 MHZ
24 MHZ
30 MHZ
125W
120W
115W
110W
105W
100W
95W
90W
85W
60N
55N
50N
45N
40N
35N
30N
25N
20N

Figure III.9

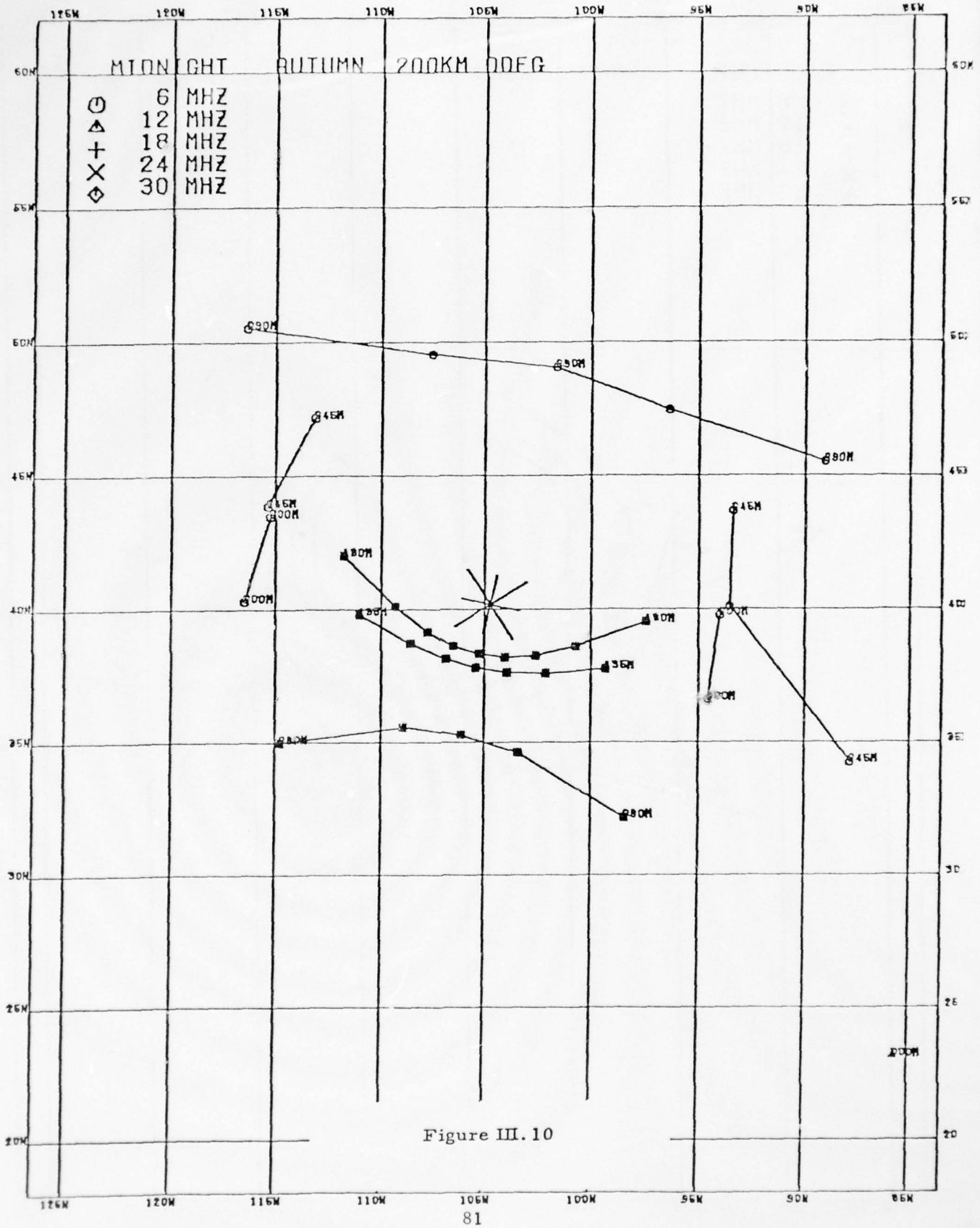

Figure III.10

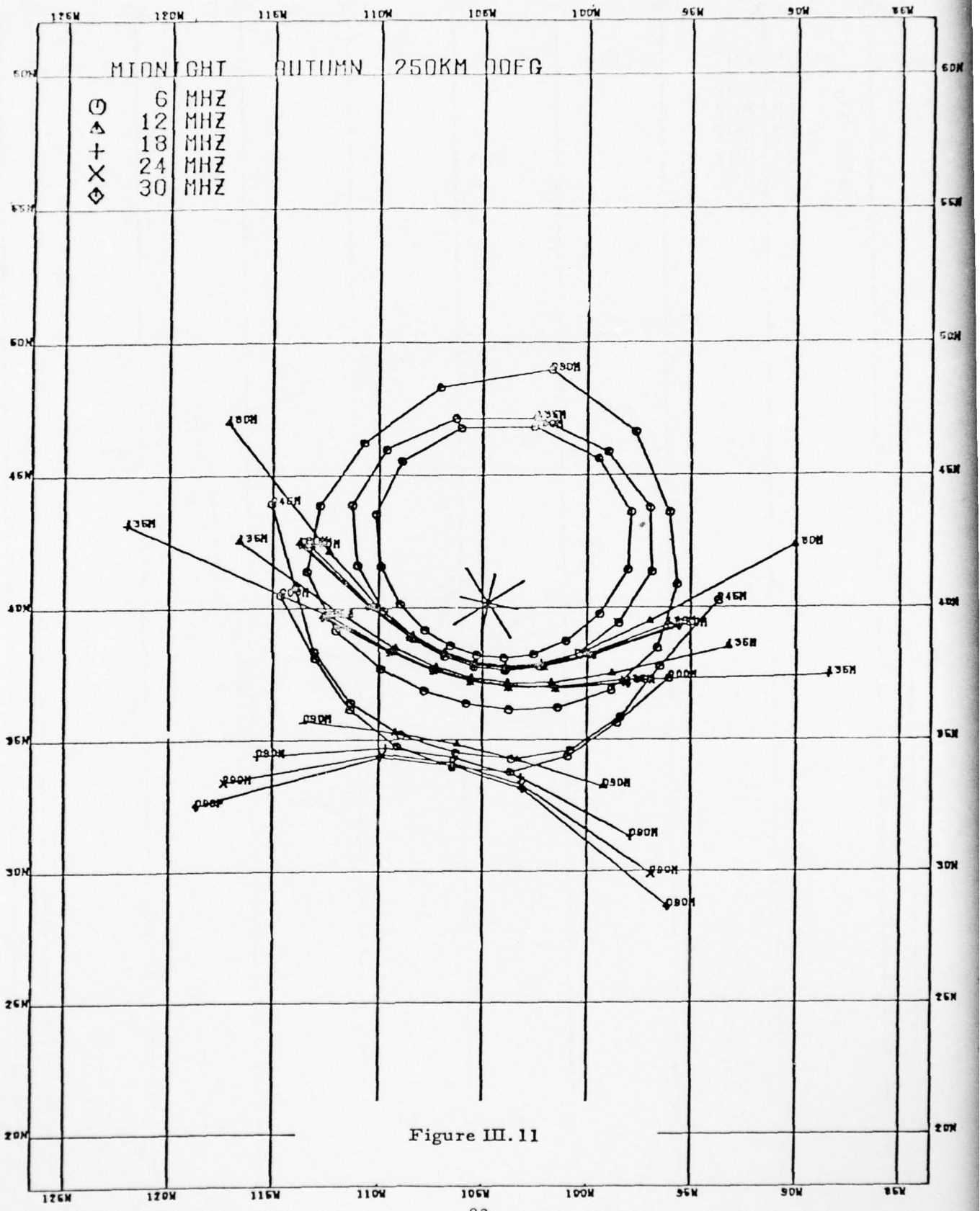

Figure III.11

curve clearly implies that this height is a normal reflection height; this inference is again reinforced by noting that the undeviated rays in the 000M and 045M scattering cone also strike the ground after refraction in the ionosphere. Thus, 250 km is the normal reflection height for a 6 MHz ray launched from the ground returning to the ground after reflection from the ionosphere at a range of approximately 1420 km from the transmitter. Therefore, we conclude that the 6 MHz ray arriving horizontally at the 250 km level is not a candidate for long distance earth detached propagation. However, a 6 MHz signal so arriving may have some energy scattered into some appropriate elevation angles for earth detached propagation.

Figures III.12 through III.16 show the intersections of the scattering cones after refraction from the Autumn Noon ionosphere, and Figure III.17 is the equivalent of Figure III.13 for the Summer Noon ionosphere.

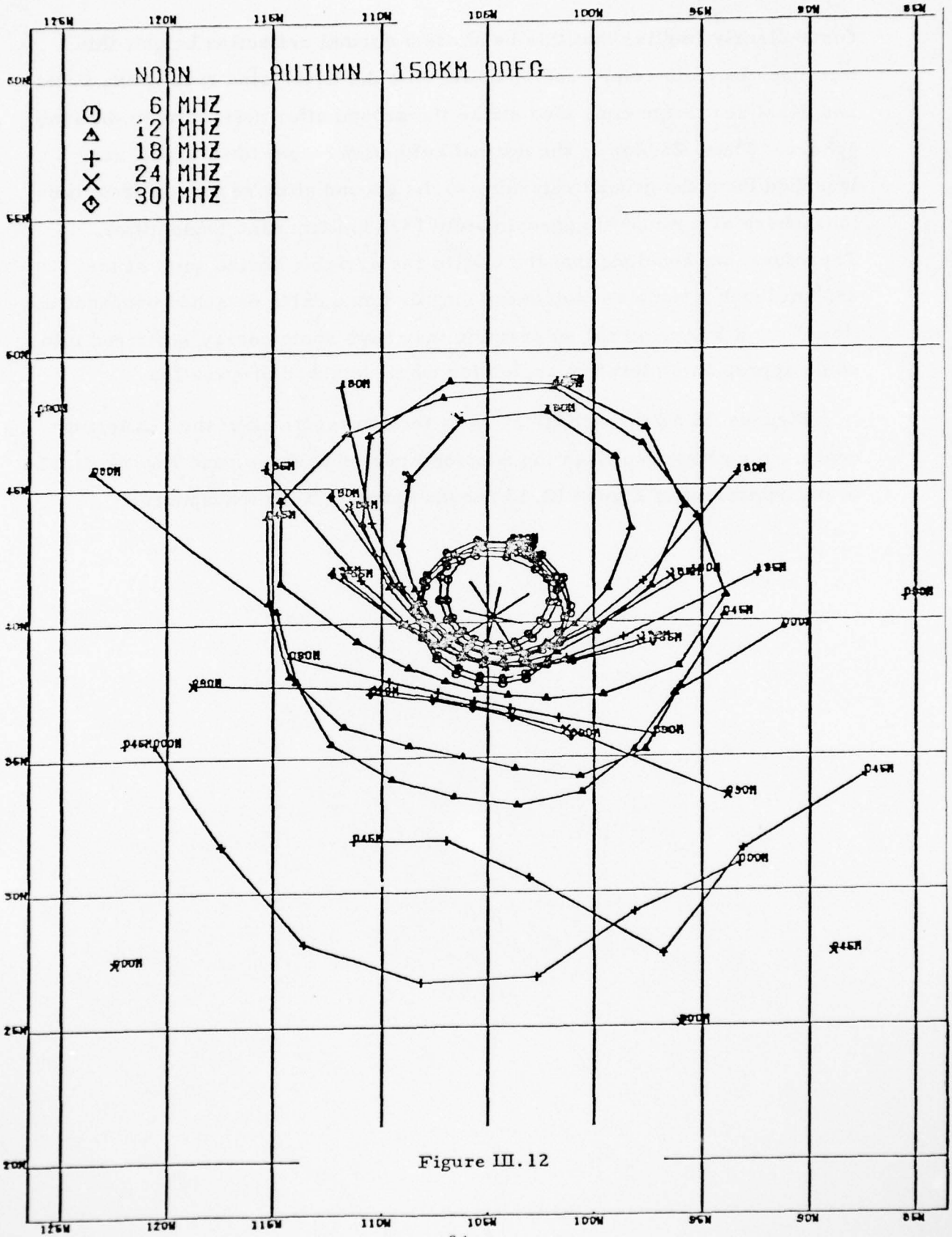

Figure III.12

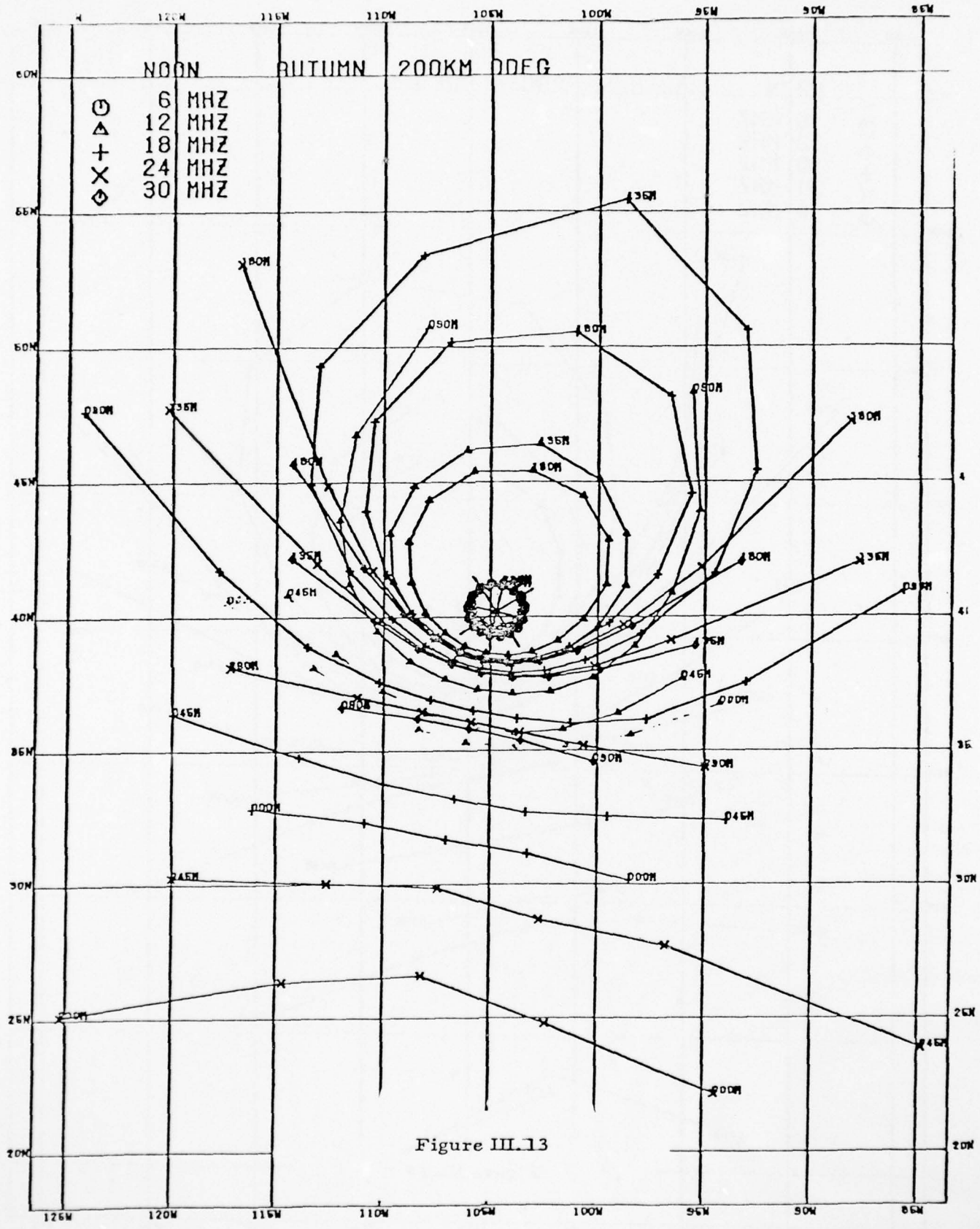

Figure III.13

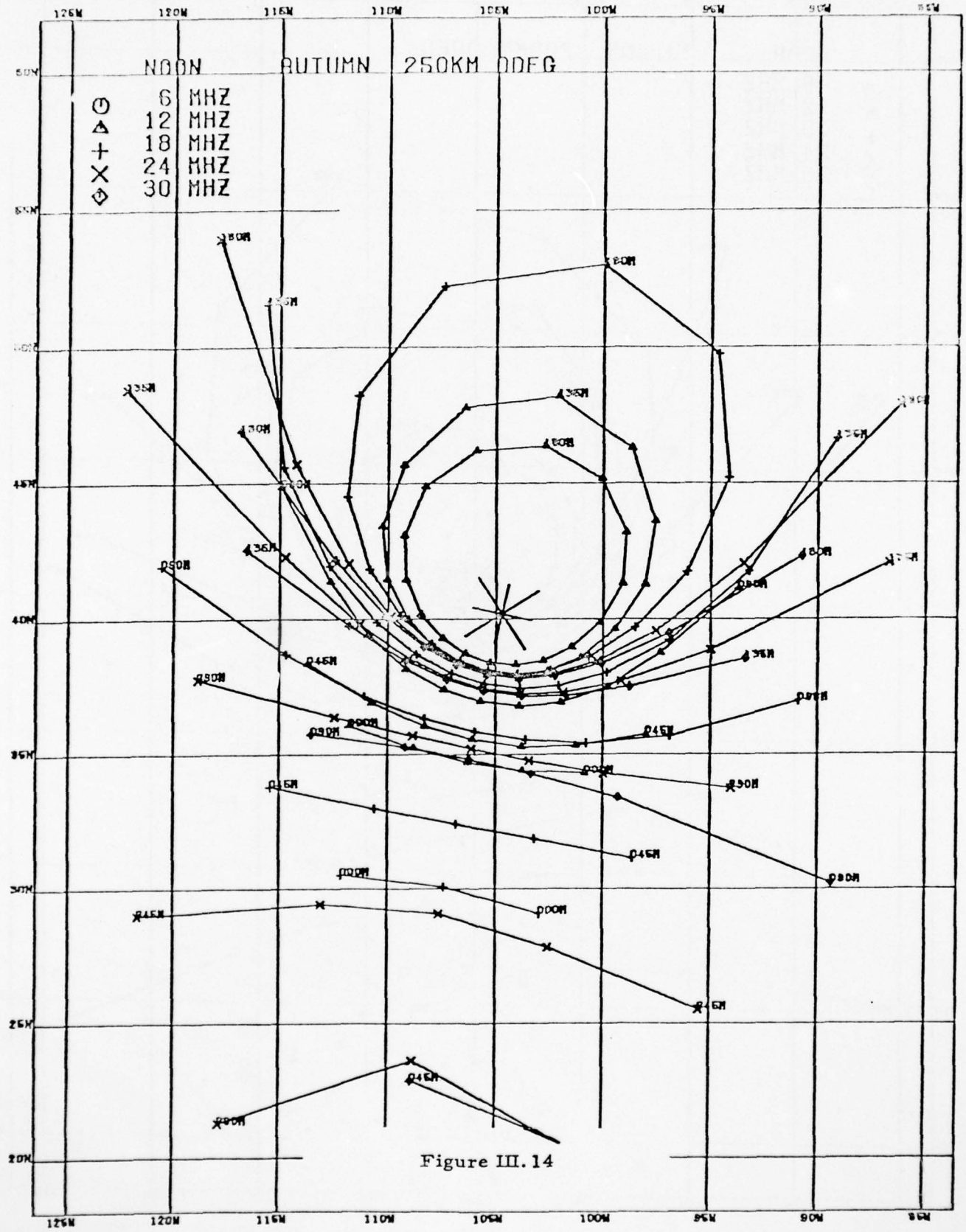

Figure III.14

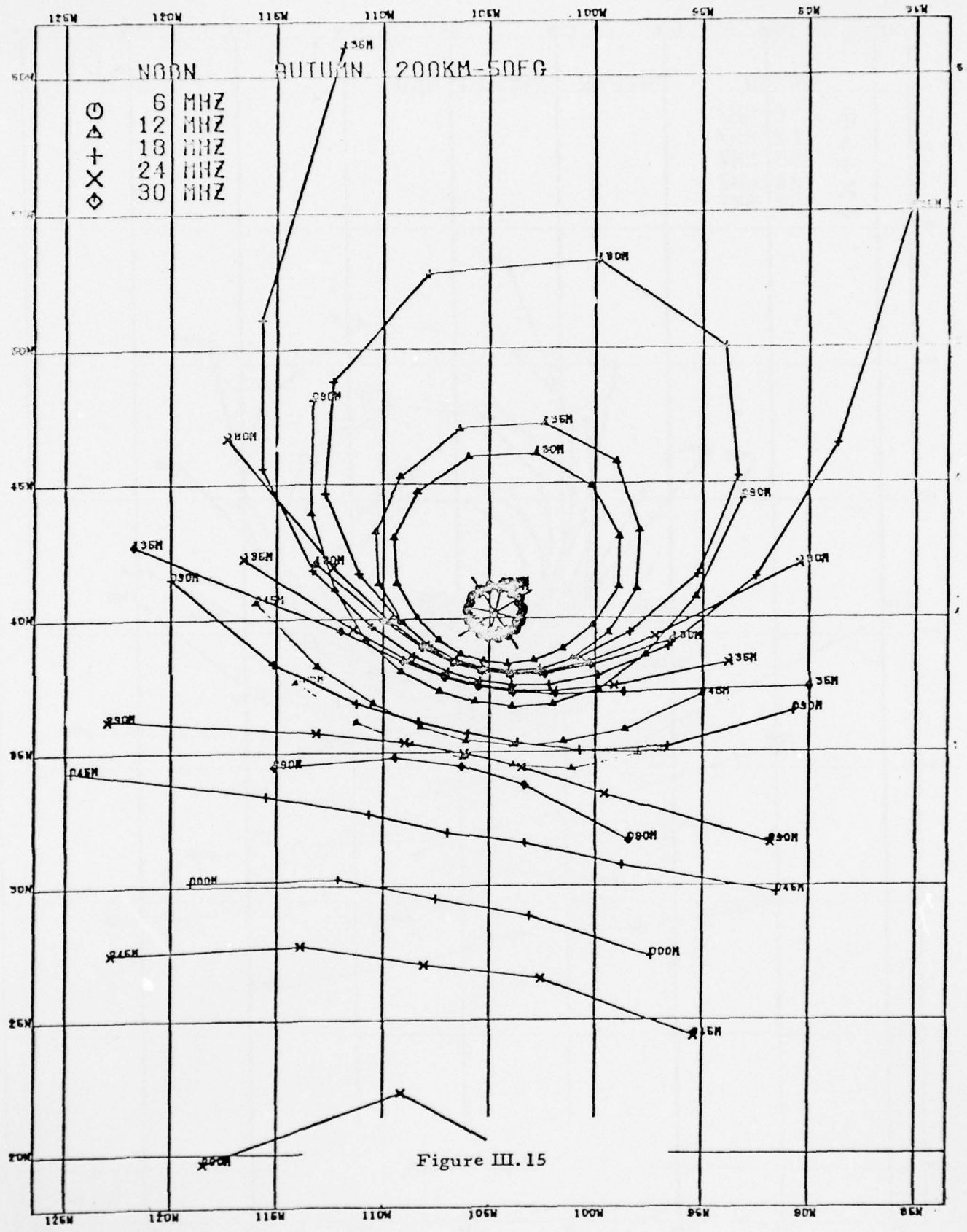

Figure III.15

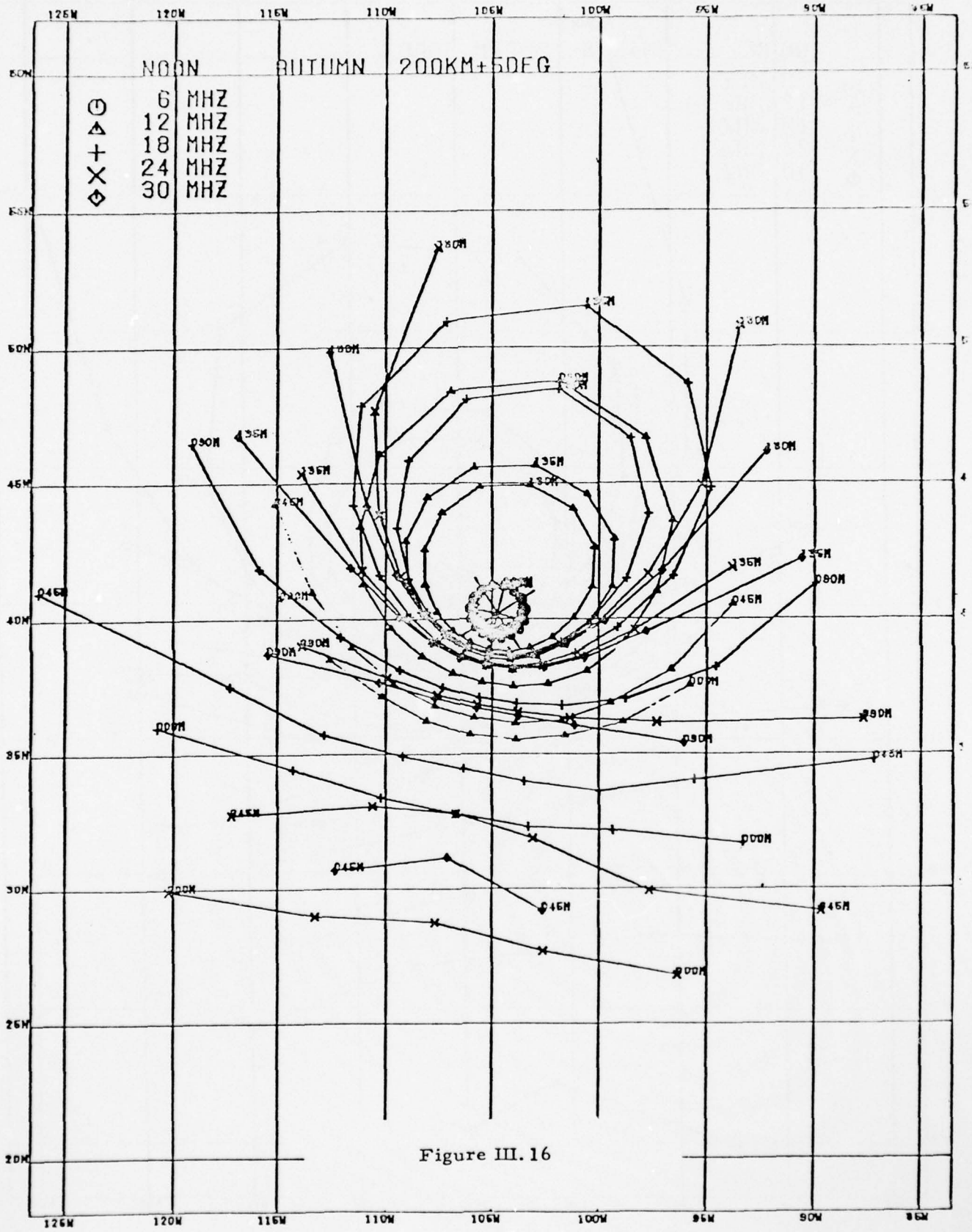

Figure III.16

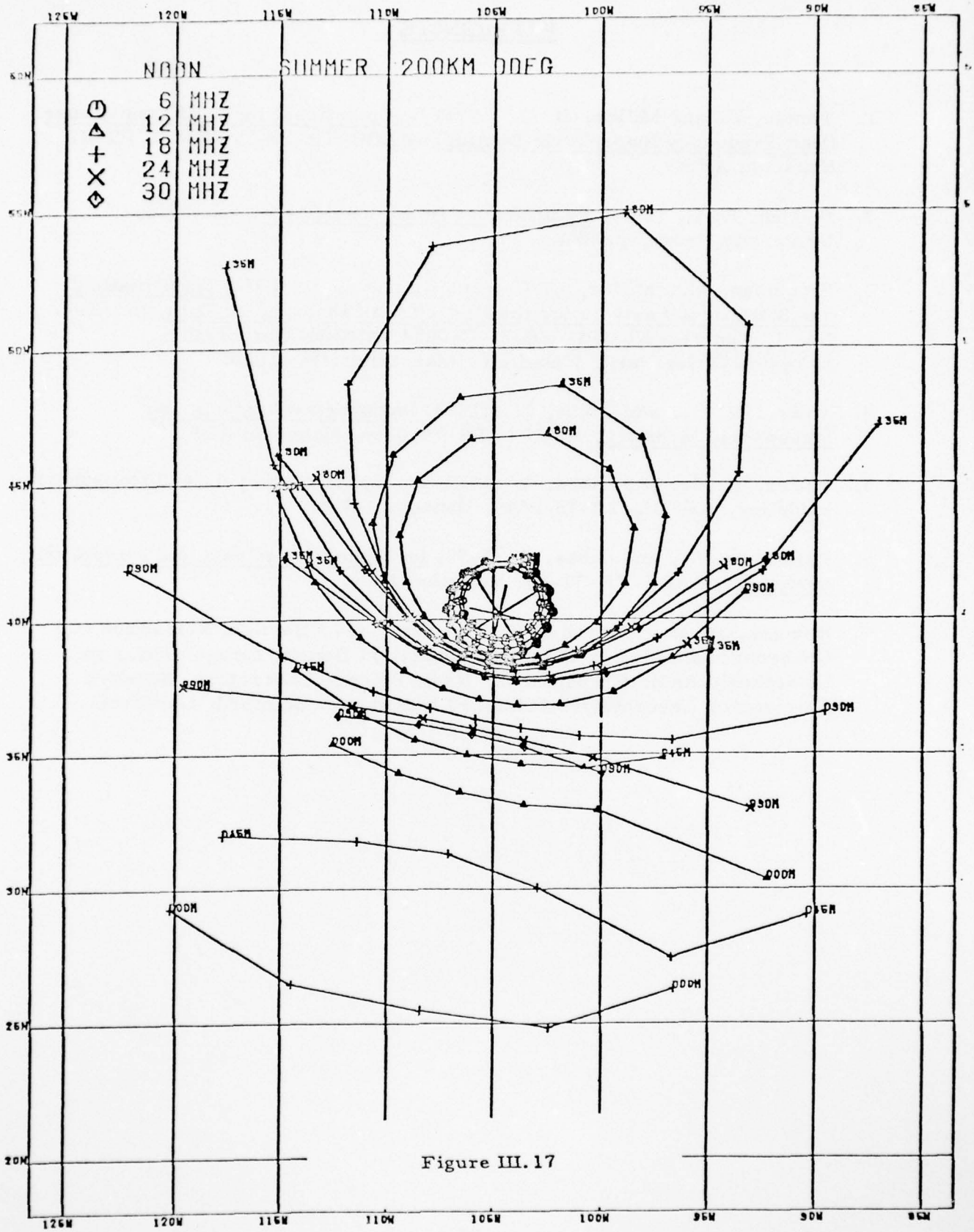

Figure III.17

REFERENCES

1. Toman, K. and Miller, D. C. (1976) Computational Study of Long-Range High Frequency Ionospheric Ducting. RADC-TR-76-359 RADC/ETEI, Hanscom AFB.

2. Budden, K. G. (1961) Radio Waves in the Ionosphere, Cambridge University Press, p. 282.

3. Friedman, M., Miller, D. C., and Reinhold, A. (1972) Mathematical and Statistical Analysis for the Reduction of Ionospheric Data, Sc. Rep. No. 1, Contract No. F19628-71-C-0034, ARCON Corporation, Lakeside Office Park, Wakefield, Massachusetts 01880.

4. Miller, D. C., and Gibbs, J., (1974) Ionospheric Analysis and Ionospheric Modeling, AFCRL-TR-74-0364, Hanscom AFB.

5. Miller, D. C., and Gibbs, J. (1975) Ionospheric Analysis and Ionospheric Modeling, AFCRL-TR-75-0549, Hanscom AFB.

6. Miller, D. C., and Gibbs, J. (1977) Ionospheric Analysis and Ionospheric Modeling. RADC-TR-77-53, Hanscom AFB.

7. Bubenik, D. M., (March 1976) The Combined Effects of Refraction and Coherent Scattering by Columnar Ionization Density Irregularities in Ionospheric Radio Propagation. Radio Science Laboratory, Stanford Electronics Laboratories, Stanford University, Stanford, California.

MISSION
of
Rome Air Development Center

RADC plans and conducts research, exploratory and advanced development programs in command, control, and communications (C^3) activities, and in the C^3 areas of information sciences and intelligence. The principal technical mission areas are communications, electromagnetic guidance and control, surveillance of ground and aerospace objects, intelligence data collection and handling, information system technology, ionospheric propagation, solid state sciences, microwave physics and electronic reliability, maintainability and compatibility.

Printed by
United States Air Force
Hanscom AFB, Mass. 01731